Thèse de doctorat

Université de Limoges

UNIVERSITÉ DE LIMOGES

ED 521 : Sciences et Ingénierie pour l'Information

Laboratoire Xlim

Pôle Electronique, Axe Systèmes & Réseaux intelligents, Equipe RESYST

Année : 2015/2016

Thèse

pour obtenir le grade de

DOCTEUR DE L'UNIVERSITÉ DE LIMOGES

Discipline : Electronique des Hautes Fréquences, Photoniques et Systèmes

présentée et soutenue par

Thierno Abdourahmane DIALLO

le 12 décembre 2016

La fibre en support du Mobile Cloud

Thèse dirigée par Christelle Aupetit-Berthelemot, Anna Pizzinat et Philippe Chanclou

JURY :

Mme Anne-Laure Billabert	Maître de conférences-HDR, ESYCOM, CNAM Paris	Rapporteur
M. Jean-François Helard	Professeur, IETR , INSA de Rennes	Rapporteur
Mme Aupetit-Berthelemot	Professeur, Xlim, Université de Limoges	Examinateur
M. Philippe Chanclou	Ingénieur, Orange Labs, Lannion	Examinateur
M. Xavier Lagrange	Professeur, LabSticc, Telecom Bretagne	Examinateur
Mme Anna Pizzinat	Ingénieur, Orange France, Arcueil	Examinateur

UNIVERSITY OF LIMOGES

ED 521 : Sciences et Ingénierie pour l'Information

Laboratory of Xlim

Pôle Electronique, Axe Systèmes & Réseaux intelligents, Equipe RESYST

Année : 2015/2016 Thèse N° X

Thesis

for the degree of

DOCTOR OF THE UNIVERSITY OF LIMOGES

Discipline : Electronic of High Ferequency, Photonics and Systems

presented and defended by

Thierno Abdourahmane DIALLO

12 december 2016

Mobile Cloud supported by the optical fiber

Thesis supervised by Christelle Aupetit-Berthelemot, Anna Pizzinat et Philippe Chanclou

JURY :

Mme Anne-Laure Billabert	Senior Lecturer-HDR, ESYCOM, CNAM Paris	Reporter
M. Jean-François Helard	Professor, IETR , INSA of Rennes	Reporter
Mme Aupetit-Berthelemot	Professor, Xlim, University of Limoges	Examinator
M. Philippe Chanclou	Engineer, Orange Labs, Lannion	Examinator
M. Xavier Lagrange	Professor, LabSticc, Telecom Bretagne	Examinator
Mme Anna Pizzinat	Engineer, Orange France, Arcueil	Examinator

"A dream doesn't become reality through magic; it takes sweat, determination and hard work."

Colin Powell

"Ever tried. Ever failed. No matter. Try again. Fail again. Fail better"

Samuel Beckett

A mes Parents
Ndoumbé Wade et Boubacar Diallo,
Mon Oncle et sa Femme
Abdourahmane Gueye et Dominique Sazerat
Et à mon Frère
Cheikh Mbacké Samb

Acknowledgments

Acknowledgments to jury committee:

At First, I would like to express my acknowledgments to Dr Anna Pizzinat. Anna Pizzinat has been my main advisor during my thesis in Orange Labs. She has forwarded me her love for optical access network applied to radio access network. I had really appreciated to work in this domain. Also, she has included into me the rigor and the love of perfect work.

Also, I would like to express my sincere gratitude to my thesis director the professor Christelle Aupetit-Berthelemot. Christelle Aupetit-Berthelemot has permitted me to have a global and academical point of view on a new and innovative architecture which has been the center context of my thesis. She has given me the sense of the pedagogy, of analysis and of the patience in the difficult life of a young research fellow.

Then I would like to thank Dr Philippe Chanclou for the effective and relevant advices which he has delivered me during my thesis at Orange Labs. Phillipe Chanclou has been a model and a reference for me, so much I have been impressed by his working and his thinking speed, his great optical knowledges and his mastery of domains linked to my thesis subject. He has transmitted into me his love of big challenges.

In addition, I would like to thank once again Anna Pizzinat, Christelle aupetit-Berthelemot and Phillippe Chanclou to have given me a chance to realize my dream in excellent conditions: become a doctor of telecoms. I feel especially lucky and fortunate to have worked with you.

After my advisors, I would like to express my acknowledgments to Dr Anne Laure Billabert for two raisons. The first raison is that she accepted to review my dissertation and the second raison is the quality of the teaching delivered by Mme Anne Laure Billarbert that I had received during my master. Indeed, I had been the student of Mme Anne laure Billert and the quality of education provided by her and the others teachers during my master has facilitated my access to the PhD school.

Also, I would like to thank the professor Jean Francois Helard for agreeing to report my manuscript of my thesis. Yours relevant questions during my presentation and your relevant notices and those of Mme Anne Laure Billabert have permitted to improve the final version of this manuscript. Finally, I would like to thank the professor Xavier Lagrage for agreeing to examine my PhD works.

Acknowledgments to Colleagues:

Orange has given me the love of collective and collaborative work. For this I would like to thank the ASHA team especially Fabienne Saliouu, Gaël Simon, Zakarya Tayq, Stephane Gosselin, Bernard Landousie, Philippe Guignard, Moufida Feknous, Aurelien Lebreton, Benoit Charbonnier, Kamil Grzybowski, Justine Konopacki, Laurent Guillo, Bertand Le Guyader, Neveena Genay and Luiz Anet Neto

Also, I would like to thank my others colleagues particularly Mr Fabrice Deletre, Mr Laurent Pommerol, Mr Gilles Merour, Mr Matthieu Ferrand, Dr Btissam Er-Rahmadi, Dr Sibiri Tiemou, Dr Soumia Natouri, Mme Wafa Ben Ali, Dr Yassine Nourridine, Dr Idir Izem, and the team of reprography.

I would like to thank Mme Marie Claude le Rouge for her administrative helps concerning the PhD school and her encouragement and Also I would like to thank Mr Abdourahmane Samb, Mr Ulyss Lombudjimabicke and Mr Severin Nadji for agreeing to reread my manuscript.

Résumé en français

Introduction

En Europe, il existe une forte concurrence entre les opérateurs mobiles. Ce contexte actuel affecte et entraine une baisse du chiffre d'affaires et de la rentabilité des réseaux mobiles. Dans cet environnement de forte concurrence vient s'ajouter la problématique de la montée en débit. En effet, pour résoudre cette problématique à court et à moyen terme, la densification du Réseau d'Accès Mobile (RAN) est envisageable, mais cette solution s'avérera inefficace à long terme. En plus, cette densification de l'architecture actuelle entraine l'augmentation des coûts d'exploitation, de déploiement et accroit la complexité de gestion du RAN notamment celle liée au management des interférences.

Afin d'augmenter le débit utilisateur sur l'interface air et améliorer la qualité de service, des techniques d'amélioration de l'interface radio telles que le « coordinated Multipoint (CoMP) » ou le « enhanced Inter Cell Interface Coordination (eICIC) » sont implémentées. Ces techniques d'amélioration de débit sur l'interface radio présentent de fortes contraintes en termes de latence et leur implémentation est difficilement mise en œuvre avec l'architecture réseau d'accès mobile actuelle telle qu'elle est décrite.

Face à tous ces enjeux et afin d'augmenter la rentabilité des réseaux d'accès mobiles, les acteurs du monde des télécommunications doivent réfléchir à une nouvelle architecture qui permettra :

- La réduction des couts d'exploitation et de déploiement
- La réduction de la consommation d'énergie
- De supporter les standards actuels et futurs des réseaux d'accès mobiles.

Une nouvelle architecture innovante nommée *Cloud ou Centralized Radio Access Network (C-RAN) ou Mobile Cloud (MC)* est proposée pour satisfaire les différentes exigences non-exhaustives citées ci-dessus. Dans l'architecture traditionnelle, le site d'antennes est essentiellement constitué d'un module radio nommé *RRH (Remote Radio Head)* et d'une entité de traitement de données numériques appelée *BBU (Base Band Unit)*. L'architecture C-RAN consiste à déporter la BBU du site d'antennes vers un local distant (situé à plusieurs kilomètres du site d'antennes) sécurisé désigné par le terme de *CO (Central Office)*. La RRH reste sur le site d'antennes. Ce déport des BBU vers le CO fait apparaitre un nouveau segment réseau entre la BBU et la RRH appelé *fronthaul*. Le lien fronthaul est soumis à certaines contraintes qui imposent la fibre optique comme le média de transport idéal pour implémenter ce dernier. D'où le titre de cette thèse :*la fibre en support du Mobile Cloud*. Cette thèse se focalise donc sur l'étude des différentes

solutions potentielles permettant l'implémentation d'un lien fronthaul optique.

Ce manuscrit de thèse est constitué de trois chapitres. Le premier chapitre constitue l'état de l'art. Cet état de l'art relate les différentes architectures filaires utilisées dans le réseau backhaul et les différents standards des RAN actuels. Ce chapitre a pour but de fournir une vue d'ensemble sur la problématique. Il identifie les principaux axes de recherches abordés durant cette thèse et présente les différentes solutions étudiées permettant la mise en œuvre du lien fronthaul. Le deuxième chapitre est consacré à l'étude du paramètre de la gigue sur un lien fronthaul. Rappelons que la gigue est la variation de phase du signal et que cette dernière affecte les performances du système. Quant au troisième chapitre, il présente les principaux résultats de deux solutions potentielles qui ont pour but de simplifier l'implémentation du lien fronthaul à moindre coût. Le premier système présente une solution auto accordable en longueur d'onde qui permettra de s'affranchir des contraintes liées à la complexité de la gestion des longueurs d'onde rencontrée dans les architectures basées sur les techniques de multiplexage en longueurs d'onde classiques. Le second système présente une solution mono fibre implémentant un dispositif de supervision du lien optique. Une synthèse du document et les perspectives de cette thèse sont proposées dans la partie conclusion et perspectives.

Dans cette thèse, plusieurs expérimentations ont été menées portant principalement sur la gigue et les solutions de déploiement de l'interface fronthaul. La qualité de la transmission fronthaul est évaluée en Taux d'Erreur Binaire (TEB) et la qualité de bout en bout de la transmission radio LTE est évaluée en EVM (Error Vector Magnitude) définie par la 3GPP.

Chapitre 1 : Etat de l'art

Le réseau d'accès mobile actuel est constitué du réseau bachkaul qui permet de transporter les données du réseau d'accès radio vers le réseau cœur. La première partie de ce chapitre présente un récapitulatif succinct des normes RAN telles que la 2G, 3G, 4G, et les enjeux de la 5G. Les caractéristiques en termes de débit et des entités architecturales du RAN y sont décrites. Les technologies filaires permettant le transport du réseau backhaul telles que le xDSL (Digital Subscriber Lines) et le réseau PON (Passive Optical network) y sont également décrits. Aussi, le C-RAN vient proposer un nouveau segment réseau nommé fronthaul qui est obtenu grâce au déport de la BBU du site d'antennes vers un CO. Le réseau backhaul est donc naturellement déplacé du site d'antenne vers le CO. Le fronthaul utilise la technologie de la radio sur fibre numérisée désignée par le terme anglais de D-RoF (Digitized Radio over Fiber). La D-RoF dédiée au fronthaul est définie par trois standards qui sont : le CPRI (Common Public Radio Interface), l'OBSAI (Open Base Station Architecture Initiative) ou le ORI (Open Radio Interface). Le CPRI est le plus utilisé dans le déploiement du fronthaul et constituera la base de nos études. En plus du CPRI, nos études se cantonneront exclusivement à l'étude de la 4G à travers la norme LTE (Long Term Evolution). Signalons aussi que le déploiement de l'interface fonthaul et le CPRI sont soumis à certaines propriétés et contraintes.

La première contrainte est celle liée au débit. En effet pour pourvoir numériser les signaux radios, une quantification avec une résolution de 15 bits est appliquée aux données radios analogiques IQ. Cette grande résolution rend le signal radio numérisé plus robuste, mais entraine une inefficacité en termes de débit. En effet, il existe un facteur approximativement égal à 16 entre le débit du CPRI et débit de la LTE. Par exemple, le transport d'un débit à 150 Mbit/s issu de la LTE à 20 MHz, d'une configuration MIMO 2X2, nécessite un débit CPRI de 2.45 Gbit/s. La deuxième contrainte est liée à la latence introduite par le lien fronthaul. Cette latence doit permettre de respecter les contraintes de délai imposées par les standards de la 3GPP pour s'assurer de la qualité de service. La latence imposée par la méthode de transmission de données « HARQ (Hybrid Automatic repeat Resquest) » permet d'établir la longueur maximale d'une liaison fronthaul. La troisième contrainte indique que le taux d'erreur binaire d'une transmission fronthaul doit être inférieure ou égale à 10^{-12}. Ensuite, nous avons des contraintes liées à la disponibilité de la fibre. En effet, la fibre optique étant une ressource rare, il est donc indispensable de l'optimiser afin de permettre et de faciliter le déploiement du fronthaul. Afin de permettre l'optimisation de l'utilisation de la fibre optique, la technique de multiplexage en longueurs d'onde appelée WDM (Wavelength Division Multiplexing) est employée.

Le WDM constitue la base de toutes les solutions étudiées permettant d'implémenter l'interface fronthaul durant cette thèse. Ces solutions se divisent en trois catégories qui sont :

- La solution passive : Cette solution utilise que des éléments passifs entre le site d'antennes et le CO pour la réalisation d'un lien fronthaul. Cette solution basique est simple à mettre en œuvre et peu couteuse

- La solution semi-active : cette solution implique l'utilisation d'un équipement actif du côté du CO et d'un équipement passif du côté du site d'antennes. Comparée à la solution passive, elle permet une supervision du lien optique

- La solution active : Cette solution utilise des équipements actifs du côté du CO et du site d'antennes. Elle permet non seulement la supervision du lien optique, mais aussi le monitoring de chaque longueur d'onde implémentant un lien fronthaul.

Le déploiement du fronthaul est aussi soumis à certains aspects légaux. En effet, afin de mieux définir les offres et situer les responsabilités entre l'opérateur fixe qui est chargé d'implémenter le lien optique fronthaul et l'opérateur mobile, des points de démarcation doivent être établis d'un commun accord entre différents acteurs. Enfin la dernière contrainte présentée est la gigue. La gigue est définie comme la variation de la phase du signal numérique qui peut entraîner des erreurs de transmission sur le lien fronthaul ou dans le pire des cas une perte du signal d'horloge. La spécification CPRI définit la contribution de la gigue sur la déviation du signal d'horloge d'une interface fronthaul. Cette déviation est fixée à une valeur maximale de 2 ppb[1] . Enfin, rappelons que la gigue constitue un phénomène physique important à observer et à étudier afin de comprendre son influence sur la transmission fronthaul. Les aspects de la gigue sur un lien fronthaul sont traités dans le chapitre 2.

[1]ppb: part per billion

Chapitre 2 : Influence de la gigue sur l'interface fronthaul

Le segment fronthaul est une interface numérisée à haut débit, donc soumis au phénomène de la gigue. La gigue est une variation de phase du signal numérique qui impacte les performances de la transmission numérique et peut entraîner la rupture de la communication sur un lien fronthaul. Les sources de l'apparution de la gigue sur une interface fronthaul peuvent être nombreuse et diverses. Elle peut être dûe notamment à une variation du courant qui alimente le laser, à un mauvais calibrage du signal d'horloge ou au bruit blanc gaussien. Elle se décompose en deux principales catégories qui sont la gigue déterministe et la gigue aléatoire. La gigue déterministe peut être quantifiée, car elle est bornée tandis que la gigue aléatoire peut être estimée. Le critère d'estimation de la gigue aléatoire proposé par la spécification CPRI est le taux d'erreur binaire (TEB). On distingue aussi la gigue sinusoïdale. En ce qui concerne cette dernière, la spécification CPRI définit un niveau de tolérance de cette gigue par rapport à sa fréquence dans une transmission fronthaul. La gigue totale est égale à l'addition de la gigue déterministe, de la gigue aléatoire et de la gigue sinusoïdale. L'étude de ce phénomène physique sur un lien fronthaul, débute avec la proposition un banc de mesure qui permet de récupérer un signal optique et d'y introduire la gigue. Ce banc a été calibré et une erreur quadratique de moyenne de 3.6% a été mesurée, ce qui permet donc de justifier la fiabilité du dispositif proposé. La première étude consiste à introduire de la gigue sinusoïdale sur le lien fonthaul et de comparer le niveau de gigue mesuré au masque de tolérance proposé par la spécification CPRI. Les résultats de cette expérience montrent que les effets de la gigue sinusoïdale ne dépendent de la fréquence de cette gigue mais plutôt de son amplitude. En effet, en tenant compte du TEB à 10^{-12} comme critère fonctionnement, la transmission sur l'interface fronthaul n'est fonctionnelle qu'avec une gigue sinusoïdale mesurée de 0,4 UI pour les fréquences allant jusqu'à 10 MHz. Le masque de tolérance de la gigue indique que pour des fréquences allant de 0 à 1800 MHz la gigue sinusoïdale doit être supérieure à 0.4 UI. Par conséquent, les transmissions fronthaul actuelles ne respectent pas les recommandations indiquées par la spécification CPRI. Ce résultat est dû en partie, au fait que le codage de canal utilisé en l'occurrence le NRZ, ne facilite pas la récupération d'horloge de telle sorte qu'une gigue sinusoïdale de 0.4 UI est assez suffisante pour perturber la récupération d'horloge et par conséquence introduire des erreurs dans la transmission fronthaul. Aussi, la boucle à verrouillage de phase utilisée dans un lien fronthaul se comporte comme un filtre passe bas par rapport à la gigue sinusoïdale. Ce qui permet l'expliquer l'annulation des effets fréquentiels de la gigue.

Le comportement d'une boucle à verrouillage de phase telle que représentée dans la

littérature a fait l'objet d'une étude théorique qui a permis d'établir des équations afin de simuler les effets des boucles à verrouillage de phase d'ordre 1, 2 et 3. L'étude théorique permet aussi d'avoir un aperçu sur la manière dont dévie la fréquence porteuse de la RRH par rapport à la présence de la gigue sur l'interface fonthaul. Le résultat de la simulation de cette étude théorique montre que la déviation fréquentielle de la porteuse radio est indépendante de la fréquence de la gigue sinusoïdale, car la boucle à verrouillage de phase se comporte comme un filtre par rapport à la gigue. Néanmoins, cette déviation de la fréquence porteuse dépend de l'amplitude de la gigue. Un banc de mesure en grandeur nature mettant en œuvre une vraie plateforme commerciale impliquant une paire BBU - RRH vient confirmer les résultats de l'étude théorique.

Mesurer la contribution de la gigue sur la déviation de l'horloge du signal CPRI constitue un enjeu majeur de cette thèse. En effet, le CPRI spécifie un maximum de 2 ppb de déviation fréquentielle dûe à la gigue, mais ne propose aucune méthode de mesure de cette dernière. Dans cette thèse, un banc de mesure a été fourni afin de mesurer cette contribution de la gigue sur déviation fréquentielle. Deux méthodes sont proposées la première considère que la source d'horloge qui asservit la BBU est accessible et la seconde lorsque le signal d'horloge est récupéré à travers le signal CPRI. Dans le deuxième cas, il est nécessaire de remettre en forme le signal d'horloge et le régénérer grâce à un récupérateur d'horloge afin d'obtenir une horloge stable. Le signal d'horloge stable et les données contenant de la gigue sont mélangés par un mixeur puis le signal résultant est transmis à l'analyseur de spectre qui va procéder à la mesure.

Dans ce chapitre, plusieurs bancs de mesure ont été implémentés afin de comprendre les effets de la gigue sur un lien fronthaul et aussi sur la déviation de la fréquence porteuse de la RRH. De ces études, il en ressort que le masque de la gigue sinusoïdale proposé par la spécification CPRI n'est pas respecté par les interfaces fronthaul telle qu'elles sont implémentées présentement. Afin d'avoir les outils adéquats pour évaluer la gigue sur un lien fronthaul, il est donc nécessaire de redéfinir le masque de tolérance de la gigue sinusoïdale.

Le déploiement du fronthaul doit être optimisé en termes de coût et de gestion des ressources. Le chapitre 3 aborde la question des fronthaul à moindre coût en présentant deux architectures. La première traite un système auto-accordable en longueur d'onde à moindre coût et la seconde présente une solution complète mono fibre pour le déploiement du fronthaul.

Chapitre 3 : Solution expérimentale pour le déploiement d'un lien fronthaul

Le déploiement du fronthaul doit tenir compte des aspects d'optimisation de ressources, de coûts et du respect de règles de régulations. La technique WDM permet d'optimiser les ressources optiques en transportant les flux de données de plusieurs liens fronthaul sur une ou deux fibres optiques. Lorsque le WDM est utilisé, il vient se poser la question de la gestion des différentes longueurs d'onde. En effet, chaque lien fronthaul est affecté d'une paire de longueurs d'onde dédiée. L'augmentation de la complexité dans la gestion des stocks de ces longueurs d'onde sera prévisible lorsque le réseau fronthaul prendra de l'ampleur. Cette problématique sera plus importante dans le cas particulier du DWDM (Dense WDM). Afin d'affranchir le réseau fronthaul de la complexité en gestion de longueurs d'onde, le système auto accordable en longueurs d'onde, nommée self-seeded basé sur un RSOA (Refletive Semiconductor Optical Amplifier), appliqué sur un lien fronthaul est étudié. L'impact de ce laser est scruté sur l'interface fronthaul, sur la transmission LTE de bout en bout et sur la déviation radio de la RRH.

L'un des enjeux majeurs de cette thèse est de pouvoir proposer ou analyser des systèmes qui permettent d'optimiser au mieux la ressource fibre optique dans le déploiement du fronthaul car cette dernière est une ressource rare et couteuse. La technique du WDM est utilisée dans la mise en œuvre du fronthaul pour réduire le nombre de fibre optique utilisée. Si l'on considère un site d'antennes et un CO où l'on veut assurer la communication bidirectionnelle entre ces deux entités (BBU et RRH), une paire de fibres optiques doit être installée. Une fibre optique est utilisée pour transporter les flux de données agrégés dans le sens montant et l'autre fibre aura pour but d'assurer la communication dans le sens descendant. Cette solution s'appelle la solution WDM à double fibre. Dans notre thèse, nous proposons l'étude d'un système mono fibre où la communication bidirectionnelle est assurée sur une seule fibre optique. Les aspects de régulation imposent que ce système dispose d'un mécanisme de supervision du lien optique. Par conséquent, afin de proposer une solution complète d'un système mono fibre, nous allons présenter un dispositif de supervision de d'un système WDM mono fibre. Ce système de supervision constitue la partie innovante dans la solution WDM mono fibre proposée pour le déploiement du fronthaul.

1. L'impact du système auto accordable self seeded sur le fronthaul

Dans cette partie, une source laser auto accordable basée sur un RSOA est étudiée. Le RSOA émet un signal optique sur une large bande plus précisément dans la bande-O dans notre cas. Le signal émis est filtré par un AWG (Array Wavelength Guide) au canal désiré puis le signal est réfléchi par un miroir placé après ce denier. Le signal repasse par le canal de l'AWG souhaité et est à son tour réfléchi par la face réfléchissante du RSOA. Cette face réfléchissante du RSOA et le miroir placé après l'AWG constituent la cavité du laser. La longueur de la cavité peut varier en changeant la longueur de la fibre entre l'AWG et le RSOA. L'amplification du signal optique est obtenue après plusieurs aller-retours de ce dernier dans la cavité. Ces différents aller-retours font apparaitre des modes longitudinaux dans le laser d'où le qualificatif de source multimode attribué au laser self seeded basé sur un RSOA.

La principale contribution concernant ces travaux, est la proposition d'un banc de mesure pour étudier les effets de la source auto accordable, à moindre coût, le self seeded, sur le fronthaul. Ce banc de mesure est constitué d'une source self seeded basée sur un RSOA qui est attaquée par des trames CPRI. Le signal optique obtenu est envoyé sur de la fibre dont la longueur varie entre 0 km, 30 km et 60 km. Durant cette étude, la longueur de la cavité variera entre une cavité courte ($<$10m), 1 km, 2 km et 5 km. Aussi, le débit CPRI variera entre 1.22 Gbit/s et 2.45 Gbit/s.

Les premiers résultats présentés sont relatifs aux tests de TEB effectués. Pour les transmissions à 1.22 Gbit/s, le TEB est inférieur à 10^{-12} et respecte donc les spécifications du CPRI. Ce résultat est valable pour toutes les longueurs de cavité testées et pour des transmissions de 0 km et de 30 km. Les performances en TEB à 0 km et à 30 km de transmission sont identiques. Ceci est dû au fait que la dispersion chromatique est assez faible par rapport au type de fibre optique utilisé (SM-28) dans la bande-O. Pour une transmission à 2.45 Gbit/s, la spécification CPRI n'est pas vérifiée en termes de TEB. En effet, on mesure un TEB de 10^{-9}. Les performances pour les différentes longueurs de transmission ne sont pas équivalentes. Cette différence de performance résulte de la combinaison des effets de la dispersion chromatique qui est faible mais pas nulle et du bruit de phase important présent dans la cavité dû aux différents modes longitudinaux.

Les effets du self seeded basé sur un RSOA sur la transmission radio LTE de bout en bout sont aussi étudiés. Rappelons que la qualité radio LTE est mesurée à travers l'EVM qui traduit l'erreur d'une constellation par rapport à une constellation idéale. La 3GPP définit le niveau EVM à ne pas dépasser suivant les constellations. Pour le banc de

mesure proposé pour cette expérience, nous disposons d'un générateur de trames LTE et des modules qui permettent d'encapsuler et d'extraire les données LTE dans les trames CPRI. Durant cette expérience, nous allons procéder aux changements des longueurs de cavité et de transmission comme dans la précédente expérience décrite ci-dessus. Les tests ont été effectués pour les constellations de QPSK (quadrature Phase Shift Keying), 16-QAM (16-Quadrature Amplitude Modulation) et 64-QAM (64-Quadrature Amplitude Modulation). Pour ces différentes modulations, les recommandations de la 3GPP sont respectées dans tous les cas de figure testés. De plus, l'EVM est conforme aux spécifications indiquées bien que le TEB du lien fonthaul ne respecte pas le seuil 10^{-12} désigné par le CPRI. Ce fait traduit une certaine robustesse du signal CPRI qui malgré la dégradation du TEB permet de conserver un EVM adéquat sur une transmission de bout en bout. Ce constat s'explique par le fait que la résolution de la quantification des échantillons IQ est très élevée et est égale à 15 bits.

Aussi, la quantité de gigue a été mesurée à l'aide d'un oscilloscope. Pour les 2 débits testés (1.22 Gbit/S et 2.45 Gbit/s) la gigue n'est pas conforme à celle décrite dans la spécification. Cette quantité de gigue importante est due à la présence des modes longitudinaux dans la cavité. Ces modes entrainent un bruit de phase important synonyme de gigue dans le domaine fréquentiel. La latence a fait aussi l'objet d'étude. Le temps de transmission du signal CPRI sur un lien fronthaul employant le self seeded est égal au temps de la propagation du signal optique dans la cavité additionnée à celui de la transmission de la fibre optique. D'après [32] , en termes de latence, la LTE et la LTE-A peuvent être utilisées jusqu'à 30 km de transmission pour 5 km de cavité. Enfin, les effets du système self seeded sur la déviation fréquentielle de la RRH sont étudiés. En effet, la gigue importante présente dans une liaison fronthaul introduite par la nature multimode du self seeded ne permet pas de respecter les recommandations de la 3 GPP en termes de déviation fréquentielle et rend de ce fait l'application du système self seeded sur le lien fronthaul impossible.

2. Solution complète du système CWDM mono fibre pour le fronthaul

Pour implémenter un lien fronthaul à moindre coût, il existe la technique WDM qui permet d'agréger et de désagréger les différents flux de données grâce aux multiplexeurs optiques et passifs. Généralement, la communication bidirectionnelle est assurée par deux fibres optiques. Afin d'utiliser moins de fibre pour la transmission fronthaul, le CWDM mono fibre sera utilisé. En effet, il divise par 2 la quantité de fibre utilisée par

rapport à la configuration CWDM double fibre et parfois pour les mêmes performances. La configuration mono fibre est atteinte grâce aux transmetteurs optiques nommés SFP (Small Form Factor Pluggable). Plusieurs types de SFP ont été évalués. Ces SFP sont :

- SWSF (Single Wavelelngth Single Fiber) : ce type de SFP utilise une longueur d'onde pour l'émission et la réception du signal optique. Il utilise un coupleur 3 dB pour séparer l'émission de la réception et un isolateur pour protéger le laser du signal de réception
- RIO (Reflection Immune Operation) : Ce type de SFP utilise une seule longueur d'onde comme le précédent, mais dispose d'un annulateur d'écho afin d'éliminer les interférences à la réception. Bien sûr, l'avantage de ce dispositif permet d'améliorer les performances de ce SFP par rapport au précédent
- CSC (Cooled Signle Channel) : ce type de SFP divise le canal traditionnel CWDM en deux. Une partie est utilisée pour l'émission et l'autre pour la réception. Ses performances sont approximativement égales à celles des SFP à double fibre.

Pour obtenir une solution mono fibre complète, prête à être intégrée dans le réseau, il faut que cette dernière possède un système de supervision du lien optique de transmission. Notre système de supervision est basé sur la mesure de la puissance du mode transverse magnétique de la lumière rétrodiffusée de Rayleigh. En effet, la puissance de la lumière rétrodiffusée de Rayleigh est prépondérante lorsque qu'il y a une coupure de fibre optique. Notre système est composé d'une diode laser, d'un PBC (Polarization Beam Combiner), d'un puissancemètre optique et d'un miroir rotateur de faraday (FRM : Faraday Rotator Mirror). Le fait de mesurer que la puissance du mode transverse magnétique permet de réduire la puissance retrodiffusée de Rayleigh mesurée.

La diode laser attaque le PBC à travers l'entrée transverse électrique (TE) en envoyant une puissance optique qui va servir de signal probe à une longueur d'onde de 1610 nm. Le PBC est relié au canal qui correspond à la longueur d'onde de 1610 nm du multiplexeur. Du côté du site d'antennes, le FRM est placé à la sortie du canal à 1610 nm du démultiplexeur. Le FRM a pour rôle de renvoyer le signal vers le CO où se trouve la diode laser, le puissancemètre et le PBC. En plus, il applique une rotation de 90° à la polarisation du signal lui arrivant afin de maximiser la puissance du signal de retour à la sortie du mode transverse magnétique du PBC où y est raccordée le puissancemètre. S'il n'y a pas de coupure de fibre et en considérant le canal à 1610 nm, le signal probe de retour est prédominant sur la lumière rétrodiffusée de Rayleigh. La puissance de la lumière rétrodiffusée de Rayleigh est négligeable par rapport au signal probe de retour. Par conséquent, c'est la puissance de la composante transverse magnétique du signal

de retour qui est mesurée. Lorsqu'une coupure est observée, la lumière rétrodiffusée de Rayleigh est prédominant dans la fibre. Afin d'évaluer les performances du système de detection de coupure, le niveau de puissance correspondant au mode transverse magnétique de la lumière rétrodiffusée de Rayleigh doit être dans un premier temps mesuré. La mesure de cette puissance s'obtient en appliquant une coupure droite sur la fibre. Un atténuateur optique variable permet de simuler cette coupure sur le lien optique fronthaul. Lorsque la puissance mesurée correspond à la puissance mesurée lors de la coupure droite décrite précédemment, alors, on peut considérer qu'il y a une coupure de fibre dans la transmission optique. Ce système proposé permet de superviser un lien fronthaul avec un budget optique de 20 dB.

Conclusion générale et perspectives

Durant cette thèse consacrée à l'étude d'un nouveau segment réseau nommé fronthaul, nous avons identifié les questionnements et les enjeux cruciaux concernant la mise en place de l'architecture C-RAN basée sur le média fibre optique. Plusieurs solutions basées sur les techniques de multiplexage en longueur d'onde ont été étudiées. L'une des contraintes et un des enjeux de l'implémentation du fronthaul est la gigue. Ce paramètre essentiel a fait l'objet d'étude approfondie dans le chapitre 2. Plusieurs bancs de mesures ont été mis en place afin de comprendre l'impact et l'influence de la gigue sur un lien fronthaul. Il en résulte que pour des raisons intrinsèques à la nature des transmissions de l'interface fronthaul actuelle, le masque de de tolérance de la gigue sinusoïdale décrit par la spécification CPRI ne peut pas être respecté. Afin de posséder un outil significatif d'évaluation de la gigue sinusoïdale, il est donc nécessaire de réévaluer le masque de tolérance de cette gigue proposée par la spécification CPRI. Cette étude révèle aussi, que les effets de la gigue sinusoïdale sur la précision de la déviation du signal d'horloge du signal fronthaul et de la déviation sur la fréquence porteuse de la RRH ne dépendent pas de la fréquence de la gigue, mais plutôt de l'amplitude de la gigue. Il a été montré de manière théorique et empirique que la PPL de la RRH se comporte comme un filtre passe bas par rapport à la gigue ce qui permet d'inhiber les effets de la fréquence sur un lien fronthaul.

Afin de simplifier la gestion des stocks des SFP colorisés, un système auto accordable en longueur d'onde nommé self-seeded basé sur un RSOA a été étudié. L'étude en laboratoire montre que la spécification en termes de TEB est respectée que pour les transmissions à 1.22 Gbit/s. La gigue mesurée ne respecte pas les valeurs indiquées par le CPRI à cause de l'important bruit de phase présent dans la cavité dû aux modes longitudinaux. La transmission LTE de bout en bout est conforme aux recommandations de la 3GPP. L'étude en grandeur nature, avec une plateforme BBU-RRH nous permet d'affirmer que ce système ne peut pas être utilisé pour implémenter le fronthaul, car elle provoque des déviations fréquentielles importantes qui ne correspondent pas aux recommandations de la 3 GPP ou même parfois une rupture de la communication entre BBU et RRH.

La dernière partie de cette thèse est consacrée à solution mono fibre complète. Cette solution est utilisée pour pourvoir réduire le nombre de fibres implémentées par rapport à la solution CWDM double fibre. La solution complète comprend des transmissions fronthaul sur une seule fibre et un dispositif de supervision de la fibre optique de transmission. Les liens fronthaul sont implémentés grâce aux transmetteurs optiques

appelés SFP. Le SFP SWSF utilise une seule longueur d'onde pour la communication bidirectionnelle, le SFP RIO possède un annulateur d'écho pour éliminer les interférences du côté réception, ou le SFP CSC qui divise les canaux CWDM en deux où chacune des parties est utilisée soit pour l'émission, soit pour la réception. Le système de supervision basé sur la réduction de la mesure de la puissance de la lumière rétrodiffusée de Rayleigh constitue la partie innovante de ce dispositif mono fibre. Ce dispositif de supervision est composé d'un PBC pour réduire la puissance de lumière rétrodiffusée de Rayleigh, d'un FRM et d'un puissance mètre. La réduction de cette puissance permet de superviser une liaison fronthaul avec un budget optique de 20 dB.

Après des études menées sur le fronthaul, et après avoir identifiés les enjeux futurs, nous orientons dans un premier temps, les travaux à venir vers le X-haul. En effet, le X-haul est la capacité du réseau à transporter de manière transparente tous les protocoles qui définissent le fronthaul (CPRI, OBSAI, ORI). Afin de réaliser un tel réseau, les différents protocoles devront être encapsulés dans des trames Ethernet. Ce type d'encapsulation impose l'utilisation de la transmission en mode paquet. Il serait donc intéressant d'étudier l'impact de la gigue paquet de l'interface X-haul sur les performances de la qualité radio. Dans un second temps et à plus long terme, des travaux pourront être menés sur la nouvelle génération de fronthaul nommée NGFI (Next Generation Fronthaul interface). En effet, le NGFI est une nouvelle Génération de l'interface fronthaul qui est en cours de réflexion et qui permettra l'implémentation des futures normes telle que la 5G. Elle consiste à déplacer certaines fonctions de la BBU vers la RRH. La communication entre la BBU et la RRH se fera via le protocole Ethernet ce qui entrainera l'utilisation du mode paquet sur les nouveaux liens fronthaul. Par conséquent l'impact de la gigue paquet du NGFI peut aussi être étudié sur les performances radio.

Contents

List of Figures

List of Tables

Glossary

A

ADSL Asymmetric Digital Subscriber Lines.

APC Angle Physical Contact.

ARQ Automatic Repeat Request.

ASE Amplified Spontaneous Emission.

ATM Asynchronus Transfer Mode.

AWG Arrayed Waveguide Grating.

AxC antenna-carrier Container.

B

B-PON Broadband Passive Optical Network.

BBU Base Band Unit.

BER Bit Error Rate.

BF Basic Frame.

BFN Frame Number.

BS Base Station.

BSC Base Station Controller.

BSS Base Station Subsystem.

BTS Base Transceiver Station.

BUJ Bounded Uncorrelated Jitter.

C

C-RAN Centralized or cloud Radio Access Network.

CA Carrier Aggregation.

CAPEX Capital Expenditure.

CD chromatic dispersion.

CDR Clock Data Recovery.

CN Core Network.

CO Central Office.

CoMP Coordinated MultiPoint.

CPRI Common Public Radio Interface.

CSC Cooled Single Channel.

CW Control Word.

CWDM Coarse Wavelength Division Multiplexing.

D

D-RoF Digitized-Radio over Fiber.

DCD Duty Cycle Distortion jitter.

DDJ Data Dependent Jitter.

DDMI Digital Diagnostics Monitoring Interface.

DeMUX De-multiplexer.

DJ Deterministic Jitter.

DoP Degree of Polarization.

DP Demarcation Point.

DSLAM Digital Subscriber Lines Access Multiplexer.

DSO Digital Storage Oscilloscope.

DU Digital Unit.

DWDM Dense Wavelength Division Multiplexing.

E

E-UTRAN Evolved-UTRAN.

ED Error Detector.

EDGE Enhanced Data GSM Evolution.

eICIC enhanced Inter-Cell Interference Coordination.

EMI electromagnetic interference.

eNB evolved-Node B.

EPON Ethernet Passive Optical Network.

ETSI European Telecommunication Standards Institute.

EVM Error Vector Magnitude.

F

FEC Forward Error Corrector.

FR Faraday Rotator.

FRM Faraday Rotator Mirror.

FSAN Full Service Access Network.

FTTA Fiber To The Antenna.

FTTC Fiber To The Curb.

FTTH Fiber To The Home.

FTTN Fiber To The Node.

FTTx Fiber To The x.

G

G-PON Gigabit capable Passive Optical Network.

GEM GPON Encapsulation Method.

GPRS General Packet Radio Service.

GPS Global Positioning System.

GSM Global System Mobile.

H

HARQ Hybrid Automatic Repeat Request.

HDLC High Level Data Link Control.

HDSL High Digital Subscriber Lines.

HF Hyper Frame.

HSPA High Speed Packet Access.

I

IEEE Institute of Electrical and Electronic Engineers.

ISI Inter-Symbol Interference jitter.

ITU International Telecommunication Union.

L

Lo Local oscillator.

LTE Long Term Evolution.

LTE-A Long Term Evolution Advanced.

M

MIMO Multi Input Multi Ouput.

MUXs Multiplexers.

N

NG-PON2 Next Generation Passive Optical Network 2.

NGFI New Generation Fronthaul Interface.

NRZ Non Return to Zero.

NSS Network Switching System.

O

OAM Operation Administration and Maintenance.

OB Optical Budget.

OBSAI Open Base Station Architecture Initiative.

ODN Optical Distribution Network.

ODU Optical Data Unit.

ODU2r overlocked Optical channel Data Unit 2.

OLT Optical Line Terminal.

ONU Optical Network Unit.

OPEX Operational Expenditure.

OPU Optical Payload Unit.

ORI Open Radio equipment Interface.

OTN Optical Transport Network.

OTU Optical Transport Unit.

OTU2r overlocked Optical channel Transport Unit 2.

P

PBC Polarization Beam Combiner.

PCS Phase Changing Speed.

PDV Packet Delay variation.

PED Phase Error Detector.

PJ Periodic Jitter.

PLL Phase Locked Loop.

PMD Polarization Mode Dispersion.

PON Passive Optical Network.

PtMP point to multipoint.

PtP point to point.

PtP WDM Point to Point Wavelength Division Multiplexing.

Q

QAM Quadrature Amplitude Modulation.

QPSK Quadrature Phase Shift Keying.

R

RAN Radio Access Network.

RAT Radio Access Technologies.

RAU Radio Aggregation Unit.

RB Rayleigh Backscattering.

RCC Radio Cloud Center.

RE Radio Equipment.

REC Radio Equipment Control.

RIN Relative Intensity Noise.

RIO Reflection Immune Operation.

RJ Random Jitter.

RM Radio Mobile.

RMS Root Mean Square.

RMSD Root Mean Square Deviation.

RNC Radio Network Controller.

RoF Analog Radio over Fiber.

RRH Remote Radio Head.

RRS Radio Remote System.

RRU Remote Radio Unit.

RSOA Reflective semiconductor Optical Amplifier.

RU Radio Unit.

S

SAP Service Access Point.

SFP Small form Factor Pluggable.

SJ Sinusoidal jitter.

SLAs Service Level Agreements.

SNR Signal to Noise Ratio.

SoP State of Polarization.

SWSF Single Wavelength Single Fiber.

T

TDM Time Division Multiplexing.

TEC thermo-electric cooler.

TJ Total Jitter.

TWDM Time and Wavelength Division Multiplexed.

U

UI Unit Interval.

UTMS Universal Mobile Telecommunication System.

UTRAN UMTS Terrestrial RAN.

V

VCO Voltage Controlled Oscillator.

VDSL Very high Digital Subscriber Lines.

VOA Variable Optical Attenuation.

W

WDM Wavelength Division Multiplexing.

WDM-PON Wavelength Division Multiplexing - Passive Optical Network.

WFM Wireless Fronthaul Module.

X

XAUI 10 Gigabit Attachment Unit Interface.

xDSL xDigital Subscriber Lines.

XG E-PON 10 Giga Ethernet Passive Optical Network.

XG-PON 10 Gigabit capable Passive Optical Network.

XGEM XGPON Encapsulation Method.

General introduction

1. Context

In Europe, the competition between the mobile operators is so strong that the profitability of the mobile network has decreased. The cost to implement, to operate and to upgrade the mobile network is increasing while the revenues generated by the latter are not sufficient. Therefore, the operators should find the way to reduce the Capital Expenditure (CAPEX) and the Operational Expenditure (OPEX).

The mobile network constituted by the Radio Access Network (RAN) and the Core Network (CN). The backhaul transport based on the access network, permits to link the RAN and the CN [1]. The deployment of RAN is more expensive than the CN. Several issues are met during the deployment and the operation of the RAN. Indeed, one of several problems is the rent of the platform to install the antenna sites. Generally, the rent of these platforms is expensive (31% of OPEX per year and per cell site [2]) and the mobile operators have some difficulties to access to these platforms making the interventions of maintenance and upgrade infrastructure difficult on the cell site. Another problem of traditional RAN is that the antenna sites are far from the entities which control them. This geographical configuration affects the performance or the radio interface and do not promote the deployment enhanced technologies of radio mobile like Coordinated MultiPoint (CoMP). In addition, the development of small cells increases the risk of the interference in the air interface and constraints the traditional RAN to evolve and be more scalable. In summary, the traditional RAN has become expensive for the mobile operator thus making it difficult the implementation of enhanced radio technics or the future standard of radio mobile. In order to keep competitive, the operators have begun to think about a novel RAN architecture.

The new architecture should allow:

- Reducing CAPEX and OPEX
- Reducing the power consumption (the energy saving is estimated 68% relative to the traditional RAN [3])
- Implementing high spectral efficiency for signal transport
- Supporting the present and future radio mobile standards
- Providing a platform for additional revenue generating services.

The Centralized [2] or Cloud [3] Radio Access Network (C-RAN) is the innovative architecture proposed to meet the requirements listed above. The C-RAN architecture supports all the Radio Access Technologies (RAT) as 2G, 3G, 4G but in the following of this work we focus only on the 4G technology. The traditional antenna site consists of the Remote Radio Head (RRH) which performs the radio processing, and the Base Band Unit (BBU) which carries out the digital processing [4] [5]. The principle of C-RAN consists to move the BBU from antenna site towards the local secured belonging to an operator called Central Office (CO). The move of BBU from antenna site to CO leads to the appearance of a new network segment called *"fronthaul"*. The fronthaul link has some requirements which impose the optical fiber as the best candidate to support the transmission of data.

The general objective of this thesis is the study of different solutions available or potential candidates allowing the implementation of fronthaul segment based on the optical fiber.

2. Expectations of this thesis

The new fronthaul segment constitutes a big market opportunity. Its deployment has been ongoing in Asia and has been announced in Europe. For this reason, the telecoms manufacturers are interested in and propose several solutions to support the fronthaul link. To permit ORANGE to understand the strengths and the weakness of different solutions proposed by the different vendors, several studies have been performed on different prototypes aiming had checking the requirements in order to confirm or invalidate these fronthaul solutions. This document does not describe all tested solutions but only the operation principle of those considered as relevant by ORANGE.

The transport of wireless signal from the antenna site to the CO requires a specific technique. Analog Radio over Fiber (RoF) is one of possible candidates for wireless signal distribution over optical fiber transmission [6]. Although this technology is considered as a potential solution, it presents low performances for the transmission of broadband wireless signals on a long distance. To face to these poor results, the wireless signal is digitized hence the appearance of Digitized-Radio over Fiber (D-RoF) technology. Therefore, the D-RoF technology is used to transmit the data on the fronthaul interface and per some specifications. Generally, these specifications specify the use of 15 bits as resolution bandwidth.

[2] Centralized: means that the BBUs are stacked in the CO
[3] Cloud: means that the resources of BBU are pooled and shared between several antenna sites

This high-resolution bandwidth ensures a high performance of the radio signal over optical fiber transmission but entails a poor spectral efficiency on the fronthaul link. One consequence of this poor spectral efficiency is a high data rate on the fronthaul link. The high data rate of fronthaul makes more sensible the data to the jitter phenomenon. The jitter is a physical phenomenon which affects the digitized data. It causes the errors and the loss of the clock on the transmission link. One part of this thesis is to analyze this phenomenon on the fronthaul link. Test setups to study the impacts of jitter on the frontaul link have been proposed.

3. Contents of the manuscript

The objective to this thesis is to provide tools to assess different fronthaul solutions based on requirements for possible deployment of Centralized or cloud Radio Access Network (C-RAN) architecture in the ORANGE network. It is a thesis for which the studies are oriented to experimental works. The manuscript is made up of an introduction, three chapters, and a conclusion. The three chapters are:

- **Chapter 1: State of the Art**
  In this chapter, a brief description of the evolution of radio mobile, fixed network and backhaul network is presented. The goal is to have a global vision on the context in which the novel architecture C-RAN has been proposed. Then, the C-RAN architecture is depicted. The different steps and the different requirements of this architecture are described. Then, the operation principles of some assessed solutions for C-RAN are presented. Finally, the future fronthaul generation to allow the deployment of future standard of radio mobile is also described. This state of the art permits to better understand the context and the challenge of this thesis.

- **Chapter 2: Jitter parameters on a fronthaul link**
  The objective of this chapter is to better understand the impact of the jitter on a fronthaul link. At first, the jitter and its effects are defined. Then measuring setups are proposed to measure and to study the effects of jitter on a fronthaul link and the jitter impact on the radio frequency deviation of RRHs is studied. According to the commercial RRH used, the response to this frequency deviation is not the same. A theoretical study is performed on a basic electronic system of RRH. The goal of this study is to provide a reference on the jitter impact on the radio frequency deviation. Finally, the impact of jitter on the frequency deviation of a commercial RRH is deeply analyzed.

- **Chapter 3: Experimental solution for a fronthaul link**
  In this chapter, some experimental solutions for the fronthaul link are presented. A low cost and colorless solution is described. Then a single fiber solution implementing a monitoring scheme is introduced.

Then after a synthesis of the previously described chapters, conclusions are drawn. It summarizes the results of different experiences performed during this thesis and presents the perspectives for the works ahead

Chapitre 1 :

State of the art

1.1 Radio mobile technologies

The main goal of Radio Mobile (RM) is to permit to everyone to communicate everywhere and whenever. To achieve this objective, a quick and great evolution of RM technology has been performed during the last thirty years. Currently, four generations of RM technologies exist and the standardization of the fifth generation is ongoing. Generally, the Radio Mobile (RM) architecture is divided in two parts:

- The Radio Access Network (RAN)
- The backhaul and Core Network (CN).

Relative to the subject we deal with, only the RAN and backhaul will be presented. The RAN is constituted of:

- Base Station (BS): It is the equipment that manages the Radio link between the end users and the network
- BS controller: It is the entity that controls and manages the BS.

The main goal for successive generations of the RM technology, the main issue has been the increasing the throughput in the air interface. Nowadays, more people use the data through the RAN. Thus, the volume of the data has significantly grown. A linear increase of the number of Base Stations (BS) (antenna cell sites) to solve the increasing data volume is not suitable. Indeed, to face to this problem, a new RAN architecture must be thought. In order to understand the different challenges of this new architecture, the evolution of the RAN is presented in this section. For the 2G, 3G, and 4G RAN technologies, a general description and the evolution of each technology are given. A brief description of the future 5G is also provided.

1.1.1 2G technology

2G or the second generation of mobile systems is the first digital RAN. Several standards exist for 2G among them the Global System Mobile (GSM) that is mainly used in Europe [7] . GSM is composed of the Base Station Subsystem (BSS) and the Network Switching System (NSS) [8]. The BSS is a part of GSM that assure the communication between the user equipment and the core network (NSS) [8]. The BSS is constituted of the Base Transceiver Station (BTS) and the Base Station Controller (BSC). The figure 1.1 describes the general architecture of GSM.

The BTSs are connected to the BSC via the interface A bis (backhaul network) and the BSCs communicate with the core network through the interface A. The BTSs contain

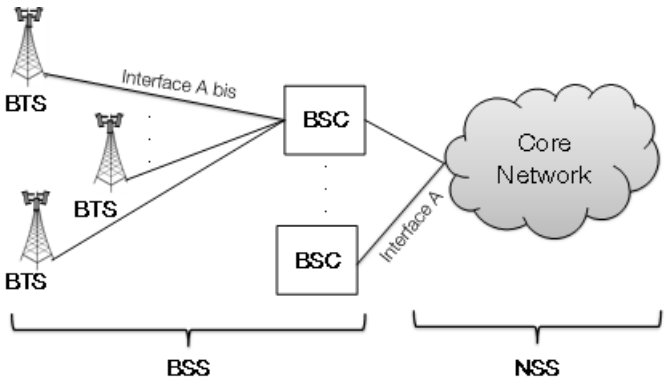

Figure 1.1: Basic architecture for GSM

of radio Transmitter/Receiver Modules (TRX) which perform the signal processing (digital and analogue signal processing). The BSC switches the traffic from the core network to the corresponding A-bis interface. Furthermore, it aggregates this traffic from BTS to the core network.

GSM has been designed for voice communication. The air transmission rate of GSM is 24.7 kbit/s. The GSM has two major evolutions:

- The General Packet Radio Service (GPRS) achieves a theoretical maximum rate of 171 kbit/s
- The Enhanced Data GSM Evolution (EDGE) achieves a theoretical maximum rate of 473.6kbit/s.

The backhaul segment uses copper interface based on E1 (2Mbit/s) over xDigital Subscriber Lines (xDSL). Nevertheless, optical access and microwave technologies are not excluded to support the 2G backhaul. The source of synchronisation for BTS is also provided by the backhaul.

1.1.2 3G technology

3G is the third generation of Radio Mobile. As 2G, several standards based on different technologies exist in 3G. The common requirement imposed to the data rate of these standards must be at least of 2 Mbit/s for indoor, 384kbits/s for outdoor and 144 kbit/s for vehicular environment. In Europe, the standard called Universal Mobile Telecommunication System (UTMS) [9] [10] is the most used. UMTS system is also divided in two parts which are for one part the backhaul and Core Network (CN) and for a second part the RAN called UMTS Terrestrial RAN (UTRAN). UTRAN consists of:

- A node B: represents the base station
- A Radio Network Controller (RNC): manages the nodeB elements.

The figure 1.2 depicts the basic architectures of UMTS.

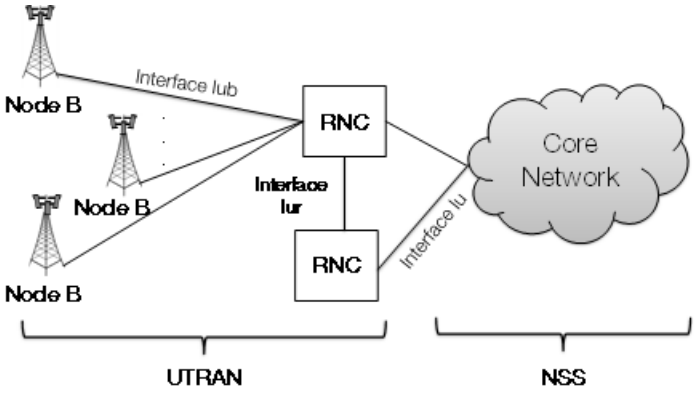

Figure 1.2: Basic architecture for UMTS

A set of node B elements controlled by a RNC is called Radio Network Systems (RNS). Generally, the nodeB is separated in two entities that are:

- Radio Unit (RU): performs the radio processing
- Digital Unit (DU): performs the digital processing.

The main evolution of UMTS is the High Speed Packet Access (HSPA) standard described in the 3 GPP Releases 5 [11], 6 [12] and 7 [13]. The HSPA permits to achieve a theoretical rate of 14.4 Mbit/s on downlink and 5.8 Mbit/s on uplink. The HSPA+ can reach 42 Mbit/s on downlink and 11.5 Mbit/s on uplink. Notice that optical fiber and microwave are considered as the preferred medium for 3G backhaul.

1.1.3 4G technology

The Long Term Evolution (LTE) is the standard of 4G technology introduced by the 3GPP Release 8 [14]. The theoretical rate is 100 Mbit/s on downlink and 50 Mbit/s on uplink, LTE RAN is named Evolved-UTRAN (E-UTRAN) [15]. E-UTRAN introduced a new RAN concept completely different of the previous RAN architectures. It consists of a single element called evolved-Node B (eNB) which is directly connected to the backhaul and the core network (EPC: evolved Packet Core) through the S1 interface [16]. The eNBs are able to manage themselves thanks to the X2 interface. The figure 1.3 illustrates

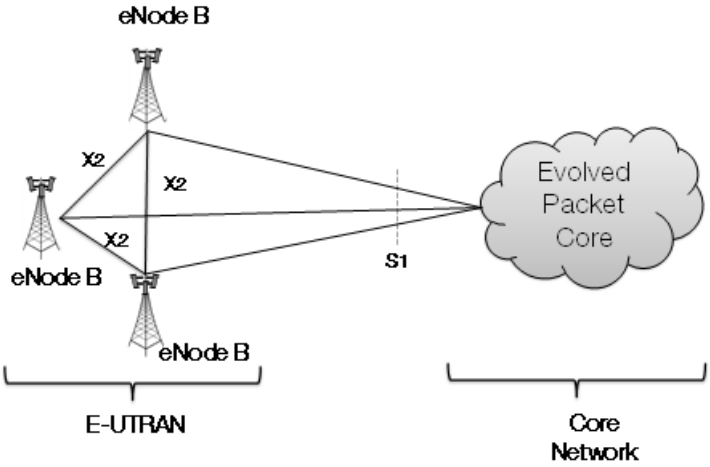

Figure 1.3: Basic architecture for LTE

the basic architecture of LTE.

Like the Node B, the eNB is also generally divided in two entities that are the Radio Unit (RU) and the Digital Unit (DU). These entities can have several names like Remote Radio Head (RRH) for the RU and Base Band Unit (BBU) for the DU. At the beginning of LTE, RU and DU tasks were managed by the same device. Then the separation of these tasks in two entities has been performed in order to optimize the space and reduce the losses between the antenna and the equipment that processes the radio signal. The main enhancement of LTE is the Long Term Evolution Advanced (LTE-A) [17] [18]. In order to increase his throughput, LTE-A develops several technics focused on the physical layer, such as Carrier Aggregation (CA) [19], Coordinated MultiPoint (CoMP) [20] and enhanced Inter-Cell Interference Coordination (eICIC) [21]. Its target is to get 1Gbit/s on downlink and 0.5Gbit/s on uplink. The preferred medium for backhaul is optical fiber but microwave could support such backhauling throughput.

1.1.4 5G technology

5G or fifth generation of mobile networks is the future generation of RM. It is ongoing standardization through the 5GPP. Some 5G expectations and features are defined [22] and are listed below:

- Capacity and throughput improvement high data rate (approximately 10 Gbit/s as cell data rate)
- Save up to 90% of the energy
- Network densification

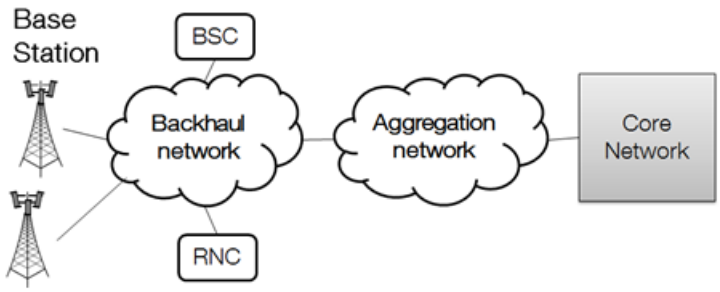

Figure 1.4: Backhaul network

- Reduce the latency
- Autonomous applications and network management, allowing Internet of Things.

The beginning of the commercial deployment of the future 5G system is expected in years 2020.

In order to establish the connectivity between the transmitted stations (BTS, NodeB) and the radio controllers (BSC, RNC) for 2G and 3G or between the eNodeB and the core network, the fixed infrastructures (copper, microwave, fiber) are generally used. In this way, a network segment appears between these entities and this segment is called backhaul. The following section describes some infrastructures used in the mobile backhaul.

1.2 Mobile backhaul

The communication between the RAN and core elements is essentially based on the backhaul network. The backhaul network can be supported by the fixed network and by the wireless network. Regarding the bandwidth necessary to the data transmission different physical mediums like cooper, microwave or fiber are used. The figure 1.4 shows the mobile backhaul in the mobile network architecture.

The backhaul network is based on two network segments: the access and the aggregation networks. In the following part, only the access architectures based on the wired technologies are presented.

1.2.1 Access network architecture based on the copper

1.2.1.1 xDigital Subscriber Lines (xDSL)

The xDSL architecture consists of the Digital Subscriber Lines Access Multiplexer (DSLAM) which is connected to the customers with a twisted-pair copper and the network

operator by the optical fiber [23]. The copper presents about 1 MHz of bandwidth of which 4 kHz is used by the voice in the telephony grid. The xDSL technologies permit to use the remaining part of the bandwidth to transmit the data and synchronization. The figure 1.5 draws the architecture of xDSL technologies.

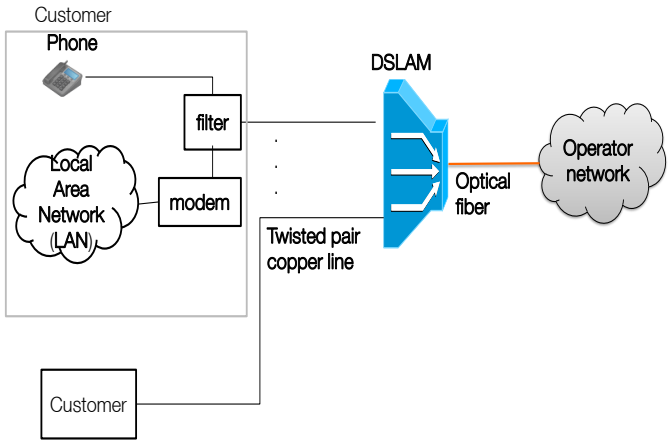

Figure 1.5: xDSL technologies architecture

There are two categories of xDSL technologies following the transmission mode:

- Asymmetric transmission mode: The bit rate between uplink and downlink are different. Generally, the bit rate of downlink is higher than the uplink
- Symmetric transmission mode: the uplink and downlink bit rate is the same. Following the standardization, one or several twisted copper lines can be used.

Concerning, the copper infrastructure, the Asymmetric Digital Subscriber Lines (ADSL) and the High Digital Subscriber Lines (HDSL) are the most used in fixed access network by the different operators to provide different services to the customers. The Very high Digital Subscriber Lines (VDSL) technology is used to complete the Fiber To The x (FTTx) infrastructures. In 2011 the ITU has started to develop a new standardization through the G. Fast project (Gbit/s working in duplex mode). The idea is to realize a hybrid architecture mixing fiber and copper that should provide ultra-high speed over the last meters (20 m – 250m) before reaching the customers, reusing the twisted pair copper lines.

The table 1.1 describes the different xDSL technologies standards. It gives the features like: the bit rate, the maximum distance between the customers and the DSLAM, the transmission mode and number of the twisted pair cooper lines used.

xDSL Technologies	Rate (Mbit/s)	Operating channel	Maximum Distance (km)	Number of twisted pair copper	Transmission mode
High bit-rate DSL	1.544 up to 2.048	Full-duplex	3.6	2 or 3	Symmetric
High bit-rate DSL 2	2	Full-duplex	2.5	1	
Symmetric DSL	0.128 up to 2	Full-duplex	3.6	1	
Symmetric High DSL	192 up to 4.6	Full-duplex	5	1 or 2	
Asymmetric DSL	0.128 - 8	Downlink	5.4	1	Asymmetric
	0.01 - 0.64	Uplink			
Asymmetric DSL 2	0.128 - 12	Downlink			
	0.016 - 0.64	Uplink			
Asymmetric DSL 2+	0.128 - 24	Downlink			
	0.016 - 1	Uplink			
Very high DSL	15 - 53	Downlink	1.3		
	1.54 - 2.3	Uplink			
Very high DSL 2	50 -100	Downlink			
	15 - 32	Uplink			
Rate Adaptive DSL	0.6 - 7	Downlink	5.4		
	0.128 - 1.024	Uplink			

Table 1.1: The features of xDSL technologies

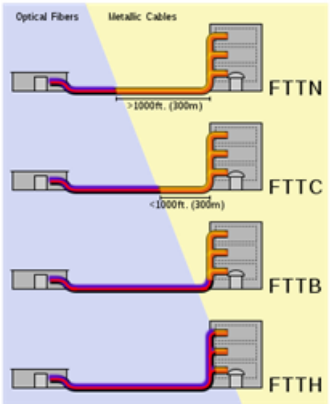

Figure 1.6: Representation of differentnotions of FTTx
[24]

1.2.2 Optical Access Network

Nowadays, with the development of different applications (video streaming, social networks) the customers require more bandwidth and more date rate. To face this request; the limits of xDSL technologies are achieved for fixed customers and also for mobile backhaul. In addition, the network of copper lines is old and gives rise to more OPEX. The optical fiber is presented as the best candidate to overcome the limits of xDSL technologies. In order to rise up the bit rate provided to the customers (here, for backhaul and antenna cell site), the fiber must be brought nearest to the client. The set of the technics necessary to bring the fiber near to the customers is designated by the term: Fiber To The x (FTTx):

- The Fiber To The Node (FTTN): fiber is terminated in the street cabinet
- The Fiber To The Curb (FTTC): fiber is terminated in the cabinet which is close to the premises of the customers
- The Fiber To The Home (FTTH): the fiber is provided until the home of the user
- The Fiber To The Antenna (FTTA): the fiber reaches the antenna cell site.

The figure 1.6 represents the different notion of FTTx and the figure 1.7 describes the basic configuration of FTTA.

In the access network, the roll out of the fiber is based on the Optical Distribution Network (ODN). At the end parts of this ODN, it exists two systems of transmission:

- The active system: This system uses the physical topology point to point (PtP). The transmitter and the receiver are linked by either a dedicated pair of optical fiber or a single fiber using two wavelengths. In case of massive deployment, this

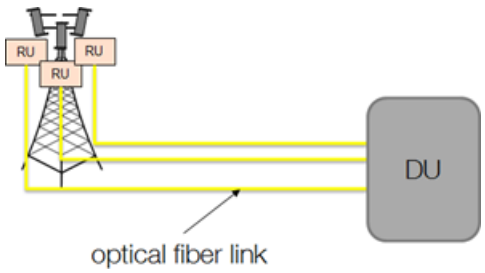

Figure 1.7: Basic FTTA

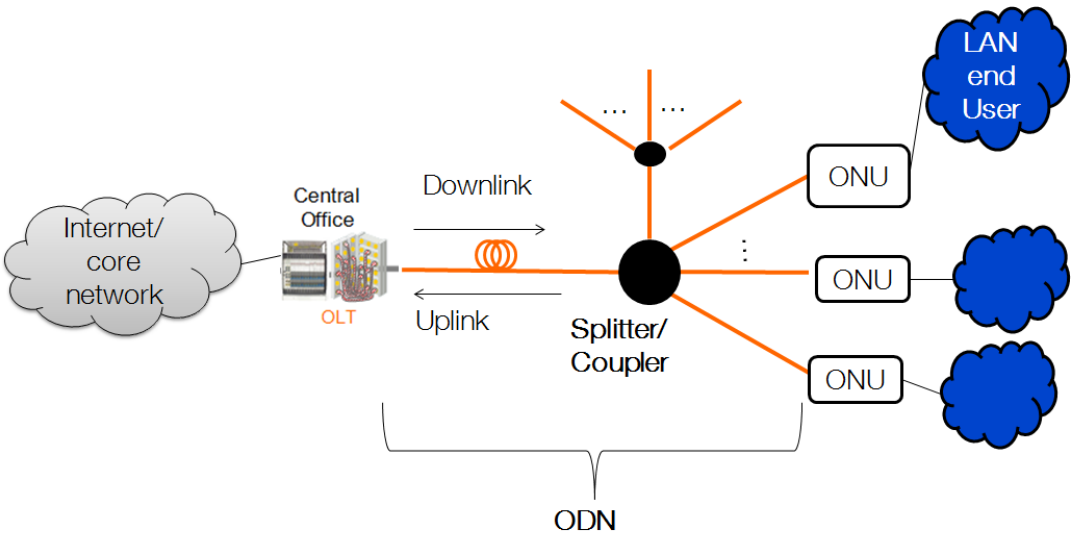

Figure 1.8: General architecture of PON

active system is very expensive due to the high number of transceivers and optical fibers that are required

- The Passive system: This system has a tree topology. In the access network, the passive system runs in the Passive Optical Network (PON). In France, ORANGE uses the Gbit/s capable PON for the deployment of FTTH.

The PON is a point to multipoint (PtMP) architecture which consists of the Optical Line Terminal (OLT) localized in the Central Office (CO), the optical power splitter situated in the cabinet and the Optical Network Unit (ONU) or Optical Network Terminal (ONT) which is installed to the end user [25] [26]. The OLT provides an interface between the optical network access and service provider. The ONU provides the services to end users. The figure 1.8 represents the basic architecture of PON.

Generally, PON uses the Time Division Multiplexing (TDM) to share the resources on the uplink and the broadcast on the downlink. Different standardization entities working on PON technology have already defined several generations [27]. The Broadband Passive

	B-PON	G-PON	XG-PON1	EPON	XG-EPON
Standards	ITU-T G983	ITU-T G984	ITU-T G987 ITU-T G9807	IEEE802.3ah	IEEE802.3av
Bitrate (Gbit/s)	Downlink: 0.155/0.622 /1.244 Uplink: 0.155/0.622	Downlink: 1.244/2.488 Uplink: 0.155/0.622 /1.244	Downlink: 10 Uplink: 10 and 2.5	Symmetric 1.25	Downlink: 10 Uplink: 1 (asymmetric) 10 (Symmetric)
Wavelength (nm)	Downlink: 1490 Uplink: 1310	Downlink: 1490 Uplink: 1310	Downlink: 1575-1580 Uplink: 10 and 2.5	1260-1360	Downlink: 10 Uplink: 1 (asymmetric) 10 (Symmetric)
Optical budget (dB)	15/20/25	15/20/25/28	29-31	21-26	20-33
Traffic mode	ATM	GEM (ATM, TDM, Ethernet)	XGEM	Ethernet	Ethernet
Distance (km)	20	60	40	20	20
Distance (km)	256	256	128	16 or more	2016 or more 64

Table 1.2: The standards of PON

Optical Network (B-PON), Gigabit capable Passive Optical Network (G-PON), 10 Gigabit capable Passive Optical Network (XG-PON) and the Next Generation Passive Optical Network 2 (NG-PON2) have been defined by the International Telecommunication Union (ITU) in coordination with the Full Service Access Network (FSAN). Furthermore, the Ethernet Passive Optical Network (EPON) and the 10 Giga Ethernet Passive Optical Network (XG E-PON) have been defined by the Institute of Electrical and Electronic Engineers (IEEE). The main difference between these two standardizations (ITU and IEEE) is the protocol used to provide some services. Indeed, the standards defined by the IUT and FSAN use in the preliminary system the Asynchronus Transfer Mode (ATM) for the voice, the Ethernet for the data. Now Ethernet is the common protocol supported at the end faces of ITU PON systems. ITU systems are more oriented than IEEE for network operator operation due to the support of interoperability, operation and management channel, and class of service definition. The standards defined by the IEEE use the Ethernet for a market oriented of data center and campus. The table 1.2 summarizes the characteristics of the different standardization.

The wavelength at 1550 nm is used for video service in coexistence with all PON

Transmission systems	categories	Downlink Rate(Gbit/s)	Downlink Rate(Gbit/s)	Wavelengths (nm)
TWDM	Basic rate	9.95	2.48	Downlink: 1596-1603 Uplink: 1524-1544
	Rate option 1	9.95	9.95	
	Rate option 2	2.48	2.48	
PtP WDM	Class 1	1.22 - 1.25	1.22 - 1.25	Downlink/uplink: 1524-1625
	Class 2	2.45 – 2.66	2.45 – 2.66	
	Class 3	9.8 – 11.09	9.8 – 11.09	
	Class 4	Still under study		

Table 1.3: The mains characteristics of NG-PON2 standard

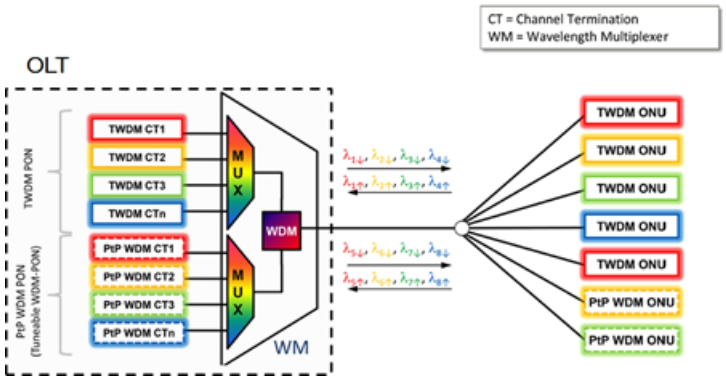

Figure 1.9: General architecture for NG-PON2

technologies.

A new standard of PON designated by the term New Generation PON2(NG-PON2) is ongoing to standardization [28]. Furthermore, NG-PON2 proposes the Time and Wavelength Division Multiplexed (TWDM) PON and the Point to Point Wavelength Division Multiplexing (PtP WDM) as two transmission flavors systems (figure 1.9). This system should be able to reach 40 Gbit/s [29]. The main characteristics of NG-PON2 are listed in the table 1.3 [30]:

The data rate of the backhaul depends on the RAN technologies. For example, for LTE, the data rate of the backhaul (S1 and X2 interfaces described in figure 1.3) changes with the Multi Input Multi Ouput (MIMO) configurations and the bandwidth. The data rate could achieve up to 3 Gbit/s on S1 interface for 8 X8 MIMO antennas. The following figures give the data rate on the S1 interface and the X2 interface for the LTE-A [31] .

In terms of bitrate, some PON standards are not suitable to support LTE backhaul. The following table summarizes the different PON standards that can support 3G and 4G RAN technologies. Depending on the technologies, the backhaul protocol is different. Indeed, for the 2G RAN, the TDM mode is used. For the 3G, the ATM and Ethernet are

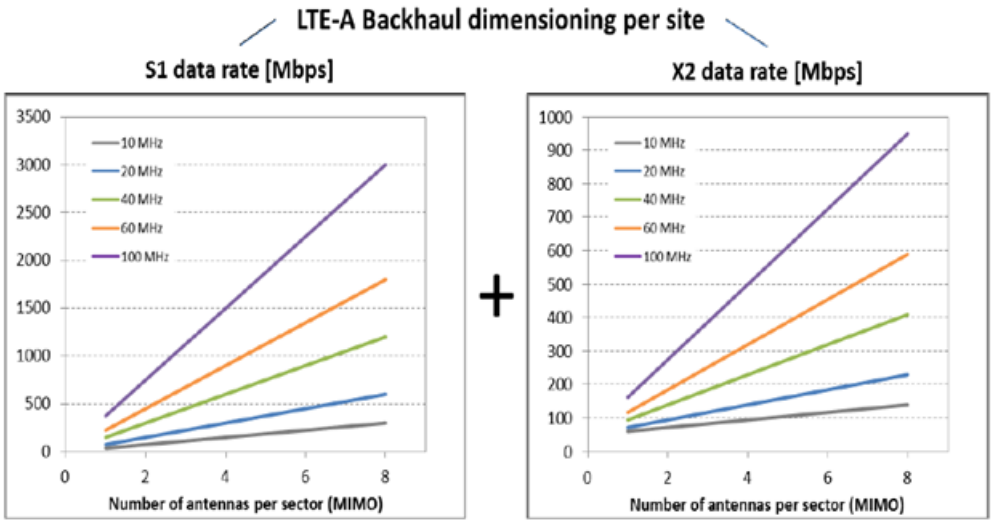

Figure 1.10: Data rate for LTE-A backhaul

.

RAN technology	Backhaul bitrate for one cell	PON standards compatibility
3G HSPA	20 Mbit/s	GPON, EPON, XG-PON1
LTE	200 to 800 Mbit/s	XG-PON1
LTE-A	200 Mbit/s to 3 Gbit/s	XG-PON working in symmetrical line rate mode

Table 1.4: Backhaul supported by the PON standards in terms of data rate

the preferred protocols. For LTE, the backhaul is supported by an IP/Ethernet interface. The overall tendency is going toward full IP for all technologies. The synchronization is also provided by the PON systems and the OLT will act as the unique source of synchronization for PON.

1.3 Mobile Fronthaul

One part of the deployment of the present RAN consists to lease some antenna cell sites and to install there the base stations. The management and the maintenance of the different base stations in these leased sites are not easy for the mobile operator because some of them are not available every time. Furthermore, the base stations in the antenna site consume a lot of power energy and footprint. In addition, the actual RAN architecture makes difficult some RAN applications like the CoMP or the roll out of the future RAN standards like 5G. Indeed, the delay of 5 ms on the X2 interface introduced by the CoMP and the goal to reduce the latency in the 5G will be difficult to reach with the actual configuration of the RAN architecture. Additionally, to the delay issue, for LTE, the

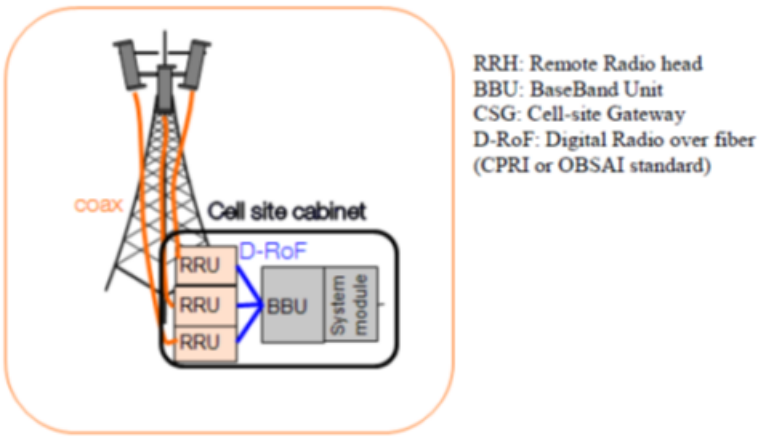

Figure 1.11: Step 1 of C-RAN: traditional base station

traffic on the X2 and S1 interfaces is not natively secured. Indeed, the communication between eNB and the core network or between eNB is not encrypted. It is necessary to secure the user data plane and the control plane. To address this issue two options are possible. First of all, IPsec can be used to secure the communication on the X2 and S1 interfaces. The second option is to place the eNB in a safe operator site (like central office). In order to face the limits of this present RAN architecture it is essential to think to a new RAN architecture concept. This new RAN architecture is called Centralized or Cloud RAN (C-RAN) and is presented in the next section.

1.3.1 Descriptions of C-RAN

The C-RAN is lined to an innovative architecture solution. It is described in 4 steps detailed below [32].

The step 1 concerns the traditional generation of macro base stations. The radio-frequency transmit and receive electronics (RRU) are located at the base of antenna tower or in the building. Large diameter coaxial feeder cables are used to connect the electronics and the antennas [32]. The figure 1.11 depicts the traditional generation of macro base station. The step 2 also called *"distributed base station"* [33] consists to place the RRH close to the antenna thus allowing a gain of 3 dB of losses (replacement of the long coaxial feeders by a short one from RRH to antennas). This has a beneficial effect also in terms of energy saving [34]. The BBU stays in the cabinet and is connected to the CO via the optical fiber as shown in the figure below. The RRH and the BBU are also connected by the optical fiber and use the Digital Radio over Fiber (D-RoF) technology [35] [36] which is defined by the standard interfaces such as Common Public

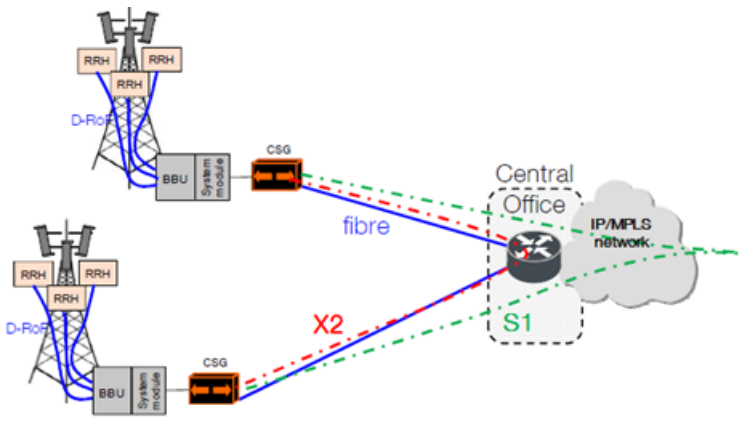

Figure 1.12: Step 2 of C-RAN: Distributed base station

Radio Interface (CPRI) [37], Open Base Station Architecture Initiative (OBSAI) [38] or Open Radio equipment Interface (ORI) [39] . The Cell Site Gateway encapsulates the data for antenna cell site in order to transport them on the backhaul network. All of this interfaces transport three types of information:

- The digitalized radio signal
- The management channel
- The synchronization.

Concerning the last bullet about synchronization, for these interfaces, the line rate acts as the clock source for RRH. That is the main reason why in this manuscript we will take attention to the jitter and wander of the transport of fronthaul interfaces.
In the step 3, the BBU is located remotely from the RRH, outside the cell site, in the CO. This configuration is called BBU centralization or BBU hosteling with stacking. BBUs of different base stations are co-located in the same CO. This central office is a restricted site which reduces the security risks that are present in the unsecured cell site. In this case, it is possible to reduce the delay of X2 interface because the BBU can be directly connected between them. The figure 1.13 depicts the step 3 of C-RAN. The BBU and the RRH are connected by the optical fiber through the ODN. The D-RoF technology defined by the standard interface such as CPRI or OBSAI is used to transport the data between the RRH and the BBU. A new network segment appears between the RRH on the cell site and BBU in the CO called *"Fronthaul"* [40].
The step 4 of C-RAN is the *Cloud-RAN*, also called BBU pooling. In this case, a centralized set of BBUs with resource pooling is capable of handling a large number of RRHs located at different antenna sites [41]. The next figure shows the step 4 of C-RAN. In the BBU pooling, the management aspects can be simplified because the BBU can

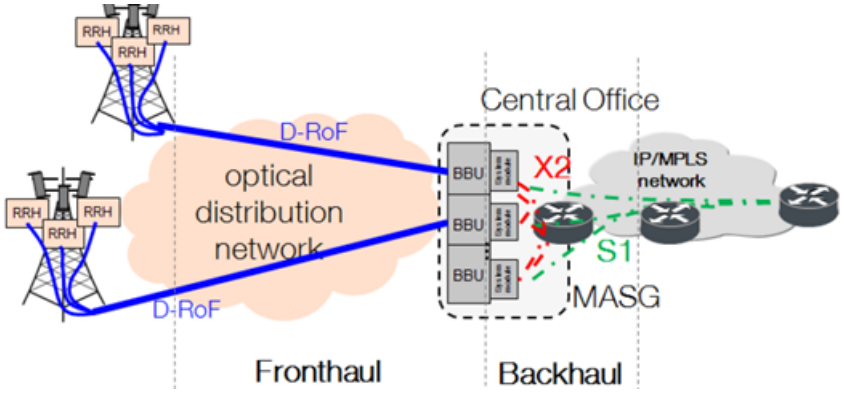

Figure 1.13: Step 3 of C-RAN: BBU centralization or hosteling

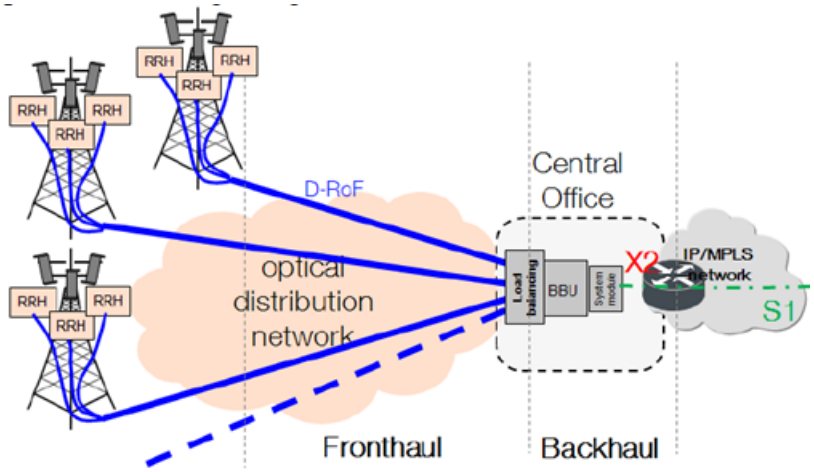

Figure 1.14: Step 4 of C-RAN: BBU pooling

handle soft handover which implies less signaling traffic instead of hard handover. One BBU controls several antennas of different cell sites, thus the control plane related to mobility in the mobile network is drastically reduced. Moreover, the number of S1 and X2 interfaces is also reduced.
The C-RAN architecture has several advantages.
It permits to:

- Reduce the cost of infrastructure
- Reduce the cost of CAPEX and OPEX
- Improve the capacity of the system easing the implementation of radio transmission technic such as the CoMP

In the following section, specifications about the fronthaul interface are described. The requirements and the involved protocols on the fronthaul link are presented.

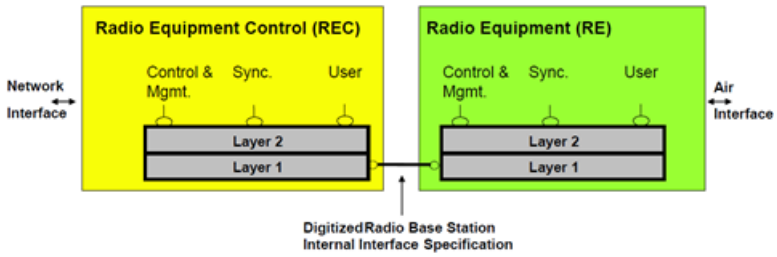

Figure 1.15: Schematic of CPRI Interface

1.3.2 Standard interface of the fronthaul link

1.3.2.1 Open Base Station Architecture Innitiative (OBSAI)

OBSAI is a specification that has been developed in 2002 by different companies which are: Hundai, LGE, Nokia, Samsumg, and ZTE and defines the architecture of base station. It has been developed to face the pressure to reduce the rising cost of base stations . Also, the OBSAI should have to allow the interoperability and the compatibility between modules of radio equipment providers. OBSAI is based on electrical standard Ethernet 10 Gigabit [42]. It defines several data rates from 728 Mbit/s to 6.8 Gbit/s. OBSAI sets the Bit Error Rate (BER) at 10^{-15} or better. The jitter aspects have been described by OBSAI. The details of this parameter have been presented in the Chapter 2.

1.3.2.2 Common Public Radio Interface (CPRI)

The CPRI is a protocol designed by Ericsson AB, Huawei Technologies, NEC Corporation, Alcatel Lucent and Nokia Siemens. It permits to establish a digitized interface between the BBU and the RRH. The specification covers the physical layer (Layer 1) and the Data Link layer (layer 2). Three kinds of information flows are multiplexed and transported over the interface. These information flows are: the user data plane, the control management and the synchronization plane data. Figure 1.15 illustrates the different flows and layers involved in the CPRI.

The Radio Equipment Control (REC) and the Radio Equipment designate respectively the BBU and the RRH. The data of CPRI is transported through the digitized IQ data. Each IQ data flow of user plane data reflects the data of one antenna for one carrier called antenna-carrier Container (AxC). The control management plane is composed of a Fast Control and Management supported by Ethernet, a Slow Control and Management supported by the High Level Data Link Control (HDLC), a L1 Inband Protocol and information relative to the vendor. The BER is set at 10^{-12}. Several data rates from

614.4 Mbit/s to 24.33 Gbit/s are defined [37]. The characteristics of jitter are described in chapter 2.

1.3.2.3 Open Radio equipment Interface (ORI)

The Open Radio equipment Interface (ORI) has been developed by the European Telecommunication Standards Institute (ETSI) in 2010, in order to bring more flexibility and equipment interoperability with respect to the others standards such as CPRI and OBSAI [43]. The ORI is based on the CPRI protocol. Indeed, ORI modifies the layer 2 of CPRI as shown in the igure 1.16. All data rate of CPRI are available in the ORI standard excepted the 614.4 Mbit/s. One of specificity of ORI is the compression of digitized IQ data. The data compression is supported by the LTE and concerns only the bandwidths of 10 MHz, 15MHz and 20 MHz. The IQ data compression should be compliant with the following requirement [44]:

- The Error Vector Magnitude (EVM) deterioration caused by the compression/decompression should be 3% most. Average measurement should be made at least over 10 ms (10 consecutive subframes of LTE)
- The compression rate should be a minimum of 50%
- The maximum tolerated one-way latency caused by the compression and decompression process should be 100 μs (preferably 20μs) for LTE.

More details about the compression and decompression requirements and the specification of low layers are provided in [39].

1.3.2.4 Comparison between CPRI, OBSAI and ORI

Both CPRI and OBSAI are used to send digitized radio IQ data. They are based on the electrical standards from Ethernet 10 Gigabit Attachment Unit Interface (XAUI). They have the same value of tolerated jitter but for different BER values. Despite of the similarities between these two standards, the CPRI presents more capacity and simplicity than the OBSAI. For example, when data rate of 3.072 Gbit/s is considered for both CPRI and OBSAI standards, the CPRI permits to use 93.75% of the frame capacity to send the used data, at least of 80% for the OBSAI. The following table shows the link bandwidth allocation for CPRI and OBSAI. CPRI has not fixed overheads unlike the OBSAI protocol. The characteristic brings more flexibility at the CPRI. In spite of OBSAI is the first defined interface between RRH and BBU, it has not succeeded to impose itself on the market. Indeed, the CPRI is the most usual standard protocol due to

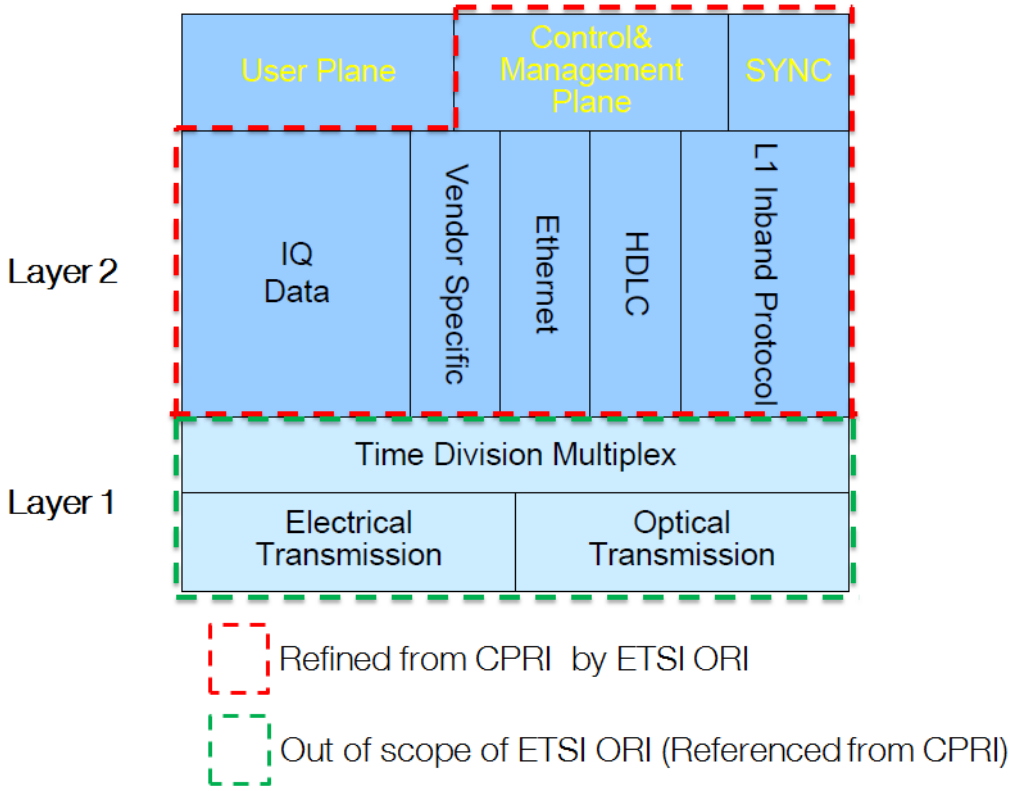

Figure 1.16: Refined field from CPRI protocol overview by ORI

	OBSAI	**CPRI**
User Data (IQ)	80%	93.75%
Control data (C&M)	4%	6.22%
Synchronization	0.25%	0.02%

Table 1.5: Comparison between CPRI and OBSAI for a bit rate of 3.072 Gbit/s

its simplicity and its flexibility. In 2010 a new standard interface called ORI is established by ETSI. There are few difference between the ORI and the CPRI because the ORI refines only the layer 2 of the CPRI in order to bring more interoperability between the elements of the base station. Compared to the CPRI, the ORI also allows the compression of the data permitting to use less of bandwidth. However, ORI is not yet implemented by base station vendors.

Nowadays, among the set of three standards (CPRI, OBSAI, ORI), the CPRI is the most used on the fronthaul segment in the market. Indeed, the providers like ERICSSON AB, Alcatel Lucent, or Huawei have base stations implementing the CPRI. Up to now, ERICSSON AB and ALCATEL Lucent provide CPRI option 3 (2.45 Gbit/s). In France, ORANGE has begun the test of C-RAN for the 4G deployment on several sites using a fronthaul segment which implements the CPRI standard with the date rate of 2.45 Gbit/s.

Because the CPRI is the most popular standard, our works and experiments will be based on this standard interface on the fronthaul segment.

1.3.3 Fronthaul requirements

To implement a fronthaul segment, it is mandatory to respect some interdependent requirements such as the technical aspects, business aspects, regulation and operation administration management constraints.

1.3.3.1 Data rate

The bit rate of CPRI interface is constant. It can be set form 614.4 Mbit/ to 24.33 Gbit/s following the radio configuration. The CPRI data rate is obtained by the following formula:

$$Data\ rate = M \times S_r \times N \times 2(\frac{I}{Q}) \times C_w \times C \tag{1.1}$$

Where:

- M: is the number of antennas per sector.
- S_r: is the sampling rate used for digitization (sample/s/carrier).
- N: is the sample width (bits/sample).
- $2(\frac{I}{Q})$: is a multiplication factor for $in-phase(I)$ and $quadrature-phase(Q)$.
- C_w: represents the factor of CPRI control word.
- C: is a coding factor. C can be equal either 10/8 for 8B/10B coding or 66/64 for 64B/66B.

CPRI specification provides sampling rates corresponding to the different radio access technologies and channels bandwidths as well as minimum and maximum values for IQ sample width. To illustrate the formula 1.1, we consider a LTE sector with 20 MHz of bandwidth with a 2×2 MIMO configuration. In this case $M = 2$, $S_r = 30.72MHz$, $N = 15$, $C_w = 16/15$ and $C = 10/8$ thus leading to 2.457 Gbit/s. The table 1.6 indicates the data rate of CPRI following the RAN configuration corresponding to one carrier and one sector.

1.3.3.2 Latency Parameters

Since the link between RRH and the BBU is at the level of the physical radio signal the total latency that the radio signal can tolerate, includes the latency of the fronthaul. The

RAN	GSM 1T1R	GSM 1T2R	UMTS 1T1R	UMTS 1T2R	LTE 10 MHz 2X2	LTE 10 MHz 4X2	LTE 20 MHz 2X2	LTE 10 MHz 4X4
CPRI Date rate	12.304 Mbit/s	24.608 Mbit/s	307.2 Mbit/s	614.4 Mbit/s	1.228 Gbit/s	2.457 Gbit/s	2.457 Gbit/s	4.915 Gbit/s

Table 1.6: CPRI data rate in versus radio access technologies

most critical parameter comes from the uplink synchronization method Hybrid Automatic Repeat Request (HARQ). The HARQ consists of an Automatic Repeat Request (ARQ), an Error Detector (ED) and a Forward Error Corrector (FEC). It is used in the RAN to ensure that the data is sent reliably from a transmitter to a receiver. The uplink HARQ processes concerns the UE and the base station. In the LTE uplink HARQ process, if the HARQ is transmitted in the subframe "n" the response ACK/NACK[1] is received through the subframe "n+4" [45]. Therefore, the eNodeB should handle the request and response within the next three subframes [46] after receipt the uplink data. The figure 1.17 illustrates the uplink synchronization HARQ method. In LTE, uplink and downlink subframes are time-aligned at the eNB. Thus, the eNB processing should be less or equal to 3 ms. In the case of C-RAN based on the optical fiber introduces between the RRH and the BBU, the propagation delay of the signal on the fronthaul link must be considered. In order to complete the timing requirement of uplink HARQ, the maximum latency on fronthaul must be determined. This latency on the fronthaul link has to consider the apropagation time on the optical fiber and in the air interface and the processing time of the BBU. The most common round trip time values for fronthaul between the RRH and the BBU is to 700 μs for LTE and 400 μs for LTE-A [32] based on RAN vendor specification (no standard value by 3GPP). In LTE-A, if the BBU and the RRH are connected without active equipment, the time delay allows to reach 40 km one way of optical fiber (80 km round trip time) between BBU and RRH. The figure 1.18 shows the impact of the fronthaul on the delay processing.

The CPRI specification defines some time requirements. These requirements concern the accuracy of delay on one way (uplink or downlink) or the round trip delay. The link delay accuracy without cable length is $\pm$8.138 ns and the absolute accuracy of round trip is $\pm$16.276 ns. The maximum absolute round trip delay without cable length is 5 μs. This latter constrains the RRH processing to be less than 5 μs.

[1]ACK/NACK: is an acknowledgement message which is used in communicating processing to signify the reception or not of message

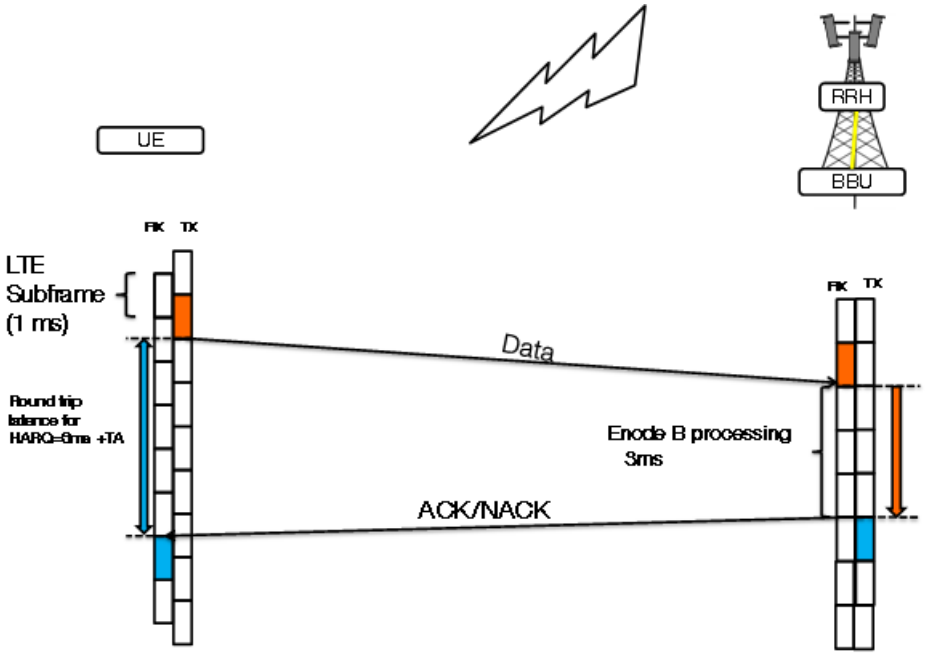

Figure 1.17: Uplink synchronous HARQ processing

1.3.3.3 Synchronization and jitter

The synchronization clock is provided to the BBU either by the Global Positioning System (GPS) or by the network through the backhaul link using the Synchronous Ethernet. The RRH clock for frequency generation is dependent on the BBU through the fronthaul clock signal. Indeed, the CPRI generates a Basic Frame (BF) for each 260.42 ns corresponding on the chip time (Tc=1/3.84 MHz). A BF contains one Control Word (CW) and fifteen (15) Words of I/Q sample bits from the different AxCs. The Hyper Frame (HF) is constituted by 256 BF and the first CW of the HF is used to synchronize the BBU and the RRH.
The 10 ms CPRI Frame is formed by 150 HFs. the HF is designated by node B Frame Number (BFN) (figure 1.19) in the 10 ms CPRI Frame.

The first BFNs sent from BBU to RRH serve to synchronize them. The HFs and the BFs are set to zero except the first CW of the first HF that contains the first synchronization byte called K28.5 used when the 8B/10B line coding is implemented. When the RRH receives the first synchronization byte, the HFs and the BFs are set to zero and the first K28.5 is sent back to the BBU. The BBU and the RRH are synchronized (figure 1.20).

The maximum time to synchronize the BBU and the RRH is set to 10 s. The central clock of RRH is based on the CPRI signal. The degradation of the CPRI signals such as the jitter should affect the accuracy of the RRH frequency clock (figure 1.21). When the

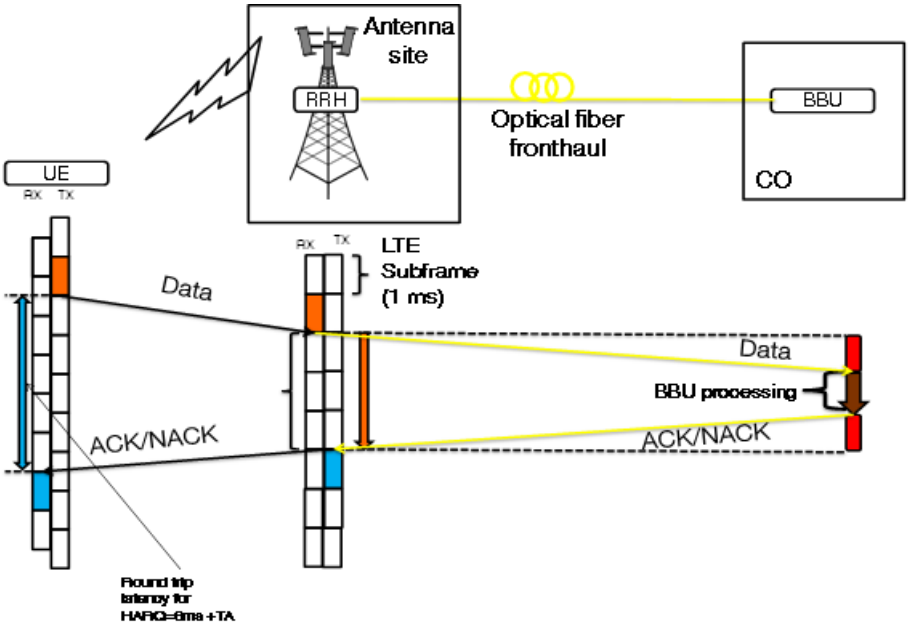

Figure 1.18: Determination of the fiber length for a fronthaul link

clock is inaccurate, errors could appear in the converting radio data. The jitter impact on the frequency accuracy budget of the interface to the radio station is estimated according to the following formula:

$$\Delta jitter_{f_0} = \frac{1}{f_0}\sqrt{\int_0^{f_1} 2.\ f^2.\ 10^{\frac{L(f)}{10dB}}.\ df} \tag{1.2}$$

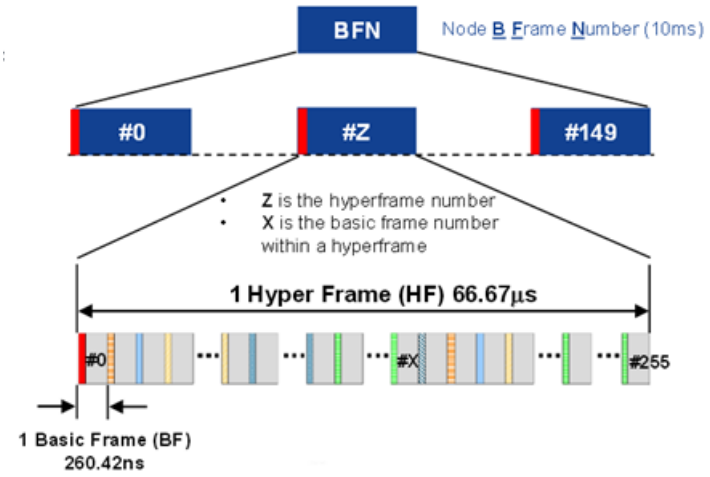

Figure 1.19: BFN structure in CPRI

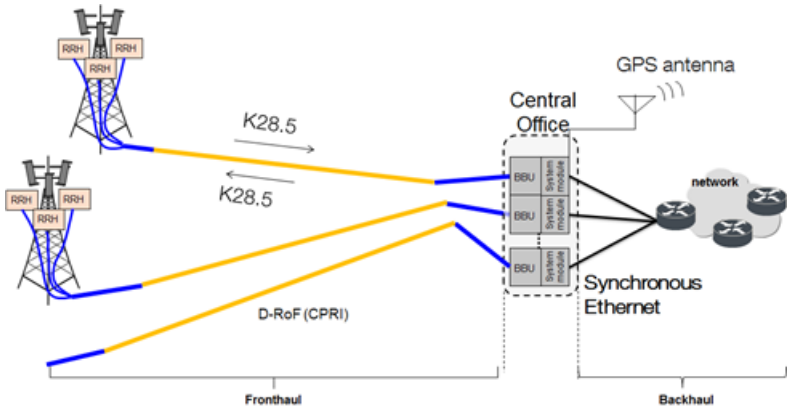

Figure 1.20: Synchronization mechanism in C-RAN

Where:

- $\Delta jitter_{f_0}$: is the contribution of jitter on the frequency accuracy
- f_1: designates the cut-off frequency of the RE synchronization mechanism
- $L(f)$: is the single side band phase noise in dBc/Hz acquired on the CPRI interface
- f_0: is the frequency of the stable clock signal at the Service Access Point SAPs which is the reference point for the jitter and the phase noise measurements.

The maximum cut-off frequency f_1 is fixed at 300 Hz and the maximum contribution of jitter is fixed at ±2 ppb relative to the radio base station frequency accuracy budget (between Master Service Access Point (SAP) and the slave SAP). A Phase Locked Loop (PLL) produces the received clock on the RRH slave port with the reference clock of

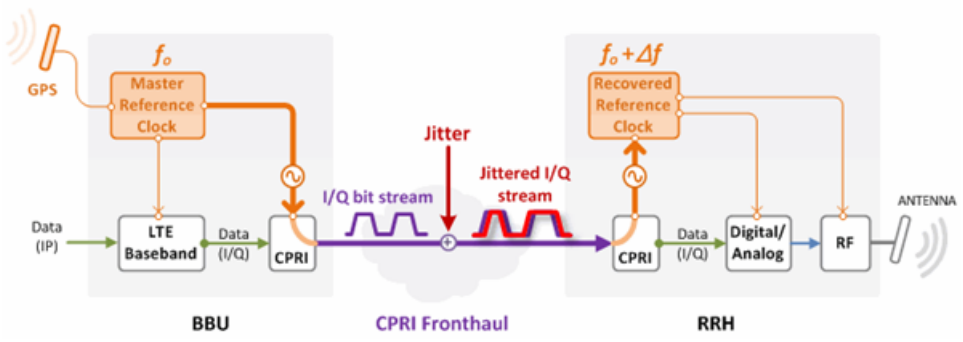

Figure 1.21: Jitter impact on the reference clock f_0 provided by the GPS

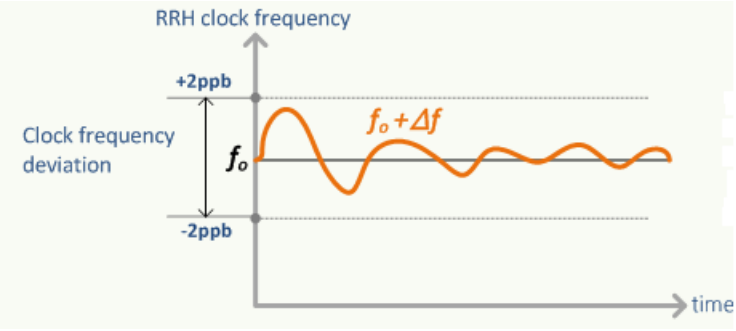

Figure 1.22: RRH clock frequency deviation

BBU. The reference clock f_0 could be provided to the GPS signal or by the network. The following figure shows the case where the reference signal is brought by the GPS [47]. The figure 1.22 illustrates the maximum contribution jitter on the reference frequency.

1.3.3.4 Legacy aspects and monitoring on fronthaul link

In France, in order to preserve a healthy competition, the regulation aspects require that the fiber provider supplies fronthaul solution to the mobile operator. In this case, the responsibility of each partner must be clarified. To address this issue, a Demarcation Point (DP) is defined. It permits to situate the responsibility limits between the mobile operator and the fiber provider (figure 1.23). The fiber provider must provide the fronthaul solution in form of wholesale offer defined by the Service Level Agreements (SLAs). Different SLA can be defined depending on the chosen fronthaul solution, but the basic and necessary one is the capacity to monitor the optical link and detect if there is failure. Indeed, the fiber provider must be able to distinguish the problems due to the optical link from the problems of the mobile network [48].

The offers based on different SLA lead the business requirements. Indeed, the goal of these latter is a low cost implementation of C-RAN. This dictates the choice of the

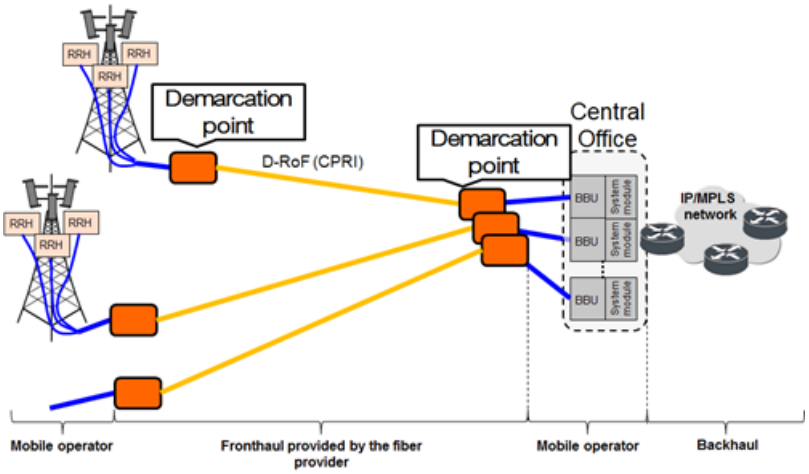

Figure 1.23: Demarcation point in C-RAN

technical fronthaul solution, but concerns also antenna cell site engineering aspects. Under this point of view, the demarcation point at the cell site will be preferred passive. In other terms, DP should not need power consumption. On top of this, the cell site DP should be most times deployed outdoor and subjected to industrial temperature range requirement (-40 to 85 °C). Low cost optical transceivers like Small form Factor Pluggable (SFP) are used. Finally, on the cell site, some local alarms are used for basic but essential indications as for instance, battery charge fire, or intrusion. The fronthaul solution should also be able to transport such signals for a centralized management.

1.3.3.5 Optical fiber resources

Radio sites can be classified in macro cells and small cells. The macro cells generally have three to six sectors. Additionally, for each sector, several Radio Access Technologies (RATs) on different bands can be present. Indeed, the 2G at 900 and 1800 MHz, 3G at 900 MHz and 2100 MHz, LTE at 800 MHz, 1800 MHz and 2600 MHz can be implemented on a same antenna site [48]. In the case of small cells, the antennas are omnidirectional, therefore it has only one RRH for each RAT and frequency band. So it can have up to 5 RRHs per small cell site. In the case of macro cells present in the urban areas, there are three sectors for each RAT accordingly 15 RRHs can be installed on the same antenna site. Each RRH must be linked to one BBU port. The use of point to point physical topology to connect the BBU and the RRH is very expensive as the number of fibers per antenna site is very important. Since the optical fiber in access network is a rare resource, other technics or topologies must be found in order to reduce the number of used optical resource. The main topologies which permit to reduce the number of fiber between the BBU and the RRH are [32]:

- Daisy chain: several RRHs could be cascaded towards the BBU. This topology reduces the number of fibers but at the same time introduces a single point of failure and a highest line rate for CPRI
- Multi Path: Ring and mesh topologies have the advantages of addressing the issue of network availability by closing the chain and providing an alternative path to maintain connectivity between the BBU and the RRHs in the presence of a link failure on any of the segments in the ring.

Two main solutions exist to achieve these topologies. These solutions are: either the active optical system or the passive optical system. In order to reduce the OPEX, CAPEX and to save energy, the passive optical system is preferred.

1.4 Transmission systems on the fronthaul link

The implementation of fronthaul is supported by the optical fiber in the most cases or by the microwave in some specific cases. Indeed, microwave permits to reach the areas where the fiber infrastructures cannot be installed. This section presents the main systems which permit the realisation of a fronthaul link. First, we discuss about the passive solutions then the active solutions are introduced. The term "active" means that the CPRI traffic is encapsulated. Generally, the equipment that encapsulates the CPRI traffic needs energy to operate. The term "passive" indicates that the CPRI frames are not encapsulated. Generally, the passive equipment does not need power consumption to operate but not necessary. A complete fronthaul solution must have a monitoring system in order to supervise the link in order to provide SLA of the different clients. During the presentation on active and passive system in the C-RAN context, the monitoring aspects will be addressed.

1.4.1 The passive solution

The passive solution is based on the Wavelength Division Multiplexing (WDM) techniques. The Coarse Wavelength Division Multiplexing (CWDM) or the Dense Wavelength Division Multiplexing (DWDM) can be used for the deployment of fronthaul. The advantage of the passive WDM is that it is possible to multiplex several links of fronthaul on one fiber [49] and that it is a low cost solution. In addition, the passive WDM does not cause a processing latency. However, the drawback of this solution is that it does not have a monitoring system.

1.4.1.1 Coarse Wavelength Division Multiplexing (CWDM)

Concerning the CWDM, it is possible to multiplex up to 18 Channels through 18 wavelengths, therefore 18 fronthaul links over 2 fibers (one for up- and one for down-stream). The spectrum grid is defined from 1271 nm to 1611 nm with 20 nm of channel spacing. Each wavelength channel can operate at any bit rate in function of the optical transceiver (Small Form Factor – SFP) ability. The colored SFPs is plugged in the BBU and the RRH to receive and transmit the CPRI signal. Nowadays, it is possible to reach up to 80 km at 2.5 Gbits/s (optical budget of 24 dB) and up to 40 km at 10 Gbit/s (optical Budget of 10 dB) with commercial SFPs. 25Gbit/s SFP is also now pre-commercially available with a reach up to 10 km.

In the case of CWDM, two configurations are possible. The first presented configuration uses the 18 wavelengths either on the uplink or on the downlink (figure 1.24). This configuration is called "the dual fiber" because a pair of optical fiber is necessary to establish the downlink and the uplink. The multiplexing and the demultiplexing is performed by means of 4 MUX/DEMUX (2 by transmission sense). The second configuration uses the half of available wavelengths (8 wavelengths) for the uplink and the other half for the downlink (figure 1.25). The kind of configuration is called *"the single fiber configuration"* because it uses 1 fiber for the 2 senses of transmission.

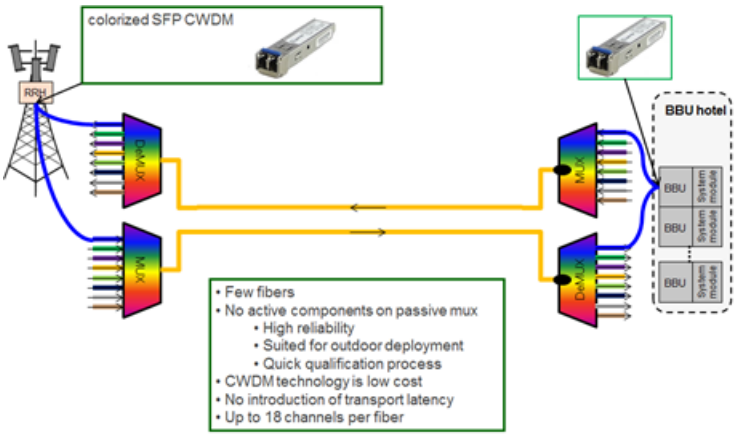

Figure 1.24: Dual fiber Passive CWDM

In the Outdoor environment (SFPs are able to operate from -40°C to 80°C) when there are 15 RRHs, it is suitable to use dual fiber configuration. If there are less than 9 RRHs the single fiber configuration is more suitable. In Practice, these two configurations cannot be deployed because they do not offer a monitoring solution. To solve this issue and benefit advantages of passive CWDM, a semi active solution is proposed.

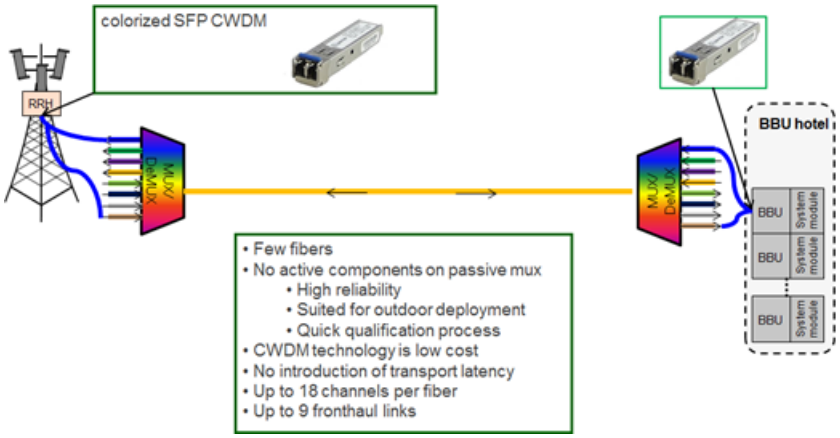

Figure 1.25: Single fiber Passive CWDM with dual fiber SFPs

1.4.1.2 Dense Wavelength Division Multiplexing (DWDM)

DWDM permits rapid network deployment and significant cost reduction. It consists to reduce the channel spacing relative to the CWDM in order to increase the number of channels. The spacing channel can be 12.5 GHz, 25 GHz, 50 GHz, 100 GHz or 200 GHz. The number of channel can reach 128 or more. It operates in the C-band from 1520 nm to 1570 nm [50] and in the L-band from 1570 to 1624 nm according ITU [51]. Generally, in the access network (based on early implementation of NG-PON2) and specifically for fronthaul, 100 GHz of spacing channel can be used. Different Array Waveguide Gratings (AWGs) such as Gaussian or flat top can be used to achieve the MUX/DeMUX function. To DWDM on a fronthaul segment, the market proposes transceivers like the colorized SFPs that can operate up to 10 Gbit/s with 10 dB as optical budget. Since the number of channels is important in DWDM, it is more suitable to use the single fiber configuration than the dual fiber configuration for the fronthaul deployment. In the massive roll-out of DWDM or CWDM using colorized SFPs on the fronthaul, the inventory issue appears. Indeed, the management and the maintenance of a great park of colorized SFPs are complicated. For each fronthaul link, it is necessary to know what kind of SFP has been used on the antenna site and the corresponding BBU in the CO. Furthermore, in CO, the difficulty is more important because the BBUs will be stacked. In the case where the colorized SFP is down it must be changed by the same colorized SFP this leads to have a double of each SFP in the stock. To solve this problem, it is necessary to implement a colorless transceiver. A self-seeded source based on Reflective semiconductor Optical Amplifier (RSOA) is proposed as a potential candidate to achieve colorless transceiver on fronthaul link. It offers the advantage of assigning automatically and passively the wavelength source. This solution has been studied and presented in the chapter 3. Like a passive CWDM, it is impossible to build a complete fronthaul solution with only passive

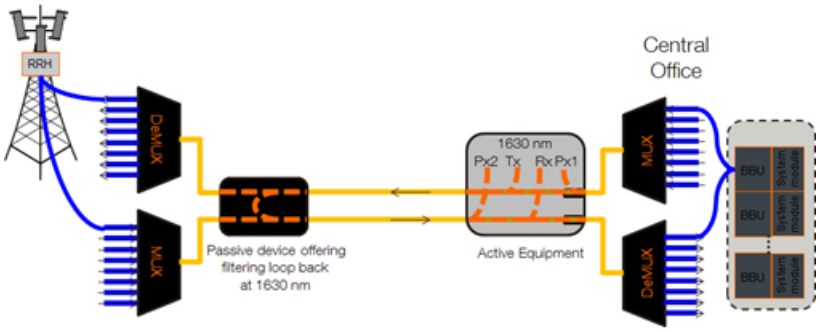

Figure 1.26: Semi active system with devices situated between the MUX and DeMUX

DWDM because it does not present a monitoring solution. A semi passive system remains a solution to build a complete fonthaul link keeping the advantages of passive WDM solution. For a sake of simplicity, we only focus on the CWDM for the presentation of semi active or active solution for fronhaul.

1.4.2 The semi active solution

A semi active solution implements an active equipment at the CO. This active device permits to monitor the fronthaul link, or for an enhanced system, each wavelength. With a semi active solution, it is possible to know if a cut of fiber has occurred on the fonthaul segment but it does not permit to localize the cutoff. Figure 1.26 describes the first presented architecture. The active equipment introduces the monitoring signal. It is placed between the Multiplexers (MUXs). In this manner, it is allowed to introduce a wavelength which is out of wavelength range used by the WDM systems. The tested equipment introduces a wavelength at 1630 nm (outside the CWDM or DWDM spectrum bands). Also on the antenna site, a passive device, situated between the MUXs, filters and sends back the monitoring wavelength to the CO. The other wavelengths are forwarded to the De-multiplexer (DeMUX).

P_{x1} measures the total power coming out of the MUX. P_{x2} measures the total power from remote antenna site. T_x introduces the optical signal at 1630 nm and Rx measures the back monitoring wavelength (a filter is also implemented in the active equipment to recover the monitoring signal). When a cut of fiber occurs no power is measured at P_{x2} and R_x. P_{x1} allows to check the power level of the signal from the set of colorized SFPs. It is possible to monitor each wavelength by putting a DeMUx at P_{x1} and P_{x2}. But if the demarcation point is constituted of the active equipment and the passive device, it is not relevant for the fiber provider to monitor each wavelength. Indeed, in this case, the task of the fiber provider is to provide the trunk fiber segment (between CO and antenna site) and ensure the quality of this latter and not to manage and monitor the different

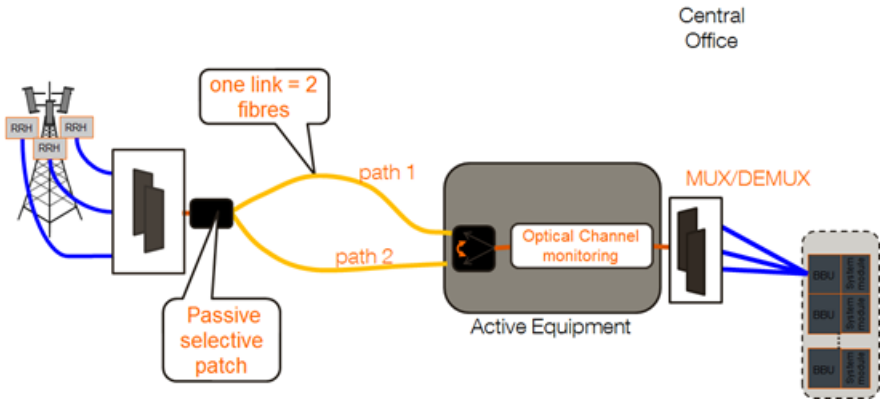

Figure 1.27: Semi active system with an automatic fiber protection

wavelengths which are transmitted through this fiber. Indeed, it could use a point to point topology or the WDM technique. This architecture can propose an automatic fiber protection. This system of fiber protection switches the CPRI traffic on a secondary optical link when a cutoff has occurred on the main optical fronthaul segment. When the optical channel monitoring notices a cut of fiber, the optical path is automatically changed (figure 1.27). In the practice case, we are not able to guarantee that the two path are the same length. When an important difference of length appears between the BBU must recalculate the delay in order to balance the frames between upstream and downstream. In other words, the BBU must synchronize again with all RRHs.

The second system positions the active equipment behind the couple of the MUX and DeMUX in the CO. It uses one wavelength of WDM system but does not need a filter relative to the concept of the previous system. Once the wavelength of the monitoring is selected among those available, the ports of the MUX and DeMUx corresponding to the monitoring wavelength are connected to realize a loop-back of the signal. The innovation of this system is brought by specific colorized SFPs that support a new interface called remote Digital Diagnostics Monitoring Interface (DDMI). In addition to the CPRI signal, this interface adds a management channel. This channel permits to get the information about optical input and output power, the temperature, the laser bias current and the power consumption of the colorized SFPs. The data provided by the remote DDMI are processed by the active equipment called transponder. The transponder has several interfaces oriented either toward the cell site or toward the BBU stack (figure 1.28). In order to reduce the cost of the SFPs and simplify the management of the SFP plugged in the BBU, gray[2] SFPs are used instead of the colorized SFPs. The fronthaul link is based on colorized SFPs implementing remote DDMI are plugged in the RRHs and in the

[2] *"gray"* means here a bidirectional method, single fiber, based on two wavelengths like 1310 nm and 1490 nm

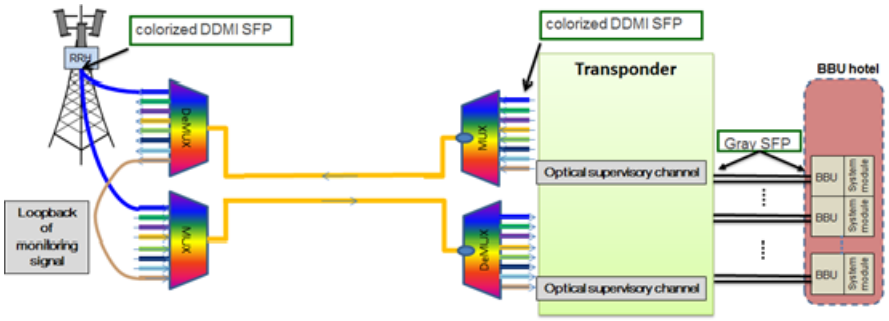

Figure 1.28: Semi active system with a transponder

transponder. Thereby, the transponder recovers all information to manage SFPs and the monitoring signal to get the status of the optical fronthaul link.

This system is suitable if the fiber operator provides each wavelength to establish the fronthaul link. In this case, the demarcation point could be the transponder and the out of the RRH. The remote DDMI SFPs on the antenna site are provided by the fiber operator or an agreement about the management of SFPs on the antenna site must be found between the mobile operator and the fiber operator.

1.4.3 The active solutions

1.4.3.1 Transponder and Muxponder

The transponder as all active element, adds a latency on the fronthaul link. The challenge is to manufacture a transponder that introduces less latency than possible. The market offers transponders which can introduce until 4ns of latency on the fronthaul link. They are manufactured to be transparent to the CPRI traffic. With this architecture, the fiber provider can propose an offer to the mobile operator that would permit to the customer to avoid the management of wavelengths. Indeed, the mobile operator would plug gray SFPs in the BBU and RRH. All colorized wavelength is managed by the fiber provider (figure 1.29).

In this case, the demarcation point could be the transponder. The responsibility between the mobile operator and fiber provider is easier to define than with the semi active system.

The Muxponder permits to achieve time aggregation of several CPRI on one frame operating over one wavelength. This device allows to save number of wavelengths. The tested muxponder has a specific frame like OTN (Optical Transport Netwotk). Indeed, it adds overheads on the CPRI frames. In this case, the muxponder is not totally transparent. Indeed, it increases the latency and modifies the clock source relative to the

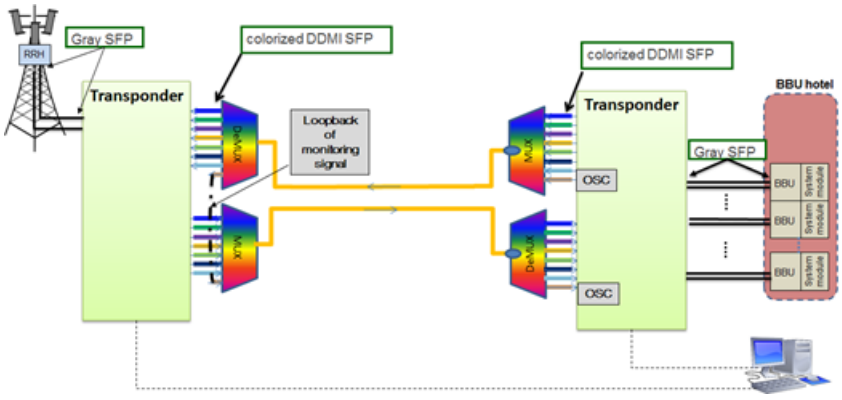

Figure 1.29: Active system with a transponder

transponder. The tested device is able to multiplex 3 CPRI links at 2.45 Gbit/s (CPRI-3) or 3.072 Gbit/s (CPRI-4) and 2 Synchronous Ethernet links, all with independent synchronization over the same 10 Gbit/s line [52]. For example, when an antenna site has 15 RRHs, only 5 wavelengths are necessary by using the muxponder and 15 wavelengths when the transponder is used.

1.4.3.2 Fronthaul over Optical Transport Network (OTN)

The Optical Transport Network (OTN) is standardized by ITU-T [53] [54]. It consists to encapsulate a digital data into specific containers and send the all through the optical network. The OTN brings some fundamental advantages [55]

- The standardization of the system allows the monitoring, the management and the maintenance of optical link
- An option for Forward Error Correction (FEC) improves the performance of the optical network
- The demarcation points between the mobile operator and the fiber provider are easily distinguished.

The CPRI signal must be transported in the OTN containers considering the stringent constraints like the jitter, the stability of frequency and the latency because these parameters directly affect the quality of the mobile service. The work to give recommendations about of CPRI over fronthaul is ongoing. Indeed, ITU focuses in this subject through the supplement 56 of the series G called OTN transport of CPRI [56]. Figure 1.30 describes the different level of OTN encapsulation [57].

The data of the client is mapped in the Optical Payload Unit (OPU). According the rate of the OPU, it is possible to map or to multiplex different OPUs in the Optical

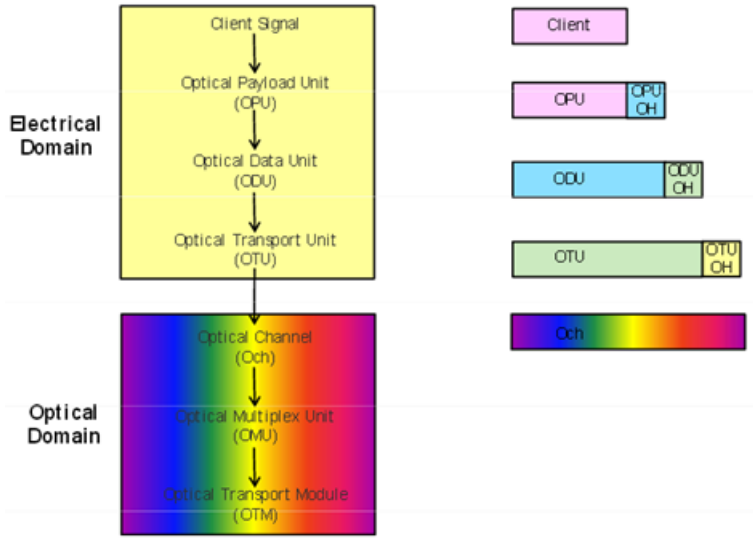

Figure 1.30: OTN containers

	Data rate (Gbit/s)		
Hierarchical level of OTN containers	**OTU**	**ODU**	**OPU**
0	-	1.24	1.23
1	2.66	2.49	2.48
2	10.79	10.03	9.99
3	43.01	40.31	40.15

Table 1.7: OTN hierarchical levels relative to the data rate

Data Unit (ODU) and this latter is itself mapped or multiplexed in the Optical Transport Unit (OTU). Several hierarchical levels exist for these different containers [58]. Table 1.7 presents some of them relative to the data rate.

There are two kinds of solution to transport CPRI over OTN. The first solution consists of a traditional OTN time multiplexing of multiple CPRI signal. This solution allows the mixing several CPRI rates with other traffic data such as Ethernet. In this case, the rates of OTN do not match well with CPRI rates (not the same sub-division of clock rate). This mismatch between the OTN containers and the CPRI data can introduce an additional jitter and an additional frequency deviation. The second method consists in using a suitable OTN container that allows a better match between the CPRI data rates and those of OTN containers. This method consists to aggregate the CPRI signals before mapping to the overlocked OTN container in order to optimize transport bandwidth efficiency. Several and only the CPRI signals (several CPRI rates are possible) can be transported per wavelength. These different overlocked containers are:

- The overlocked Optical channel Data Unit 2 (ODU2r)

CPRI signal	CPRI rate (Gbit/s)	OTN multiplexing signal in OUT2 at 10.7 Gbit/s	OTN multiplexing signal OUT2r at 12.6 Gbit/s
CPRI-2	1.22	8	12
CPRI-3	2.45	4	6
CPRI-4	3.07	2	3
CPRI-5	4.91	2	3
CPRI-6	6.1	1	2
CPRI-7	9.83	1	1

Table 1.8: Multiplexing and mapping of CPRI in OTN containers

Figure 1.31: Overview compression of ORI

- The overlocked Optical channel Transport Unit 2 (OTU2r).

Table 1.8 describes the number of CPRI clients relative to the data rate that can be multiplexed according the two solutions of CPRI over OTN.

The CPRI signal can be transported in the OTN container at 25 Gbit/s but presently, the existing solutions propose the encapsulation until OTU2r.

1.4.3.3 ORI interface

The following active system which is presented for a fronthaul is the ORI interface. Indeed, the ORI interface is a native active solution for fronthaul because it permits the compression and the decompression of the IQ data samples of CPRI in order to save the bandwidth (figure 1.31).

Remember that the objective of the ORI interface is to make the fronthaul interface fully interoperable by modifying some functions of the CPRI L2 layer. The option of compression permits to save the bandwidth. The details of ORI are presented in the section 1.3.2.3.

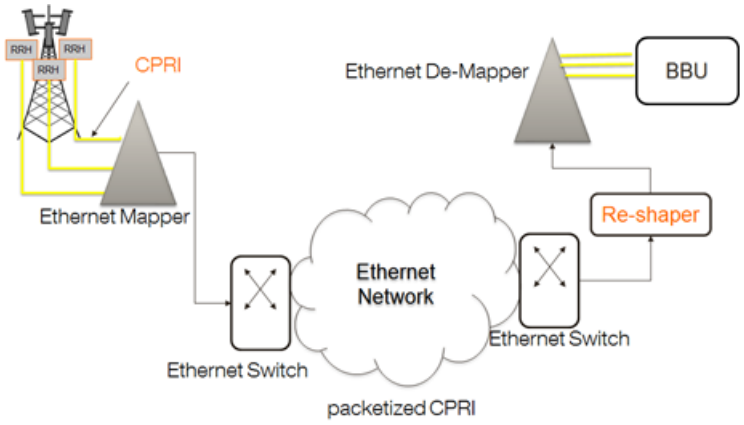

Figure 1.32: Architecture of CPRI over Ethernet

1.4.3.4 CPRI over Ethernet

Ethernet is also considered as a frame to encapsulate CPRI because it ever exists in backhaul equipment. The feasibility to re-use the existing backhaul equipment and network is considered. It is also considered the fact that Ethernet network has already the capacity to manage and monitor this network. The CPRI over Ethernet provides to the fronthaul network the propriety of Operation Administration and Maintenance (OAM) inherited from Ethernet characteristics [59]. Ethernet can bring to the fronthaul the flexibility and the scalability of the network required by the future radio standard. The CPRI over Ethernet consists of the mappers which performs the encapsulation of CPRI in the Ethernet frames in order to allow the CPRI traffic to be transported through the Ethernet network (figure 1.32) [60] .

The packetized CPRI entails an additional jitter, Packet Delay variation (PDV) and the variation of delay in fronthaul link. These aspects have a consequence on the synchronization parameter. Nowadays the debate is that Ethernet could meet the stringent latency and jitter requirements imposed by the CPRI [61]. With the traditional encapsulation of CPRI in Ethernet, the CPRI requirements does not meet. The study to resolve this question is ongoing and several solutions are proposed like:

- Dynamic reconfiguration of CPRI data rate [62]
- Special policy of Ethernet traffic (IEEE 802.Qbv) [63].

The presented solutions are based on the simulation. Currently, the standardization actors work on the equipment which allows the mapping the CPRI on Ethernet by meeting the different stringent requirements of CPRIs.

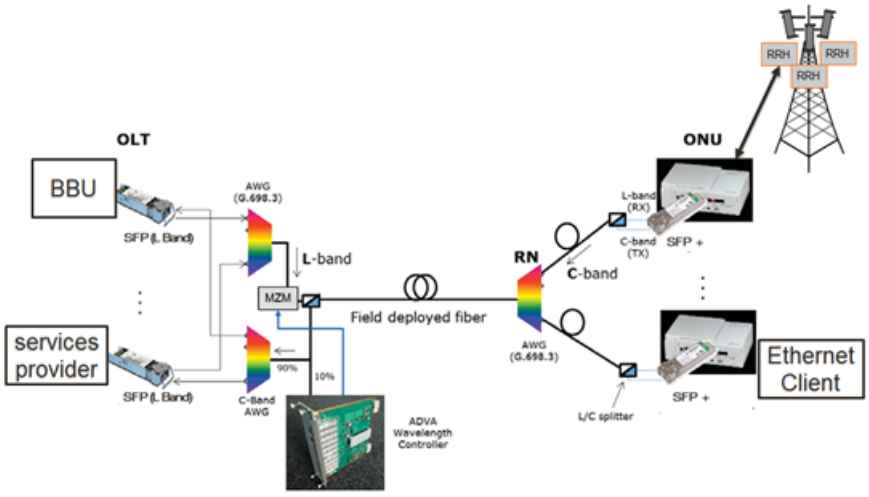

Figure 1.33: WDM-PON prototype provided by ADVA

1.4.3.5 WDM-PON

Wavelength Division Multiplexing - Passive Optical Network (WDM-PON) is an approach used by the next generation access architecture to achieve the fronthaul interface and the backhaul network. It consists to replace the optical power splitter in the classical PON architecture by a wavelength multiplexer that separates the wavelengths for individual delivery to the ONUs. To avoid the inventory issue of wavelengths and in order to simplify the operation of the system, colorless devices or tunable lasers are required in the ONUs. Several solutions implementing WDM-PON exist, but as an example, an innovative low-cost prototype (provided by ADVA) that has been tested on a fronthaul interface is presented into next figure [64] [65].

In this prototype, a SFP transmits in the L-Band[3] is plugged in the BBU. The SFP+[4] introduced in the ONU emitting in the C-Band[5], contains a high temperature low cost tunable laser (Distributed Bragg reflector Laser). This SFP+ is suitable for the outdoor environment because it is able to operate until 90°C without thermo-electric cooler (TEC). The auto tuning of one wavelength of a particular ONU does not affect the performance of the neighboring channel. The wavelength controller receives the optical signal from the ONU. This signal contains a pilot tone which permits the wavelength controller to identify the port of the AWG and the considered ONU. Then, the feedback signal is sent by the wavelength controller to the ONU in order to adjust the wavelength and the power level. The ONU contains a micro controller which receives the parameters from the wavelength controller and applies them to the laser.

[3]L-Band: wavelength range from 1565 nm to 1625 nm
[4]SFP+ is a SFP which is able to operate until 10 Gbit/s
[5]C-Band: wavelength range from 1530 nm to 1565 nm

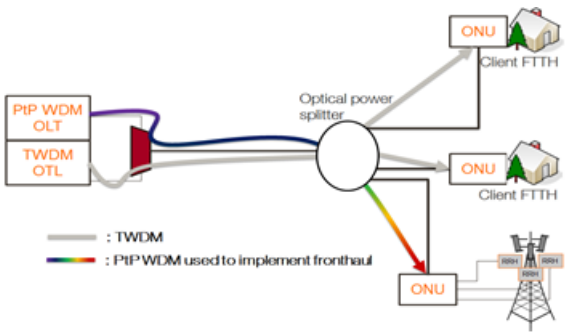

Figure 1.34: Fronthaul based on TWDM and PtP WDM NG-PON 2 solution

1.4.3.6 Point to multi-point TWDM and PtP WDM of NG-PON2

When a new TWDM ONU wants to connect to the TWDM OLT port, a ranging process is launched by the OLT. The ranging process permits to evaluate the distance between the ONU and the OLT in order to avoid the collision on the uplink. During this ranging process, a ranging time window for delay measurement is initiated by the OLT. When the ranging window is opened, the communication is dedicated to the new ONU, the other connected TWDM ONUs at the same channel pair stop the traffic with the OLT [66]. When the fronthaul is implemented in the current PON systems, the timing process such as HARQ or time advance could not be compliant to the standards because of the ranging procedure. In addition, this latter could temporarily increase the latency of fronthaul link. Also, the delay and the jitter of CPRI data would be rise by the encapsulation of CPRI frames in GEM frames or Ethernet frames and by the TDM system. In order to realise fronthaul link over the PON tree, the PtP WDM of NG-PON2 can be used. Figure 1.34 describes the basic architecture based on the NG-PON2.

The NG-PON2 is one of architectures that has been invoked in the concept of fixed and mobile network convergence described in the European COMBO project for integrating the fronthaul. Nowadays, only the TWDM prototype is developed. Therefore, it is difficult for us to test the fronthaul over WDM PON in NG-PON2.

1.4.3.7 Fronthaul microwave solution: an alternative solution

The wireless technology can be used as an alternative and a complementary solution of optical fiber in the deployment of the fronthaul. The wireless fronthaul allows the deployment of fronthaul in the areas that cannot support operation with the optical fiber. The deployment of wireless fronthaul is fast and permits to save OPEX and CAPEX. The following figure depicts the architecture of fronthaul microwave.

This solution consists of Wireless Fronthaul Module (WFM) which recovers the CPRI

Figure 1.35: Architecture of wireless Fronthaul

signal. The WFMs are connected to the BBUs and the RRHs via the optical fiber. A commercial solution had been tested. In this solution, a single wireless fronthaul link can support up to three RRHs. The WFMs recover the CPRI signal and apply him a process which permits to carry up to 7.5 Gbit/s (corresponding of the rate of 3 CPRI-3 links) in 70 MHz of bandwidth on 5.8 GHz of carrier frequency [67]. The tested wireless fronthaul solution preserves the performance of the downlink and uplink radio and meets the requirements of fronthaul.

1.5 New Generation Fronthaul Link (NGFI): Functional Split

The C-RAN offers several advantages and eases the deployment of the 2G, 3G and 4G technologies. Presently, several organisms of standardization pay attention to the future 5G technology. Regarding the requirements and the characteristic like the virtualization, the current fronthaul interface is not suitable of the 5G RAN deployment. Indeed, in the fronthaul, the constant bit rate renders the data transmission inefficient, the fixed correspondence between one BBU and one RRH does not provide the flexibility and the scalability that needs the future 5G and the sampling I/Q data rate depend to the number of antennas. To solve this issue, the fonthaul interface must be rethinking. A novel concept of fronthaul called New Generation Fronthaul Interface (NGFI) is developed. It consists to move certain functions from BBU to RRH. This procedure is called functional split [68] [69]. In [69] a C-RAN architecture based on NGFI is proposed.

In this architecture, the pool of BBU becomes the Radio Cloud Center (RCC) and

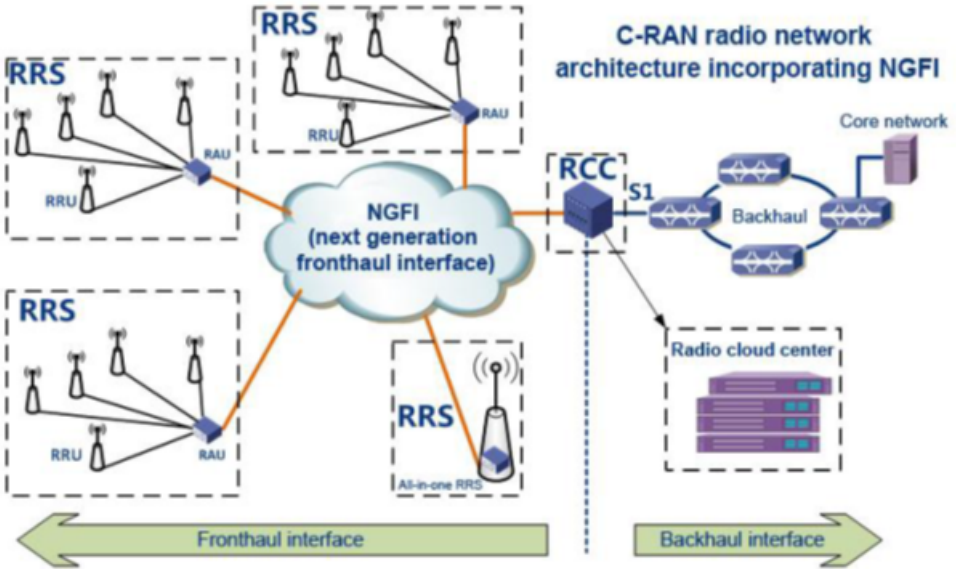

Figure 1.36: C-RAN based on NGFI

the Remote Radio Unit (RRU)[6] (RRH) becomes the Radio Remote System (RRS). The RRS consists of antenna, the RRU and the Radio Aggregation Unit (RAU). The RAU contains the functions of BBU which shift to the Radio site (part of BBUs baseband processing). The RCC includes the BBU function like radio aggregation and the higher control functions or the virtual BBU (virtualization aspect of C-RAN). It handles multiple base stations, management of cells and serves as a function pool. The figure 1.36 presents two cases. At first, the traditional RRUs is connected to the RAU via a CPRI link. The RAU permits to attack the network of the NGFI. In second case, the RAU and the RRU are not dissociated, they constitute a unique entity and are directly connected to the NGFI network. The functional split introduced by the NGFI allows the fronthaul to be packetized and transported in the packet-switched network. In this manner, the fronthaul proposes the advantages as:

- Efficiency and flexiblility
- Its bandwidth depends on the traffic
- Permits the multiple mapping relationship between BBUs and RRUs
- The data rate becomes independent of the antenna number.

Regarding [68], [69] and [70] the functions in the BBU which carry out the Cell processing and the UE processing are moved from BBU to the RRU. The different functions are listed in table 1.9. To reduce the bandwidth and make possible the packetized CPRI or

[6]RRU is equivalent to the RRH

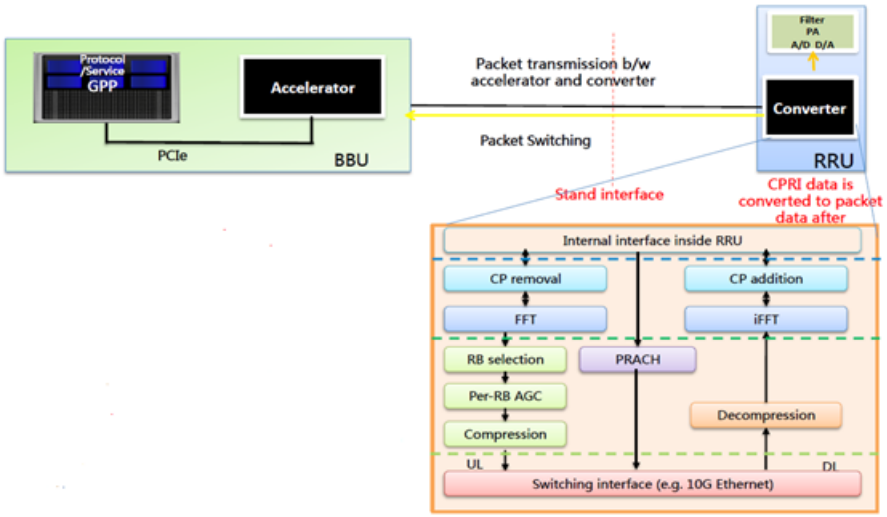

Figure 1.37: Function spilt proposed by China Mobile

the CPRI over Ethernet, China Mobile proposes to group some functions in a converter that is included in the RRU (figure 1.37). Ethernet has been proposed as candidate to transport the packets generated by the accelerator and the convertor. Indeed, the Ethernet network will provide flexibility, scalability and will facilitate the management and the control of the NGFI.
In order to avoid the constraints of stringent delay requirements like HARQ, it has been proposed the shifting of the MAC processing from BBU to RRH [69]. In this way, only the function of Radio base station control and Management and the Backhaul transport remain at the BBU (figure 1.38).
NGFI transmission jitter is defined as the fluctuation in the time taken for data to be transmitted between RCC and RSS. A challenge of the NGFI is to reduce this jitter and provide the synchronization of the data on Ethernet. The works on NGFI are ongoing and the advancement of the interface depends on the standardization of 5G.

1.6 Conclusion

This chapter has been devoted to the state of the art in order to understand the different technologies and the future perspectives that have intervened in this work. This chapter begins by a brief presentation of the current RATs: 2G, 3G, 4G and the future RAT standard that is 5G. The presentation of these RATs and the technologies used in the mobile backhaul to transport the data of RAN to the core network, permit to identify the challenges of the future RAN architecture. Then a new concept of RAN called C-RAN is presented. The different advantages of C-RAN relative to the traditional RAN are listed. This new architecture consists to move up the BBU,

Functions to shift from BBU to RRU	
Decoupling Fronthhaul bandwidth from number of antennas	**Decoupling Cell/UE processing**
• Downlink antenna mapping • Uplink antenna mapping • Fast Fourier Transform (FFT)/Inverse FFT (IFFT) • Channel estimation and equalization	• Prefix Cyclic addition/removal • Cell Specific Reference Signal, Primary Synchronization Signal, Secondary Synchronization Signal • Fast Fourier Transform (FFT)/Inverse FFT (IFFT) • Physical Broadcast Channel processing (PBCH) • Physical Downlink Shared Channel processing (PDSCH) • Physical Downlink Control Channel processing (PDCCH) • Physical Uplink Shared Channel processing (PUSCH) • Physical Uplink Control Channel processing (PUCCH)

Table 1.9: Functional split in the NGFI

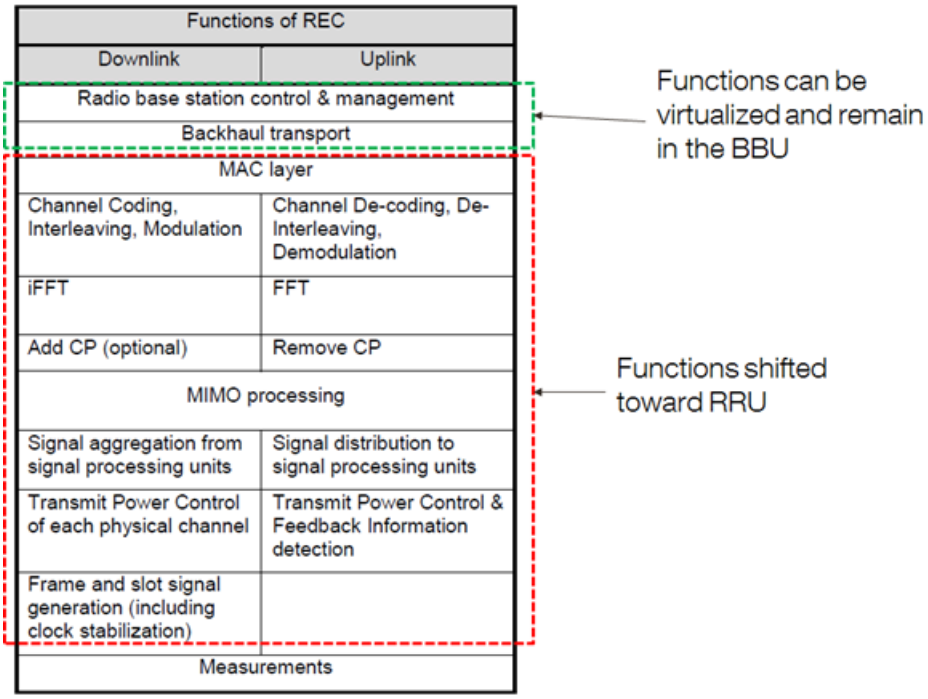

Figure 1.38: CPRI Functions decomposition of the BBUs indicatated the functions shifted to the RRU

situated at the antenna site in the traditional RAN, to CO. The consequence of the localization of the BBU to the CO is the apparition of the new network segment between the BBU and the RRH called fronthaul. The fronthaul is a digital interface based on the D-RoF technology. It is defined by the protocols like CPRI (most used) OBSAI, and ORI. The fronthaul segment has stringent requirements in terms of jitter ($maximum\ jitter\ contribution\ on\ frequency\ clock\ deviation \leq 2ppb$), BER ($BER \leq 10^{-12}$), data rate(high date rate), latency and time parameters. According to the different requirements on the fronthaul link, the optical fiber remains the best candidate to support this interface. Since the optical fiber is a scarce resource, it must be optimized. Indeed, the WDM technique is used to multiplex several fronthaul links on one or two fibers. This technique is the base of different studied solutions in the fronthaul deployment. These fronthaul solutions are divided into three main categories which are:

- **Passive solution:** it is a low cost solution and is easy to implement. The drawback of this solution is that it does not have a monitoring or a management system in order the administrate the fronthaul links
- **Semi active Solution:** it is the solution used by ORANGE. It consists of an active device generally situated in the CO. It also a low cost solution and brings a monitoring system which allows the detection of failure on the optical link

- **Active Solution:** it consists of two active devices localized on the antenna site and the CO. This solution brings a little more flexibility and security to the fronthaul links. His using in the deployment of C-RAN depends on the SLAs that the fiber provider proposes.

The future of the fronthaul is addressed through the NGFI and the new functional split of the RAN equipment. The function split consists to move some function performs by the BBU to the RRH. The NGFI is necessary to the deployment of the future 5G RAT.

Chapitre 2 :

Jitter parameters on a fronthaul link

2.1 Introduction

Since the fronthaul link uses the D-RoF technology, it is obviously affected by the jitter phenomenon. The standards which define the fronthaul have requirements about this perturbation that affects the digital communication systems. In this chapter, the jitter has been defined and the specifications about the different requirements are done. In addition, innovative setups to introduce and to measure the jitter have been implemented. The influence of jitter on the radio frequency deviation is studied. At the beginning of this study a theoretical analysis is carried out on a classical PLLs to have a reference and to understand some obtained results and finally, the influence of jitter on the frequency deviation is done on a commercial eNodeB in order to have an overview of the jitter impact on a real equipment which are presented in the ORANGE network.

2.2 Jitter description

2.2.1 General description

Jitter is the physical phenomenon which manifests by a phase variation of signal. This phase variation has wrong results on the quality of high speed digital transmission because it can cause the error decision at the reception and the loss of clock signal. In this chapter, a definition and the description of jitter are given, and then its impact on the fronthaul link is studied.

Jitter is a variation of phase at the significant moment of the signal. It concerns the phase variation above 10 Hz. When the phase variation is below 10 Hz, we talk about wander. This phase perturbation leads or lags the time decision in the digital system. The consequence of this error time decision is the appearances of errors in the digital transmission [71]. When an eye diagram is observed on an oscilloscope, the jitter is responsible to the horizontal closure of this eye diagram (figure 2.2). The following figure (2.1) illustrates the consequences of jitter.

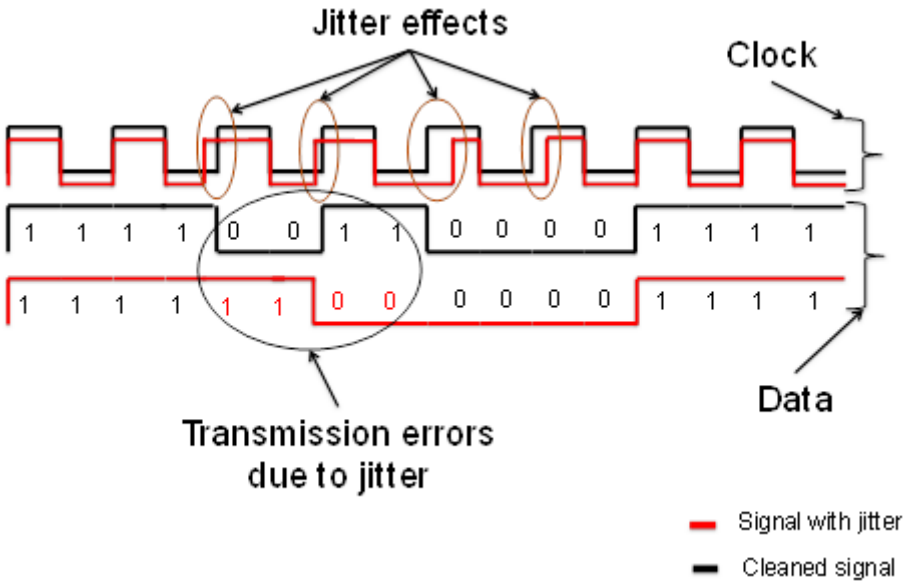

Figure 2.1: Jitter effects on digital transmission

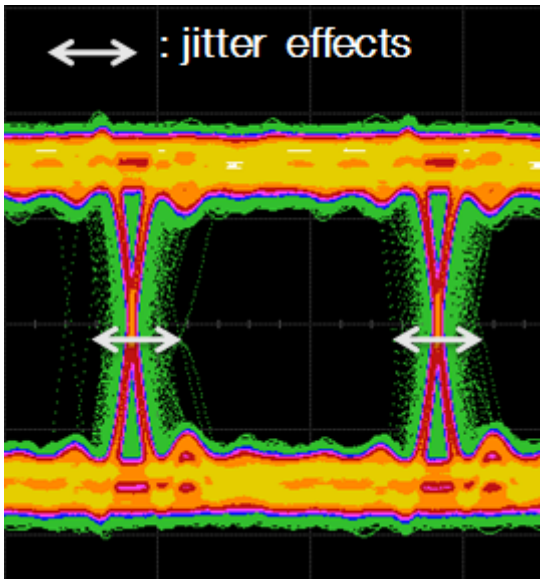

Figure 2.2: Jitter effects on an eye diagram

Figure 2.1, shows how the errors are introduced in a digital signal and figure 2.2 shows the jitter effects on an eye diagram. This figure highlights a horizontal closure of an eye diagram due to the jitter which causes a variation of edge positions (rising and falling edges) and therefore the loss of clock. We can consider that the detection of signal is done on the rising edge on figure 2.1. The jitter leads or lags the rising edges of the clock signal and introduces in this way the errors on the digital transmission. Fronthaul is a high speed digital data transmission (up to 10 Gbit/s, nowadays in practice). Before to study the effects of jitter on fronthaul, it is expected to define and give the different parameters

of jitter.
In the classic literature, jitter is divided in two parts [72] :

- **Deterministic Jitter (DJ)**: it is always bounded in amplitude. It also has several components which are:
  - **Periodic Jitter (PJ)**: Also called Sinusoidal jitter (SJ), it manifests by a periodic or sinusoidal variation of signal edges. Generally, the sources of PJ are electromagnetic interference (EMI) such as power supplies.
  - **Bounded Uncorrelated Jitter (BUJ)**: It is caused by the cross-talk of signal of different circuits. These signals are bounded by uncorrelated with the transmitted signals. Generally, the sources of BUJ are noise of power supply or the EMI.
  - **Data Dependent Jitter (DDJ)**: This type of jitter is caused by the transmitted data pattern on the link. it is subdivided into two parts:
    - **Duty Cycle Distortion jitter (DCD)**: It is the period variation of consecutive alternate patterns.
    - **Inter-Symbol Interference jitter (ISI)**: It is caused by the difference of time symbol in the transmission link.
- **Random Jitter (RJ)**: it is essentially caused by the thermal noise. RJ is unbounded and it represented by a Gaussian density function in most cases. It can be represented by a value Root Mean Square (RMS) or by a peak to peak value. Considering that RJ is unbounded the quantification of the peak to peak value must be determined by a criterion. This criterion is the Bit Error Rate (BER)

The Total Jitter (TJ) is the combination of DJ and RJ. This value is given in peak to peak value. The following figure gives a schematic representation of jitter.

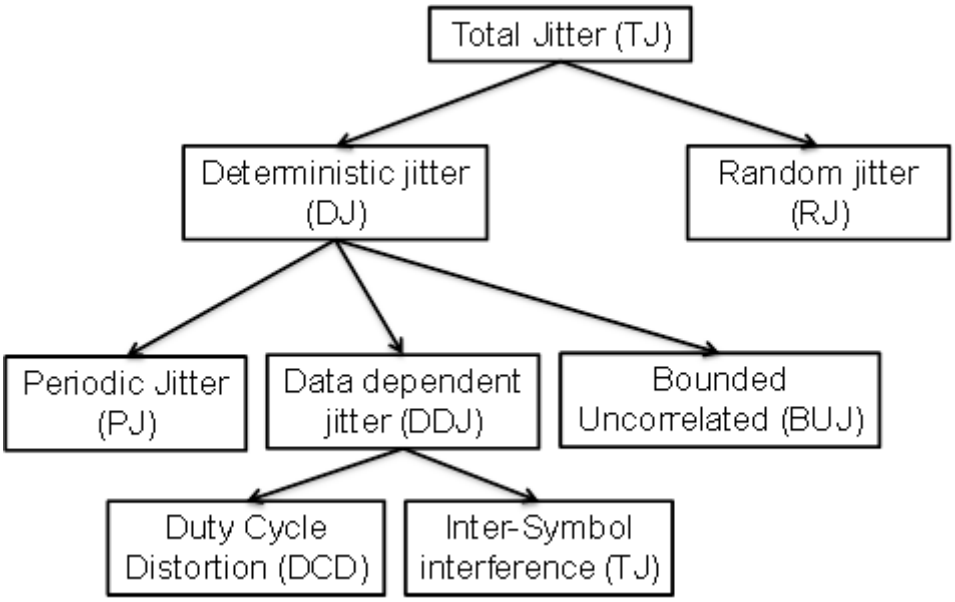

Figure 2.3: Jitter components

In addition to the decomposition of jitter, international standards [73] define and specify the limits of three categories of jitter and wander about the network equipment. These three categories are [74] :

- **Jitter tolerance** : is the minimum jitter amplitude that equipment should tolerate at input for error-free.
- **Jitter transfer** : it is the ratio between the input jitter and the jitter that is provided at the out of equipment.
- **Jitter generation** : it is the maximum quantity of jitter generated by the equipment

2.2.2 The measurement units of jitter

To distinguish the measurement units of jitter, two domains must be considered. Indeed, the measurement of jitter can be performed in the spectral domain and in the temporal domain. In the spectral domain, the measurement is carried out by a spectrum domain and the measurements concern only the means values and not the peak to peak value. The measurement units for this kind of measurement are the second (s) or the Hertz (Hz). In the temporal domain, the measurements are performed by the oscilloscope and concern both kinds of measurement mean and peak to peak. Also, the jitter measurement unit is either in second (s) or in Unit Interval (UI). The UI represents the period of the signal. It can be also represented by one bit in the eye diagram as shown by the figure 2.4.

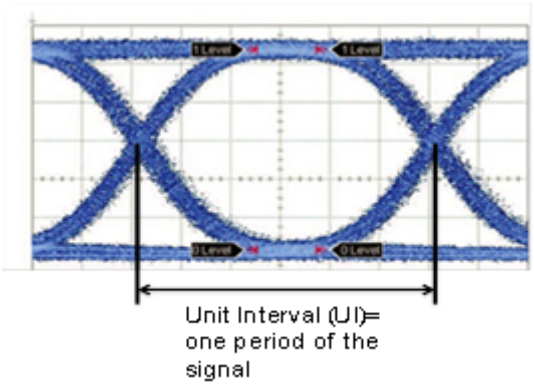

Figure 2.4: Eye diagram representing an Unit Interval (UI)

Generally, the jitter is measured in second (s) or UI. On the phase representation, a UI represents 2π In following, without precision, we can consider that the jitter is measured in UI. To understand the jitter effect and to simplify the mathematical representation, we consider that the signal clock is a sinusoidal waveform. The clock of signal (Clk) can be represented by the following simplified formula :

$$Clk = A\sin(\omega t + \theta) \tag{2.1}$$

Where :

- A : is the amplitude of the clock signal
- ω : is the angular frequency of the clock signal.
- θ: is the phase of clock signal.

Remember that the jitter is the variation of the phase θ and this fluctuation can be a time function $\theta(t)$.

$$Clk = A\sin(\omega t + \theta(t)) \tag{2.2}$$

Now the generalities have been drawn, some details about the SJ and RJ components are going to be shown in the next section because they are the most influential parameters in a fronthaul link.

2.2.3 Jitter specifications of fronthaul standards

2.2.3.1 Sinusoidal jitter (SJ)

All three standards OSAI CPRI and ORI, have the same specification about the tolerance of SJ. Indeed, the SJ for these standards is based on XAUI receiver interface

defined by IEEE [75]. Figure 2.5 presents the single tone sinusoidal jitter mask for the free standards.

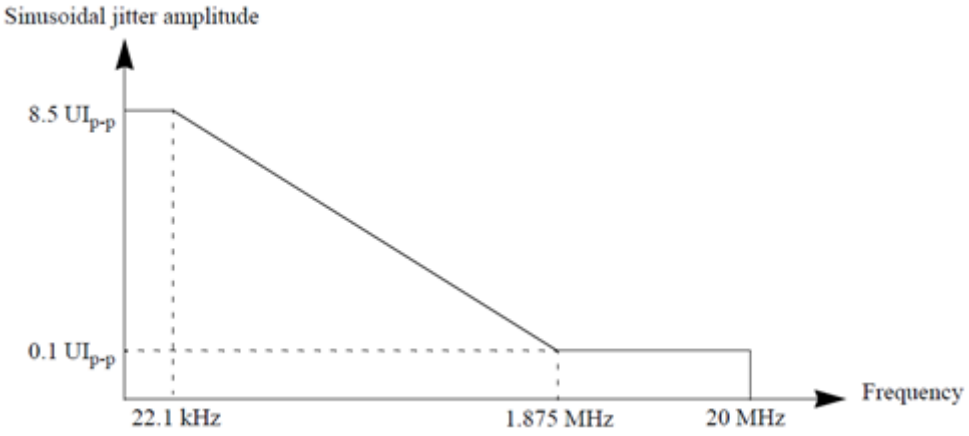

Figure 2.5: Single tone sinusoidal jitter mask

2.2.3.2 OBSAI

The total Jitter (TJ) for OBSAI is specified by the a BER of 10^{-15}. Table 2.1 summarizes the jitter parameters [76].

	Jitter Amplitude tolerance on transmitter (UI_{p-p})	**Jitter Amplitude tolerance on receiver** (UI_{p-p})
Deterministic jitter (DJ)	0.17	0.37
DJ+ Random Jitter (RJ)	N/A	0.55
Total Jitter (TJ)	0.35	0.65

Table 2.1: Jitter Characteristics for OBSAI interface

- Where UI_{p-p} means UI peak to peak.

2.2.3.3 CPRI and ORI

CPRI and ORI have the same specification in terms of jitter because ORI is based on CPRI. This jitter is specified by a BER of 10^{-12}. Table 2.2 draws the jitter specifications for the both standards. CPRI and ORI.

	Jitter Amplitude tolerance on transmitter (UI_{p-p})	**Jitter Amplitude tolerance on receiver (UI_{p-p})**
Deterministic jitter (DJ)	0.17	0.37
DJ+ Random Jitter (RJ)	N/A	0.55
Total Jitter (TJ)	0.35	0.65

Table 2.2: Jitter Characteristics for CPRI and ORI interfaces

2.3 Mathematical representation of jitter

The mathematical jitter aspect permits the representation of jitter and studies the effects and the consequences of this phenomenon by the calculation or by the simulation.

2.3.1 Determination of the peak to peak total jitter value (TJ)

To obtain the peak to peak value of the total jitter, the RMS RJ must be converted. A constant factor α is defined in function of BER. The calculation of this constant factor α and the TJ are given in the following section. This constant is determined by the following equation :

$$BER = \frac{1}{2}\, erfc(\sqrt{2}\alpha) \tag{2.3}$$

$$BER = \frac{1}{2}\int_{\sqrt{2}\alpha}^{\infty} e^{-t^2}\ \mathrm{d}t \tag{2.4}$$

$$\alpha = \frac{1}{\sqrt{2}}\, erfc^{-1}(2BER) \tag{2.5}$$

$$TJ = DJ + \alpha RJ_{RMS} \tag{2.6}$$

The relation between peak to peak TJ and RMS random jitter value is given by the equation 2.6. The decomposition of jitter describes above is the conventional representation found in the general literature. In the $CPRI$ specification, the details about jitter components are different from the convention. The TJ is divided into three parts and is represented by the formula 2.7 :

- Deterministic Jitter (DJ)
- Periodic Jitter (PJ)

- Random Jitter (RJ)

$$TJ_{CPRI} = RJ + DJ + SJ \tag{2.7}$$

The used oscilloscope measures the jitter with a conventional representation which is different to that proposed by the $CPRI$ specification. It is necessary to map the both representation in order to have a correspondence between the value of $CPRI$ specification and the measured jitter. To solve this issue, a discussion is addressed in the *section IV.1* of this chapter.

2.3.2 Sinusoidal jitter (SJ)

The SJ is a jitter that represents by a sinusoidal shape the variation of clock edges of a digital signal. The main parameters are the amplitude of this sinusoidal and its frequency. The frequency is measured in Hz and the amplitude is measured in UI because the latter is a temporal variation. When the Sinusoidal Jitter (sinusoidal variation of signal phase) appears on the signal, the clock can be written like the below formula 2.8 :

$$Clk = A\sin(\omega t + 2A_j\pi\sin(\omega_j t + \varphi)) \tag{2.8}$$

$$\theta(t) = 2A_j\pi\sin(\omega_j t + \varphi)) \tag{2.9}$$

Where :

- A_j : is the amplitude of the SJ measured in UI.
- ω_j : is the angular frequency of the SJ.

One important parameter is the Phase Changing Speed (PCS). This parameter is important for a Clock Data Recovery (CDR) in order to track the phase. It corresponds to the derivative of Sinusoidal Jitter ($\theta(t)$).

$$\frac{\mathrm{d}\theta(t)}{\mathrm{d}t} = 2A_j\pi\omega_j\cos(\omega_j t + \varphi)) \tag{2.10}$$

2.3.3 The random jitter (RJ)

The RJ is an unbounded phenomenon and it is mathematically represented by a Gaussian probability distribution function :

$$PDF_{RJ}(x) = \frac{1}{\sigma\sqrt{2\pi}}\, e^{\frac{(x-\mu)^2}{2\sigma^2}} \tag{2.11}$$

Where :

- μ : is the mean.
- σ : is the standard deviation.

Since the RJ is unbounded, its real quantity is infinite. But it is possible to estimate a value of this quantity by using the BER as reference. The BER is the probability defined from the PDF_{RJ}

$$BER(x) = \frac{1}{\sigma\sqrt{2\pi}} \int_{x}^{\infty} e^{\frac{u^2}{2\sigma^2}} \, \mathrm{d}u \tag{2.12}$$

The RJ is generally expressed as a function of the standard deviation σ. To understand this mathematical representation, the following figure is analyzed.

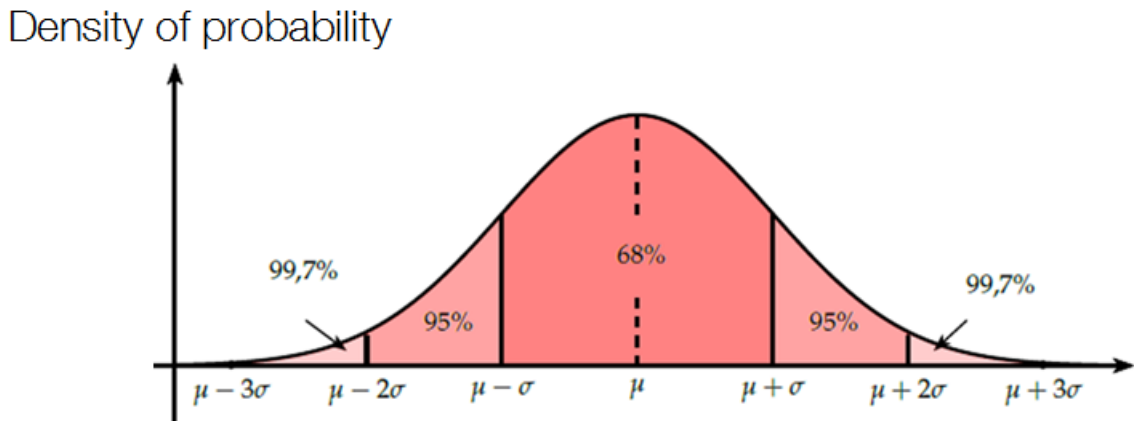

Figure 2.6: Gaussian probability in function of μ and σ

Figure 2.6 depicts the probability that an event occurs relative to the standard deviation σ. For example, considering a range of 2σ, ($[\mu-\sigma, \mu+\sigma]$), the probability that an event appears is 68%. In other hand, there are 32% that an error appears; therefore, this percentage is considered as BER ($BER = 0.32$). The random jitter can be represented by the probability that an event occurs and can be expressed like a following formula :

$$RJ = \alpha(BER)\sigma \tag{2.13}$$

Now we are going to establish the relation between the α parameter and the BER.

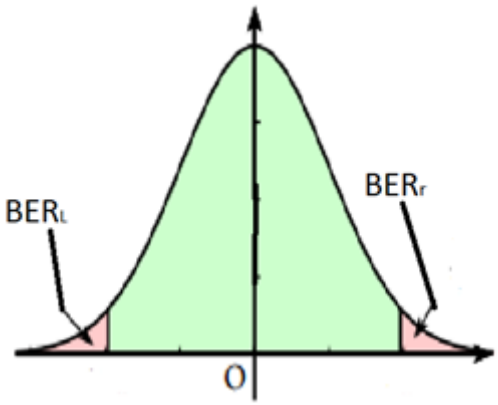

Figure 2.7: BER representation on the RJ curve

The above figure illustrates the BER_L and the BER_r. It is the probability concerning respectively the left tail and the right tail of Gaussian curve. The sum of BER_L and BER_r constitutes the total contribution of RJ with an accuracy defined by the BER. If PRJ is the probability based on the PDF_RJ and X a random variable, we have:

$$BER_L(x) + BER_r(x) = P_{RJ}(|X| \geq x) \tag{2.14}$$

Taking into consideration that the PDF_{Rj} is symmetric, the BER_L and the BER_r are equal. Therefore, the total RJ contribution can be characterized by $2BER_r$.

$$BER_L(x) = BER_r(x)$$

$$2BER_r(x) = P_{RJ}(|X| \geq x)$$

Therefore the total $BER(x)$ is:

$$BER(x) = P_{RJ}(|X| \geq x)$$

Carrying out the variable transformation :

$$y = \frac{u}{\sigma\sqrt{2}}$$

$$BER_r(x) = \frac{1}{\sigma\sqrt{2\pi}} \int_x^{\infty} e^{y^2} \, \mathrm{d}y$$

$$BER_r(x) = \frac{1}{2} \, erfc(x)$$

Considering that $u = \alpha_1\sigma$ the variable y becomes $y = \alpha/2$:

$$BER_r(x) = \frac{1}{2}\, erfc(\frac{\alpha_1}{\sqrt{2}})$$

Therefore

$$\alpha_1 = \sqrt{2}\, erfc^{-1}(2BER_r)$$

According to the equation 2.13, the RJ_r can be written as the following expression :

$$RJ_r = \sqrt{2}\, erfc^{-1}(2BER_r)\sigma$$

Therefore, the total RJ considering the $BER(x)$

$$RJ = 2\sqrt{2}\, erfc^{-1}(2BER_r)\sigma \tag{2.15}$$

where α described in equation 2.13 is:

$$\sigma = 2\sqrt{2}\, erfc^{-1}(BER) \tag{2.16}$$

Here the standard deviation σ represents the RMS value of RJ. The following table 2.3 gives the correspondence between the constant factor α and the BER [77].

BER	α
10^{-6}	9.507
10^{-9}	11.996
10^{-12}	14.069

Table 2.3: Constant factor α for different BER

The peak to peak TJ depends on the BER precision of the RJ. In terms of probability density function, the TJ is the convolution of PDF_{RJ} and of the PDF_{DJ}

$$\delta(x-\mu_l) + \delta(x-\mu_r) * \frac{1}{\sigma\sqrt{2\pi}}\, e^{\frac{x^2}{2\sigma^2}} = \frac{1}{\sigma\sqrt{2\pi}}\, e^{\frac{(x-\mu_l)^2}{2\sigma^2}} + \frac{1}{\sigma\sqrt{2\pi}}\, e^{\frac{(x-\mu_r)^2}{2\sigma^2}} \tag{2.17}$$

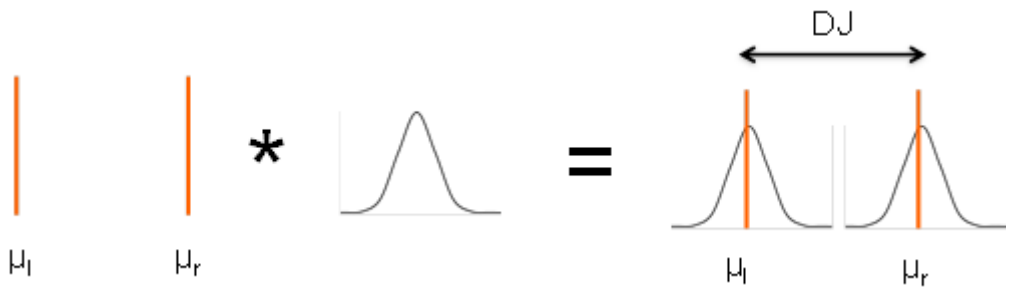

Figure 2.8: Dual-Dirac method to estimate the TJ

$$TJ = DJ + \alpha(BER)\sigma \tag{2.18}$$

The mathematical representation of jitter allows us understanding the impact of this phenomenon on fronthaul link. The following section deal with the influence of jitter on a fronthaul segment. It is necessary to understand the influence of jitter on a fronthaul link.

2.4 The jitter impact on the fronthaul link

Remember that the jitter can be represented in the time domain and the spectral domain. In the spectral domain, only the average value in Hz is considered. In the time domain, a Root Mean Square (SMS) value and the peak to peak value can be measured. In this section, we study the impact of the jitter on the fronthaul link. Noticing that in the time domain, the representation of the jitter described by $CPRI$ is different to the conventional representation used by our oscilloscope, it is necessary to have a correspondence between the two kinds of representation. At the beginning of this section, an equation allows converting the conventional representation to CPRI jitter representation is demonstrated. Then, the setup and the results of the study about the influence of the jitter on fronthaul are presented.

2.4.1 Correspondence between the representation of the jitter in CPRI specification and its traditional representation

Fronthaul is generally a high-speed data link. Therefore, it is natural that the jitter has an impact on fronthaul link. At this section, the jitter measurement technic is investigated in order to bring a correspondence between the values of jitter in $CPRI$ specification and the jitter values which are measured by the oscilloscope. Remember that in the CPRI specification, the TJ is constituted by the DJ, the RJ and the SJ. In the conventional

representation, the DJ is composed by the BUJ, DDJ and SJ. The measured DJ is not an addition between three components. It is usually determined by an estimation based on Dual-Dirac model. This method can be fitted to a Gaussian PDF. The Dirac functions are the mean of the Gaussian PDF. The DJ represents the means of the Gaussian PDF used to fit the tail of the TJ 2.9.

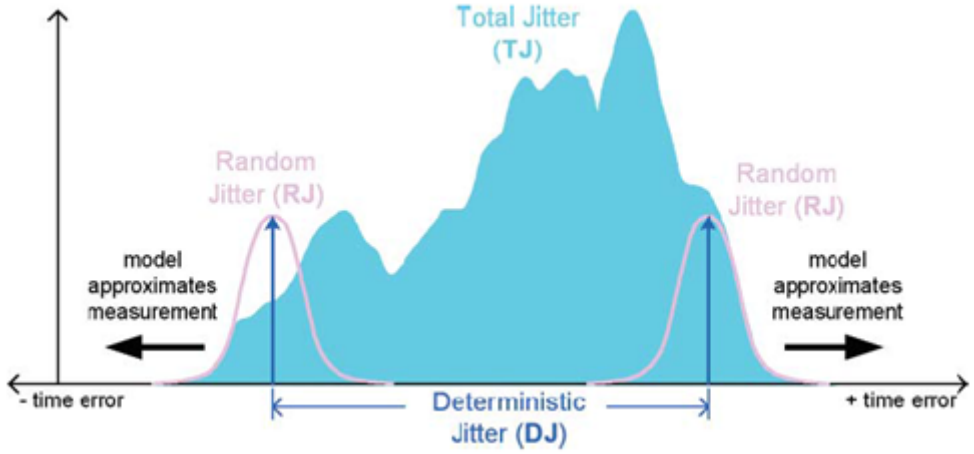

Figure 2.9: Dual-Dirac method to estimate DJ and TJ

The conventional decomposition of jitter is based on the IUT recommendations O.171 [78] and O.172 [79]. No specific technic is described to calculate the different kinds of jitter. The DJ peak to peak (DJ_{p-p}) represents the quantity of DJ which takes into consideration all different components of DJ. Its determination is possible if some conditions are met [80]. For example, when the DJ is exclusively caused by the DDJ, it is possible to calculate the DJ by comparing the average transition times of the repeating pattern [81]. The DJ obtained by Dual-Dirac method and the DJ_{p-p} can have different value. Considering that no specification or no reference is given by the $CPRI$ specification about how to determine the DJ, we suppose that the DJ is estimated by this Dual-Dirac method. At following, without a specific mention, the DJ is the deterministic jitter calculated with the Dual-Dirac method. Our equipment uses this method to estimate the deterministic jitter. In this case, the TJ_{CPRI} equals to the addition of the measured TJ (equation 2.19) and the SJ.

$$TJ_{CPRI} = TJ + SJ \tag{2.19}$$

2.4.2 The impact of jitter in a fronthaul linkn

In the previous parts, the requirements in terms of jitter are described for the fronthaul link. The influence of jitter will be studied through an experimental setup.

The goal of this study is to understand the influence of the jitter and have knowledge on the manner that the jitter can impact the performance of the fronthaul. At first, the experimental setup is described. Some important details to realize this setup are given. Finally, the results will be presented and discussed.

2.4.2.1 Description of setup

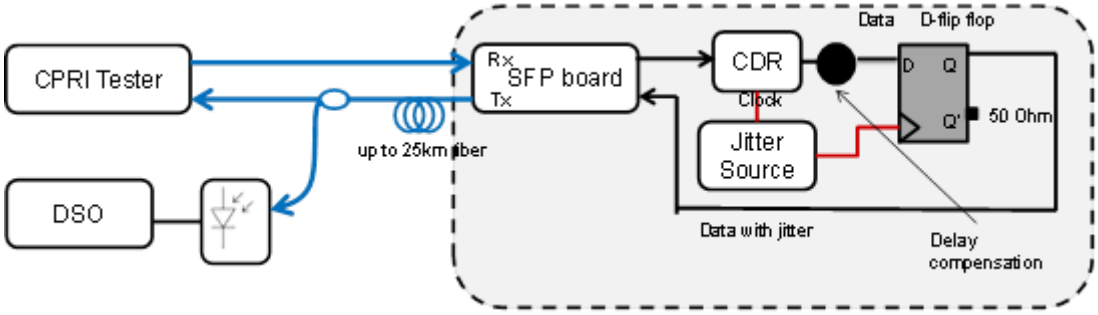

Figure 2.10: Setup to introduce the jitter in the fronthaul

The objective of this experimental setup is to introduce jitter on the fronthaul link and to measure the jitter and the BER. Indeed, several devices (figure 2.10) permits to reach this objective :

- **CPRI Tester** : This equipment permits to generate the $CPRI$ frames. It is possible to choose the length of the $PRBS$ (until $PRBS$ 23) that will be charged in the payload but in $CPRI$ all data are mixed with at $PRBS$ 31 in order to assure the recovery clock for a long distance.
- **SFP board** : A SFP is plugged in the SFP board. It permits to convert the optical signal to electrical signal and vis-versa. It is necessary to make this conversion because the other devices operate in electrical domain.
- **Clock Data Recovery (CDR)** : it allows recovering the clock of signal and then separates the clock and the data signal. It can operate until 2.5 $Gbit/s$.
- **Jitter Source** : It permits to introduce the jitter in the clock signal. Several kind of jitter can be mixed to the clock such as: Sinusoidal Jitter, Random Jitter and Bounded Uncorrelated Jitter.
- **Delay shifter** : The jitter source introduces a delay between the clock and the data. Indeed, when the length of coaxial cable is different between the path followed by the clock and the path followed by the data, a delay appears between data and

clock. This delay can introduce errors in the transmission. In order to avoid these effects of the introduced delay, a delay shifter is used. This delay shifter permits to adjust the phase of the signal before the introduction of jitter.

- 13 GHz **D-flip flop** : It permits the recombination of the clock and the data.
- **Digital Storage Oscilloscope (DSO)** : The oscilloscope is able to measure and separate the different components of the jitter.
- **Optical to Electrical Converter (OEC)** : It is a photodiode. The setup needs the photodiode which intrinsically has low noise and low jitter. The OEC used in the experience can operate from 622 $Mbits/s$ to 12.5 $Gbit/s$. It corresponds to the actual data rate range of fronthaul.

Up to now, the common data rate in the fronthaul link is 2.45 $Gbit/s$. According to this ascertainment, the $CPRI$ tester is set at 2.45 $Gbit/s$. the $CPRI$ tester provides an optical signal which is converted in electrical by the SFP board. This signal is received by the CDR which separates the clock and the data in two different ways. The clock is recovered by the jitter source which introduces it the jitter. The data signal is transmitted to the flip-flop D. The different lengths of coaxial cable and the processing of jitter source introduce a delay between clock (to trig the flip-flop D) and the transmitted data. This delay creates errors at the decision time during the acquisition of signal. The output of jitter source containing the jitter trigs the flip-flop D. To cancel the effects of this introduced latency, a delay compensator is placed between the data output of the CDR and the flip-flop D. The calibration of this delay compensator is done without an introduced jitter. A delay is added until the free error transmission is reached. The output of jitter source containing the jitter trigs the flip-flop D. The flip-flop D recombines the data and the clock containing the jitter and transmits the electrical signal to the to SFP board which converts it to an optical signal. Once the conversion is made, the signal is sent up to 25 kms. After the crossing of the transmission fiber, the signal is separated by two by a power splitter. The $CPRI$ tester receives a part of this signal to perform the calculation of BER. The other part is recovered by the OEC which converts to the electrical signal. This signal attacks the DSO which carries out the jitter measurements.

2.4.2.2 Experimental results

The system operates at 2.45 $Gbit/s$. The test consists to introduce the jitter such as described in figure 2.10. For any amplitude of SJ introduces, the jitter measurements and the measurements of BER are performed. At first, only the SJ jitter is introduced on the fronthaul link. The DSO cannot capture all the phenomenon of the jitter at low frequency

because it has not enough deep memory. In order to determine the minimum frequency of jitter that can be measured, some characteristics of DSO must to be considered. These characteristics are the deep memory and the sampling rate. After calculation, the minimum frequency is approximately 800 Hz. Several sinusoidal single tones have been tested but for the clarity of the figure 2.11, only some of curves corresponding to the measured SJ are presented. The following figure summarizes the results.

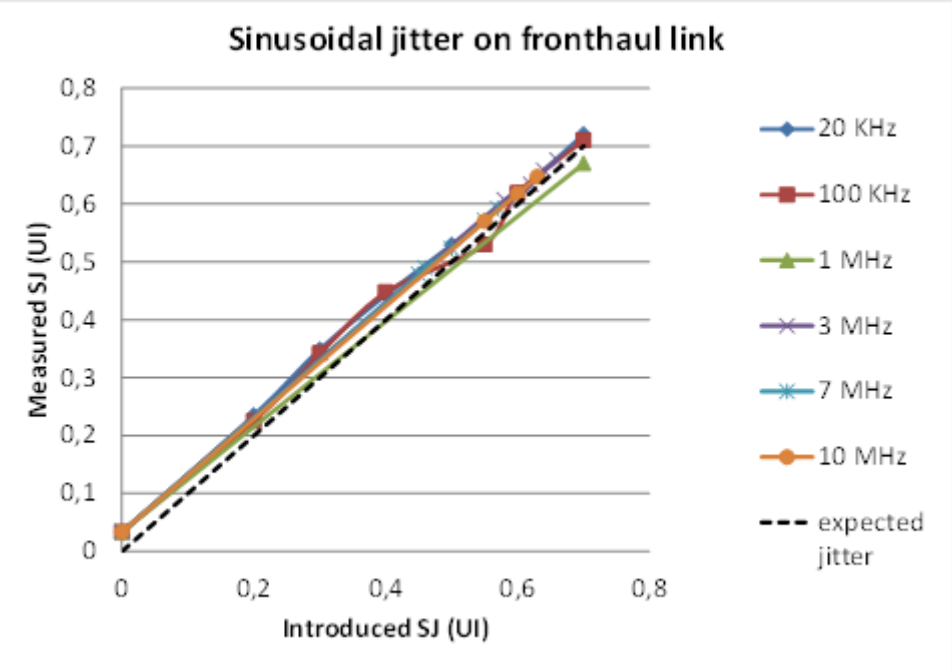

Figure 2.11: Result of sinusoidal jitter

Figure 2.11 shows that the intrinsic SJ of this dispositive is 0.03 UI. All curves are almost superimposed and the quantity of measured jitter is approximately the same that the expected jitter. To justify the reliability of this dispositive, the Root Mean Square Deviation (RMSD) between the measured SJ and the excepted jitter are calculated. This $RMSD$ concerns the range of the SJ defined by: $[0\ Hz, 20\ MHz]$.

$$RMSD = \sqrt{\frac{\sum_{i=1}^{N}\sum_{j=1}^{M}(\widehat{x}_{i,j} - x_{i,j})^2}{MN}} \tag{2.20}$$

Where :

- N is the number of tested frequencies
- M represents the number of samples
- $\widehat{x}_{i,j}$ is the measured SJ corresponding to the i^{th} tested frequency and the j^{th} sample of this frequency (i^{th} tested frequency)

- $x_{i,j}$ is the expected value of SJ corresponding to the i^{th} tested frequency and j^{th} sample of this frequency

After calculation, the $RMSD$ equals to 0.025 and after to have normalized this value the ratio of deviation is approximately 3.6%. This deviation is due to the intrinsic jitter and the transfer jitter of each involved device in this setup. The analysis of figure 2.11 shows that this setup doesn't filter the jitter in the frequency range of $[10\ kHz, 20\ MHz]$ (this test has been performed for 1 kHz). Finally, this setup can be used to introduce the jitter on the fronthaul link because it doesn't filter the SJ and introduces a low jitter deviation.

Generally, the maximum amplitude of the SJ is 0.7 UI (figure 2.11). The fact to add an amplitude of SJ more than 0.7 UI causes the failure of the fronthaul link. The tolerance jitter of the fronthaul has been evaluated below. For this to happen, an operating criterion must be defined. The first criterion which has been defined is the BER. According to the $CPRI$ specification it must be less than 10^{-12} for a functional system. The second criterion is the EVM. According to the 3 GPP recommendations, it must be less than 18% for a $QPSK$ modulation. In the following results, a comparison of SJ between the $CPRI$ specifications and the measured SJ is done. The purpose of this comparison is to know if the actual devices in fronthaul correspond in terms of SJ to the $CPRI$ specifications. The setup described by figure 2.10 is implemented to measure the jitter and the BER.

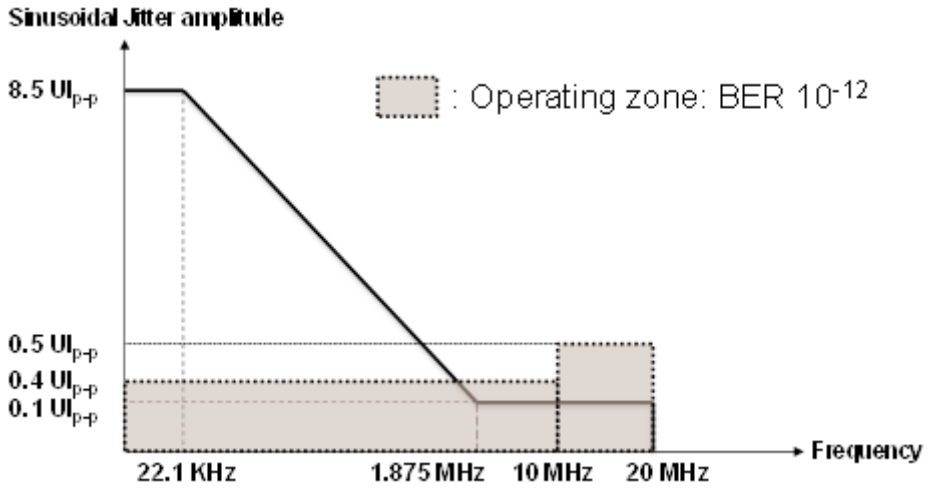

Figure 2.12: Comparison of tolerance SJ between the measured SJ and the CPRI specification

In figure 2.12, the operating zone is delimited by the jitter amplitude which corresponds on a BER equal to 10^{-12}. For the frequencies between $[1\ kHz, 1.5\ MHz]$, the maximum amplitude of the measured jitter permitting to reach a BER of 10^{-12} is 0.4 UI. This

value less than the expected tolerance jitter described in the $CPRI$ jitter. Considering the frequencies between $[1.500\ MHz, 20\ MHz]$ the tolerance jitter describes by the template of SJ is respected. The quantity of measured jitter is more important than the excepted SJ. When the EVM is considered as a criterion of operating, the end to end link is experimented. LTE frames forward through a fronthaul segment and the performance of this system is evaluated by the EVM. To measure the EVM performances of the end to end link, the setup described by figure 2.13 is realized.

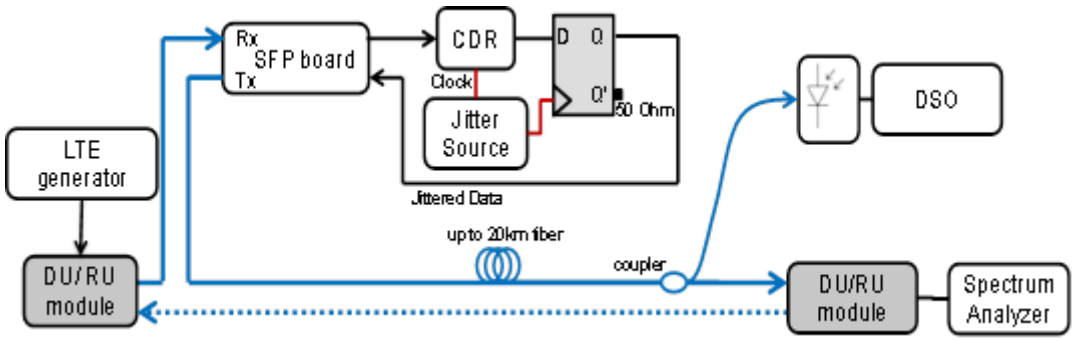

Figure 2.13: Setup of jitter and EVM measurements

This experimental system includes the setup to introduce the jitter on the fronthaul link. In addition, others devices are involved :

- **LTE generator** : It generates the LTE frames.
- **DU/RU Module** : It permits to encapsulate the LTE frames in $CPRI$ frames and make the inverse operation.
- **Spectrum Analyser** : it allows measuring the EVM of signal provided by the DU/RU Module

In this experience, LTE frames are generated by the LTE generator. The payload of LTE frame is modulated in Quadrature Phase Shift Keying (QPSK), 16- Quadrature Amplitude Modulation (QAM) and $64 - QAM$ but only the result with a $QPSK$ is presented. Notice that the results of others modulation formats are the same than these of $QPSK$. The LTE frames are transmitted to the DU/RU Module which encapsulates them in the $CPRI$ frames. Then, the SJ is introduced in the $CPRI$ signal and forward through 25 km of optical fiber. At the reception, an optical power splitter is placed and divided the signal into two. One part of the optical signal is recovered by the DSO. The other part of the signal is sent to the spectral analyser. The Analyser measures the EVM and the results of this experience is depicted by figure 2.13.

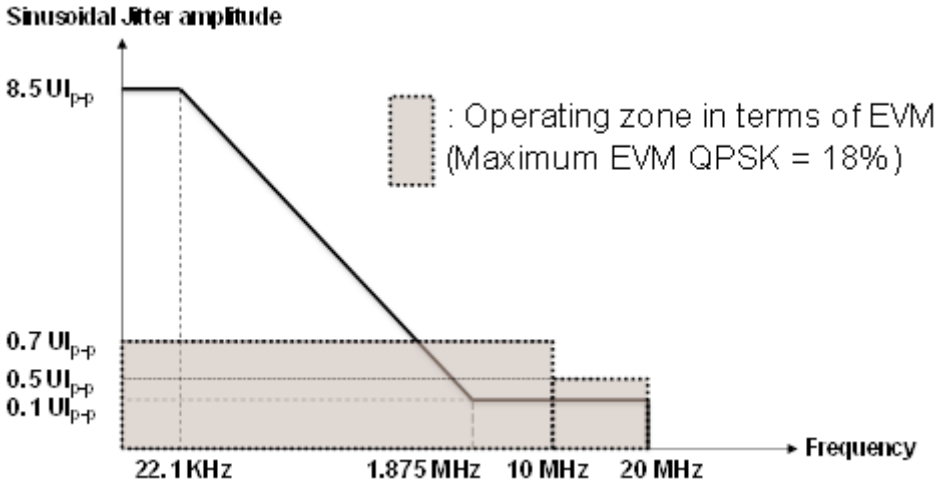

Figure 2.14: Jitter measurements with EVM as operating criteria

The maximum amount of jitter measured that allows the operation of system is 0.7 UI. Above this value, the fronthaul link is failed. The maximum amplitude of jitter to have an operating system in terms of EVM is independent to the frequency unlike the mask of SJ taken as reference. Between 10 MHz and 20 MHz, the amplitude 0.5 UI of SJ corresponds at the maximum amplitude possible to inject in the fronthaul link. It is a limit of the jitter source and it is impossible to introduce SJ up to 0.7 UI. A difference of SJ amplitude is noticed between the both considered criterion BER and EVM. This difference is due to the high resolution of bandwidth. The EVM of end to end link meets the 3GPP recommendations until a threshold of BER equals to 10^{-6}.

The previous analysis shows that for frequency of the SJ from 10 Hz to 1 MHz, the template proposed by the $CPRI$ specification is not respected. To have a better understanding of this observation, a spectral density of the $CPRI$ signal (Non Return to Zero) is studied. In theory, concerning the Non Return to Zero (NRZ) signal, there are not energy at the frequency of the signal but in practice, this signal has a spectral ray at 2.457 GHz (frequency of signal) which allows recovering clock signal.

More the power of this spectral line is high, more it is easy to recover the clock. The principle of the following setup is to introduce SJ on the fronthaul link and to measure the power of the spectral ray at 2.547 GHz. One part of $CPRI$ signal is sent to the spectrum analyser which is able to measure the power of this spectral line. Figure **??** and figure 2.16 describe respectively the setup and the results of the experience

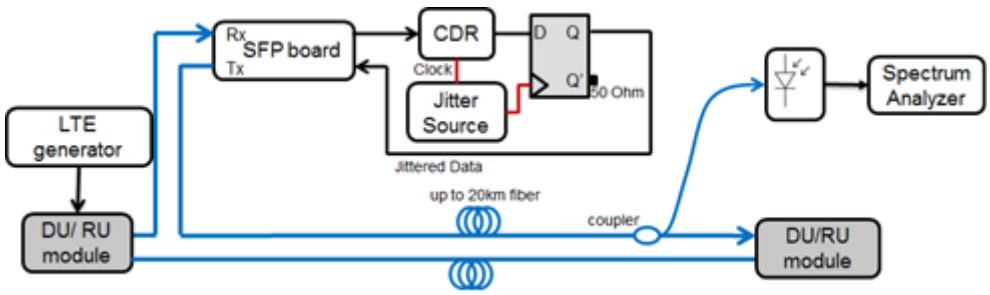

Figure 2.15: Setup to measure the Power of spectral ray at 2.457 GHz

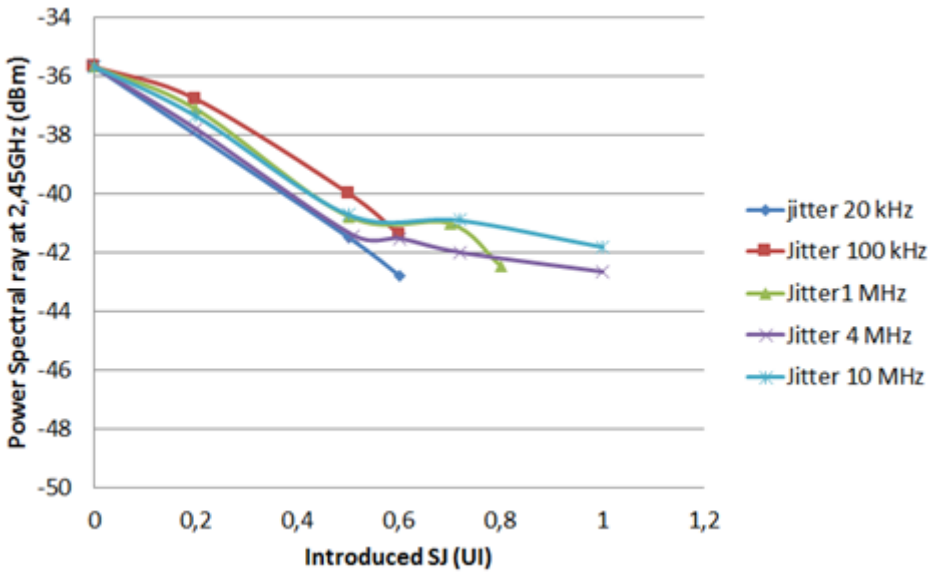

Figure 2.16: Power of spectral line at 2.457 GHz

For any frequency of SJ, the measured power is approximately equal. In other words, the power of the spectral ray at the frequency of the $CPRI$ signal is independent to the frequency of SJ. More the amount of SJ is high, less is the measured power. Indeed, when the jitter is added the power of the ray varies between -41 dBm and -42 dBm. From this power interval the system has difficulty to track the clock of signal. This results highlights and confirm the previous conclusions about the jitter on fronthaul link. In order to reduce the effects of the jitter on the detection of the clock, the line code could be changed. The RZ line code is a proposed candidate because it has a spectral ray at the frequency of signal to facilitate the recovering of the clock signal. The drawback of the RZ line code is that its electronic is more expensive than the electronic of NRZ.

2.4.2.3 Contribution of jitter on the frequency accuracy budget

There exist 2 two kinds of measurement to characterize the jitter in a digital communication. The first is carried out in the temporal domain with an oscilloscope. The jitter measurement in the temporal domain permits to distinguish the RMS value and the peak to peak value of the jitter. The second kind of measurement is performed in the spectral domain. In this domain, only the RMS value is considered and the jitter is measured in hertz. The jitter is represented by the variation of the phase noise. Let Remember that the $CPRI$ specification fixes the contribution of the jitter on the frequency accuracy at 2 ppb. To assess the contribution of the jitter on the frequency accuracy budget, the single side band of the reference clock must be obtained [82]. According to [37], the reference point for the jitter and phase noise specification is the stable clock signal provided at the Service Access Point of the synchronization (SAP_s) illustrated by the following figure 2.17.

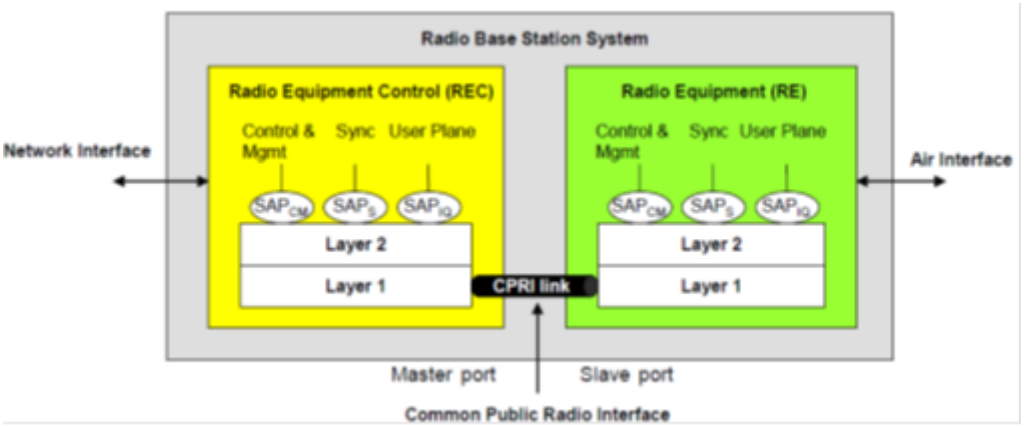

Figure 2.17: Basic Architecture of CPRI

In figure 2.17, the Radio Equipment Control (REC) represents the BBU and the Radio Equipment (RE) represents the RRH. In practice the synchronization of the BBU can be provided either by the backhaul network (network interface) or by the external source clock. The RRH is able to recover the clock signal from the received $CPRI$ signal. Hence, to measure the contribution of jitter from the $CPRI$ signal to the frequency accuracy budget, it is necessary to recover the stable clock signal. Also, as noted in [37], the evaluation of the impact of the jitter on the frequency accuracy is based on the single sideband of the $CPRI$ interface. In the $CPRI$ interface the acquired signal is coded in NRZ (Non Return to Zero). In order to obtain the single side band of the data signal, it is necessary to translate the data NRZ signal from base band to the clock frequency as shown the following formula :

$$S_{ssb}(t) = s(t)\cos(\omega_0 t) - \widehat{s}(t)\sin(\omega_0 t) \tag{2.21}$$

Where :

- S_{ssb} : the single side band.
- $s(t)$: The data signal.
- $\widehat{s}(t)$: The Hilbert transform of s(t).
- ω_0 : The angular frequency of reference CPRI signal.

The following figure 2.18 gives the setup to measure the jitter contribution of the CPRI signal.

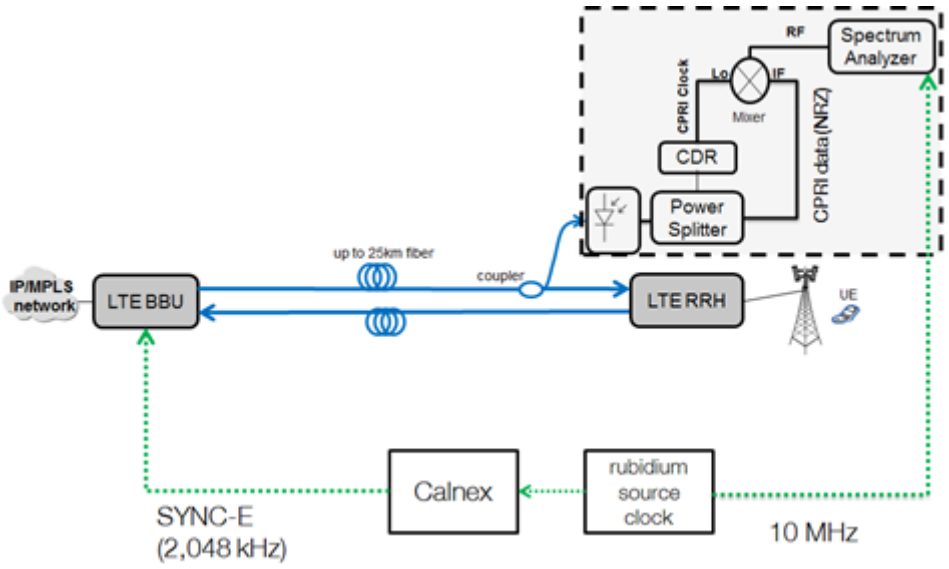

Figure 2.18: Dispositive to measure the impact of jitter on the frequency accuracy budget

In this setup, a Double Side Band mixer is used to translate the data message to the frequency clock. The Local oscillator (Lo) input of the mixer is attacked by the $CPRI$ clock. The $CPRI$ clock is recovered by the CDR. This CDR is able to retime and reshape the clock and the data signal and by the way, the latter provides a stable clock signal. Because of the retiming and reshaping of the signal done by the CDR, a power splitter is put at the output of the photodiode in order to recover the data containing the jitter. The data signal from the power splitter attacks the input IF of the mixer. The result of this operation performed by the mixer is transmitted from the RF output to the spectrum analyzer. Notice that the signal of the RF output is a double side band signal. The particularity of this spectrum analyzer is that it is able to get a single side band signal from a double side band signal. Also, it is able to perform the calculation described by the equation 1.2.

The phase noise of the single side band signal should vary according to the frequency of jitter. Therefore, to complete the study of the impact of jitter on the frequency accuracy budget, SJ is introduced to the fronthaul link (figure 2.19). This study will permit to know what is the amount of jitter on the fronthaul link which meets the requirement (R-18[1]) of $CPRI$ specification.

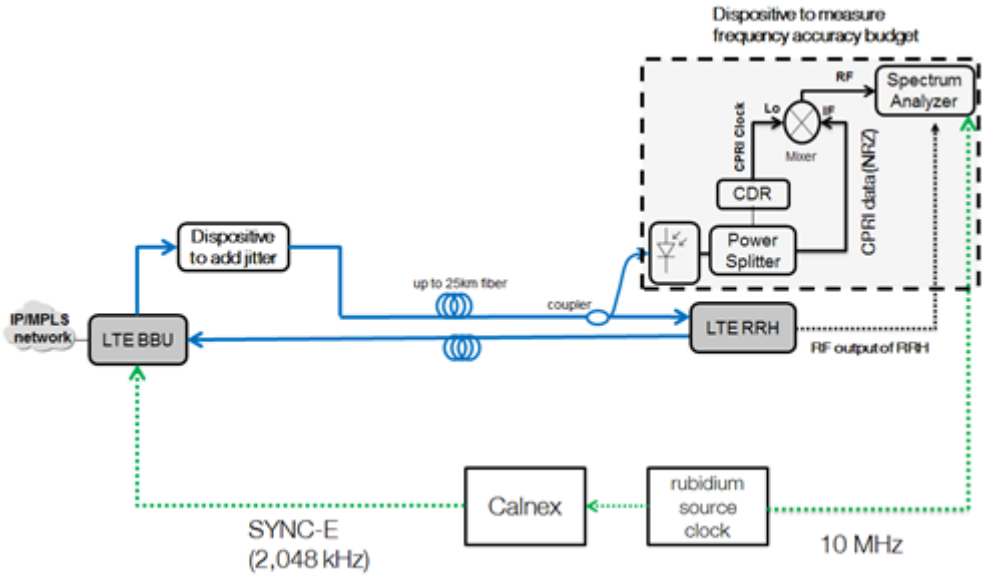

Figure 2.19: Setup to study the jitter impact from CPRI interface to the frequency accuracy budget

To measure the contribution of jitter from $CPRI$ interface to the frequency accuracy, we have to consider a central frequency. This frequency corresponds to that delivered by the CDR and it is equal to 2.457 GHz. The following figure presents the results of the test. First of all, a reference measurement is performed. During this reference measurement, no jitter is introduced on the $CPRI$ link.

Generally, for all frequencies and amplitude of SJ introduced, the maximum contribution of jitter on frequency accuracy budget is not achieved. Indeed, the maximum measured frequency accuracy budget is 1.41 ppb. The low frequencies from 1 kHz to 500 kHz are not a real impact on frequency accuracy budget because the results are approximately equal to the reference measurement. The measurements concerning the frequencies from 500 kHz to 10 kHz have the same trend but a slight increase of the frequency accuracy is noticed when the frequency of the introduced SJ rises. The general conclusion of this study is that only the SJ does not bring enough variation of the phase noise to achieve the limit proposed in specification of $CPRI$.

[1]R-18: Maximum contribution of jitter from CPRI link to the radio base station frequency accuracy budget is 2ppb.

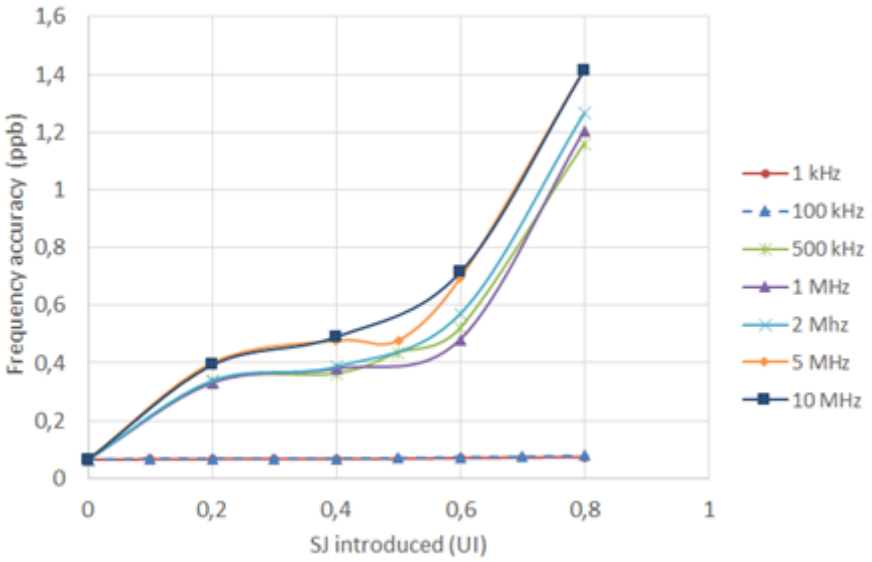

Figure 2.20: Contribution of SJ from CPRI interface to radio base station frequency accuracy budget

2.4.3 Impact of jitter on the LTE radio part

The RRH is the first point which directly communicates with the user equipment. The communication is possible thanks to the radio link. The radio link uses a carrier frequency to transmit and to receive the information. Generally, the frequency is provided by an oscillator. This oscillator is driven by a PLL. The PLL applies an electrical voltage in function of the phase difference to the oscillator. In fronthaul, the clock of the CPRI signal leads the PLL. Indeed, the phase difference which allows providing the tension to the oscillator is based on the phase of the CPRI clock. If the jitter is present in the clock of the CPRI signal, the variation of the phase can cause the variation of the carrier frequency. In this case, the user equipment should have some difficulties to synchronize with the carrier frequency. The figure 2.21 illustrates the effects of the CPRI signal on frequency deviation.

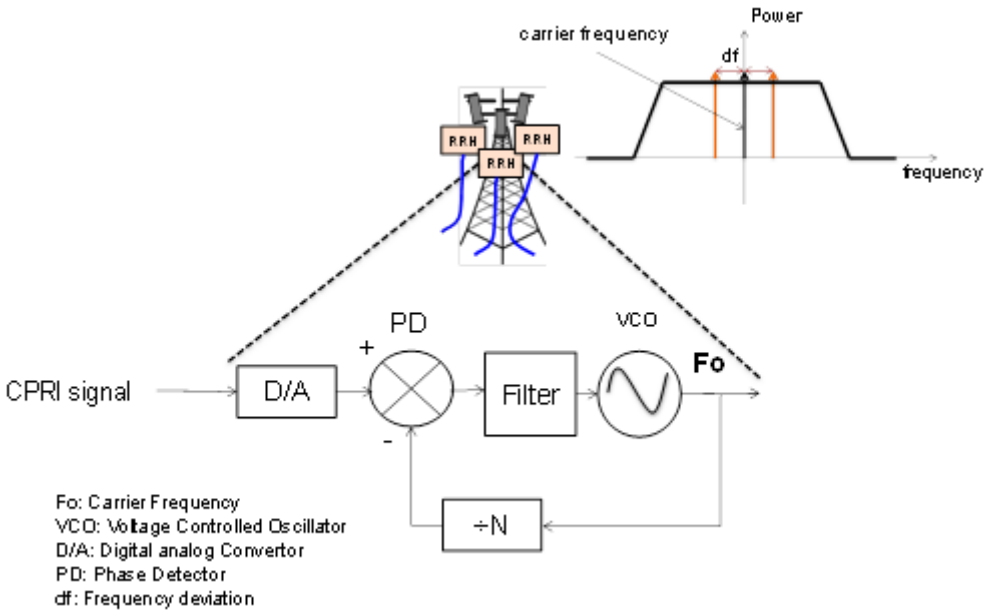

Figure 2.21: Classical representation of a PLL in the RRH

The 3GPP recommendation [83] fixes the maximum frequency deviation at 50 *ppb*. Above of this quantity of deviation the user equipment cannot synchronize on the carrier frequency. In order to investigate the impact of jitter in frequency deviation, the study is divided by two. At first, a theoretical study will be done. Given that the information concerning the PLL of the commercial Enode B is not available for confidentiality reasons, the classic PLLs described in the literature are considered as the reference model and are used for the theoretical study. The goal of the theoretical study is to provide a reference concerning the impact of jitter on the radio frequency deviation. It is also important to have an idea on the evolution of the frequency fluctuation due to the jitter in order to diagnostic the issue of end to end transmission. At a second time, a test will be done on the commercial LTE platform.

2.4.3.1 Jitter impact on carrier frequency

Remember that the jitter is the variation of the signal phase. The PLL operates with the phase difference; therefore, it is natural that the jitter has an influence on the operation of the PLL. In addition, the RRH recovers the clock from CPRI signal. When the jitter is present on the fronthaul link, the operation of the RRH could be disturbed. Each constructor implements its owner PLL system but any information about this subject is not available. In order to stay in the generality and for sake of simplicity, the classical PLL represented in the literature is considered. The purpose of this study is to have a general idea on effects of jitter present in the fronthaul link on the radio frequency carrier. Considering the [84], [85] and [86], it is possible to propose a simplified block

schema of the RRH allows studying the jitter effects on radio frequency carrier. Notice that the nonlinear effects are not considered in this study. The figure presented beyond is a simplified schema of PLL.

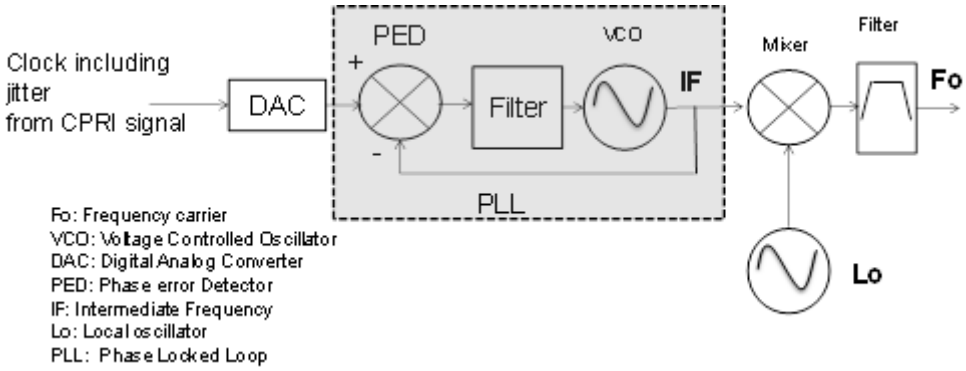

Figure 2.22: Simplified schema of frequency carrier of RRH

To understand the issue of jitter on the frequency carrier, we suppose that we have an ideal mixer and the nonlinear effects are not considered. In this configuration, after having filtered the signal provided from the mixer, the frequency carrier F_0 equals :

$$F_0 = L_0 + IF \tag{2.22}$$

Now we suppose that the jitter included in the clock signal, which attacks the PLL, causes the frequency deviation of ΔIF. The equation 2.22 becomes :

$$F_0 = L_0 + IF \pm \Delta IF \tag{2.23}$$

The equation 2.23 shows that the carrier frequency F_0 is sensible to the frequency fluctuations of the PLL.

The operation mode of the PLL is determined by the filter. Several type of filter exists but only the filters which permit a stable state of the PLL are considered. The survey is split in 3 cases. The first case, the study is performed without the filter. The Phase Error Detector (PED) is directly connected to the Voltage Controlled Oscillator (VCO). At the second case, the PLL uses a first order filter and in the third case, the second order filter is used. For each case, the effects of SJ and the TJ are treated. The ideal clock (without jitter) has a duty cycle of 50%. This signal can be represented by a sinusoidal. The DAC provides a sinusoidal signal to the PED. The PED delivers an electrical tension (V_{PED}) based on the gain of the PED (K_1) and the difference of phase between the clock from CPRI signal and the signal provided by the VCO.

$$V_{PED} = K_1(\phi_{CPRI} - \phi_{VCO}) \tag{2.24}$$

The VCO is supplied by the tension V_{PED}. It delivers a signal with a frequency F_{out} where K_2 is the gain of VCO and F_0 is the nominal frequency.

$$F_{OUT} = F_0 + K_2 V_{PED} \tag{2.25}$$

1. **Fist case: First order PLL (PLL without filter)**
   The phase at the output of the VCO ω_{VCO} can be written:

$$\omega_{VCO} = \omega_0 + 2\pi aV \tag{2.26}$$

The absolute phase of the VCO is defined by :

$$\theta_{VCO}(t) = \int_0^t \omega_{VCO}\ \mathrm{d}t = \omega_{VCO}t + 2\pi K_2 \int_0^t V_{PED}(t)\ \mathrm{d}t \tag{2.27}$$

The relative phase of VCO is defined such as :

$$\Theta_{VCO}(t) = \theta_{VCO}(t) - \omega_{VCO}t = 2\pi K_2 \int_0^t V_{PED}(t)\ \mathrm{d}t \tag{2.28}$$

The tension V_{PED} can be written in function of the relative phase where Θ_{CPRI} is the relative phase of the clock signal.

$$V_{PED} = K_1(\Theta_{CPRI} - \Theta_{VCO}) \tag{2.29}$$

The function derived of the relative phase Θ_{VCO} gives the frequency deviation of the VCO. Therefore, the derived of Θ_{VCO} can be written as equation 2.30 :

$$\frac{\mathrm{d}\Theta_{VCO}}{\mathrm{d}t} = 2\pi K_1 K_2(\Theta_{CPRI} - \Theta_{VCO}) \tag{2.30}$$

The equation 2.30 can be written in the frequency domain thanks to a Laplace transform and the following transfer function is obtained :

$$\frac{\Theta_{VCO}(P)}{\Theta_{CPRI}(P)} = \frac{2\pi K_1 K_2}{P + 2\pi K_1 K_2} \tag{2.31}$$

According to the equation 2.31, the PLL can be considered as a phase low filter with a cut frequency equals to K_1K_2. Relative to the jitter, the PLL filters the SJ jitter having a frequency higher than K_1K_2. In the following, the term $2\pi K_1K_2$ is designed by $\omega_{C_{PLL}}$.

The equation 2.32 can be considered as the relative phase of clock signal provided by the CPRI ($\Theta_{CPRI}(t)$). The latter represents the jitter. In the frequency domain, $\Theta_{CPRI}(P)$ written as :

$$\Theta_{CPRI}(P) = 2\pi A_j \frac{\omega_j}{\omega_j^2 + P^2} \tag{2.32}$$

Where:

- A_j: is the amplitude of jitter
- ω_j: is the frequency of SJ

The combination of equation 2.31 and 2.32 allows obtaining the relative phase of the PLL including the SJ effects in the frequency domain. The inverse Laplace transform of $\Theta_{VCO}(p)$ gives the relative phase of the PLL in the temporal domain. Considering the SJ, the temporal expression of the relative phase writes :

$$\Theta_{VCO}(t) = 2\pi A_j \omega_{C_{PLL}} \omega_j [A_1\, e^{i\omega_j t} + A_1^*\, e^{-i\omega_j t} + A_2\, e^{-i\omega_{C_{PLL}} t}] \tag{2.33}$$

$$\Theta_{VCO}(t) = 4\pi A_j \omega_{C_{PLL}} \omega_j [\Re(A_1)\cos(\omega_j t) - \Im(A_1)\sin(\omega_j t) + \frac{1}{2} A_2\, e^{-i\omega_{C_{PLL}} t}]$$

$$\frac{\mathrm{d}\Theta_{VCO}}{\mathrm{d}t} = -4\pi A_j \omega_{C_{PLL}} \omega_j [\Re(A_1)\sin(\omega_j t) + \Im(A_1)\cos(\omega_j t) + \frac{1}{2}\omega_{C_{PLL}} A_2\, e^{-i\omega_{C_{PLL}} t}] \tag{2.34}$$

Where A_1 and A_2 equals :

$$A_1 = -\frac{1}{2(\omega_j^2 + \omega_{C_{PLL}}^2)} - i\frac{\omega_{C_{PLL}}}{2\omega_j(\omega_j^2 + \omega_{C_{PLL}}^2)} \tag{2.35}$$

$$A_1 = \frac{1}{\omega_j^2 + \omega_{C_{PLL}}^2}$$

The equation 2.33b gives information about the evolution of the relative phase during the time. It allows studying the effects of SJ in terms of amplitude or jitter frequency on the frequency of the PLL. To get the angular frequency deviation, the derivative of the relative phase is done (equation 2.33c). A Simulation of the evolution of the phase and the frequency fluctuations during the time is carried out.

First of all, the parameter $\omega_{C_{PLL}}$ has to be fixed. According to the maximum frequency deviation of 50 *ppb* [83] and the maximum phase gap that is of 2π *rad*, it is possible to determine the angular frequency. We suppose that the local oscillator is stable, therefore the frequency fluctuation is essentially caused by the variation of the frequency delivered by the PLL. In this way, the maximum cut frequency $f_{C_{PLL}}$ of the PLL is :

$$f_{C_{PLL}} = \frac{50F_0 10^{-9}}{2\pi} \tag{2.36}$$

To have a scale of this cut frequency $f_{C_{PLL}}$ the LTE 800 MHz and 2.6 GHz are considered. Our simplified PLL used in the eNodeB of LTE 800 MHz should approximatively have a cut frequency of 6.36 Hz. We remember that the jitter concerns the phase variation is equal or higher than 10 Hz. In this case, the PLL filters the effects of any jitter. Concerning the enodeB of LTE 2.6 GHz, this value should approximatively equal to 20.7 Hz. Any frequency jitter above 20.7 Hz is filtered. At the following for the simulation, the cut-off frequency of the PLL is fixed at 6.36 Hz. To study the influence of frequency jitter, the simulation of equations 2.34 are performed. The amplitude of the SJ is fixed in order to assess the influence of the frequency of SJ. The following figure gives an example of frequency deviation corresponding to 0.5 UI of SJ at 10 KHz.

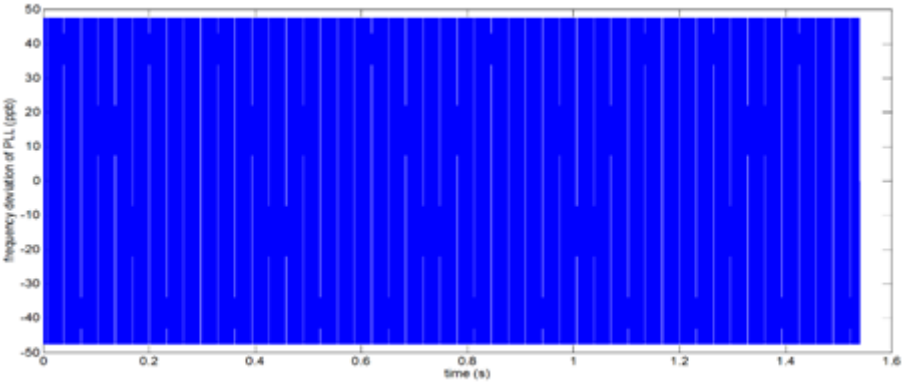

Figure 2.23: Frequency deviation of the first order PLL due to 0.5 UI at 10 KHz of SJ

The following figure summarizes the result of the simulation about the first order PLL.

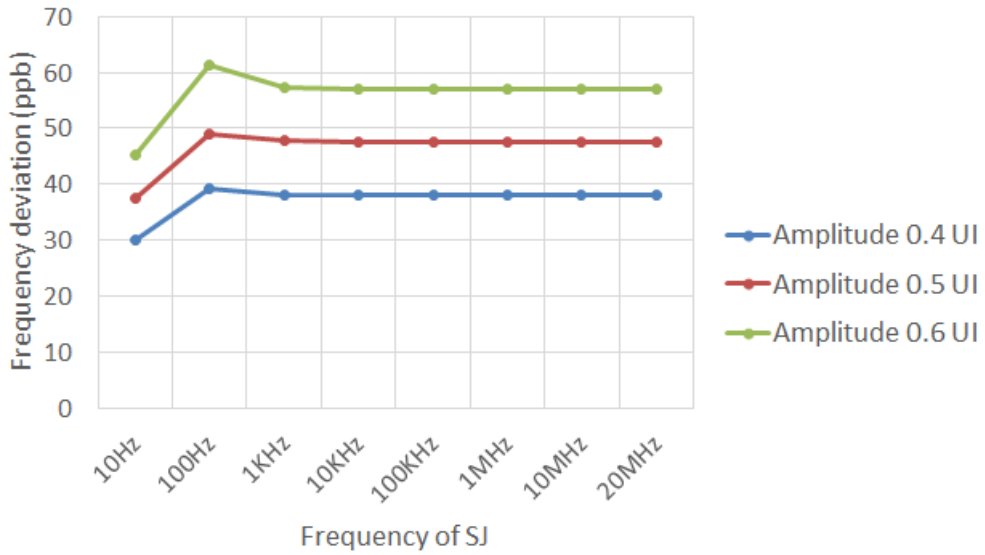

Figure 2.24: Frequency deviation of the first order PLL

Through figure 2.24, the effects of the amplitude and the frequency of SJ on the frequency deviation are highlighted. Indeed, for the frequencies between 10 Hz and 1 kHz, the frequency deviation varies and reach its maximum at 100 Hz. Also, figure 2.24 confirms that more the amplitude of SJ is high, more the frequency deviation is important. For any frequency, higher than 1 kHz, the frequency deviation is constant. Finally, for this kind of PLL, the frequency deviation increases when the amplitude of the SJ rises. This situation opens the discussion on the choice of criteria that should be considered to assess the impact of the SJ on radio frequency deviation. The jitter frequency is generally filtered by the PLL. For the high jitter frequencies, the radio frequency deviation is constant. Accordingly, in this case, the jitter frequency is not very important criterion. The increase of the jitter amplitude automatically causes the rise of the radio frequency deviation. In addition, when the jitter amplitude increases, the lock range limit of the PLL can be achieved. In this situation, the PLL could not lock and could cause the loss of the synchronization. After this analysis, it is more suitable to consider the jitter amplitude to establish the tolerance standard of SJ.

2. **Second case: second order PLL**

   The second order PLL is a PLL which contains the filter of first order. It is the most common in practical systems. In the frequency domain, the filter can be written of two different kinds such as [74] :

$$F_1 = \frac{1 + PT_2}{PT_1} \tag{2.37}$$

$$F_2 = \frac{1 + PT_2}{1 + PT_1}$$

The transfer function of the PLL writes :

$$H(P) = \frac{EP + F}{P^2 + 2\xi\omega_n P + \omega_n^2} \tag{2.38}$$

The table beyond provided by [74] summarizes the different parameters relative to the filter.

	Passive FIlter		**Active Filter**	
	$\frac{1}{1+PT_1}$	$\frac{1+PT_2}{1+PT_1}$	$\frac{1}{PT_1}$	$\frac{1+PT_2}{PT_1}$
E	0	$2\xi\omega_n\left(1-\frac{\omega_n}{K_1K_2 2\xi}\right)$	$2\xi\omega_n$	$2\xi_n$
F	ω_n^2	ω_n^2	ω_n^2	ω_n^2
ω_n	$\sqrt{\frac{K_1K_2}{T_1}}$	$\sqrt{\frac{K_1K_2}{T_1}}$	$\sqrt{\frac{K_1K_2}{T_1}}$	$\sqrt{\frac{K_1K_2}{T_1}}$
ξ	$\frac{\omega_n}{2K_1K_2}$	$\frac{T_2\omega_n}{2} + \frac{\omega_n}{2K_1K_2}$	0	$\frac{T_2\omega_n}{2}$
T_1	$\frac{K_1K_2}{\omega_n^2}$	$\frac{K_1K_2}{\omega_n^2}$	$\frac{K_1K_2}{\omega_n^2}$	$\frac{K_1K_2}{\omega_n^2}$
T_2	0	$\frac{2\xi}{\omega_n}\left(1-\frac{\omega_n}{K_1K_2 2\xi}\right)$	0	$\frac{2\xi}{\omega_n}$

Table 2.4: Parameters of transfer function of second order PL

The jitter expression can be written such as indicated by the equation 2.32. In this case, the relative phase of VCO writes :

$$\Theta_{VCO_{2nd}}(P) = \frac{EP + F}{P^2 + 2\xi\omega_n P + \omega_n^2} \frac{2\pi A_j \omega_j}{(P^2 + \omega_j^2)} \tag{2.39}$$

$$\Theta_{VCO_{2nd}}(P) = \frac{EP + F}{(P - x_1)(P - x_2)} \frac{2\pi A_j \omega_j}{(P + i\omega_j)(P - i\omega_j)} \tag{2.40}$$

For the value of x_1 and x_2, two cases are distinguished :

$$\text{If } \xi \in [-1;1] \Rightarrow x_1 = \omega_n(-\xi + i\sqrt{(1-\xi^2)}) \text{ and } x_2 = -\omega_n(\xi + i\sqrt{(1-\xi^2)})$$
$$\text{else } x_1 = \omega_n(-\xi + \sqrt{(\xi^2-1)}) \text{ and } x_2 = -\omega_n(\xi + \sqrt{(\xi^2-1)})$$

Thus, the equation 2.40 permits to obtain the expression of the relative phase in the temporal domain thanks to the inverse Laplace transformer. Indeed, the expression of the relative phase in function of the time is given by the equation 2.32.

$$\Theta_{VCI_{2nd}}(t) = 2\pi A_j \omega_j (A_1\, e^{x_1 t} + A_2\, e^{x_2 t} + A_3\, e^{-i\omega_j t} + A_4\, e^{i\omega_j t}) \tag{2.41}$$

Where :

- $A_1 = \frac{Ex_1+F}{(x_1-x_2)(x_1^1+\omega_j^2)}$
- $A_2 = \frac{Ex_2+F}{(x_2-x_1)(x_2^1+\omega_j^2)}$
- $A_3 = \frac{F+iE\omega_j}{(2i\omega_j)(-x_1+i\omega_j)(-x_2+i\omega_j)}$
- $A_4 = -\frac{F-iE\omega_j}{(2i\omega_j)(x_1+i\omega_j)(x_2+i\omega_j)}$

According to the table 2.4.3.2, the factor ξ (damping factor) is positive. When the latter is between 0 and 1, the values of x_1 and x_2 are complex. A_1 becomes complex and A_2 is the conjugate of A_1. A_3 is a complex and A_4 is its conjugate. Consequently, the relative phase of the PLL attacked by the CPRI signal including the jitter writes :

$$\begin{aligned}\Theta_{VCO_{2nd}}(t) =& 4\pi A_j \omega_j \Big[\Re(A_1)\, e^{-\omega_n t}\cos\left(\sqrt{1-\xi^2}t\right) - \Im(A_1)\, e^{-\omega_n t}\sin\left(\sqrt{1-\xi^2}t\right) \\ &+ \Re(A_3)\cos(\omega_j t) - \Im(A_3)\sin(\omega_j t)\Big]\end{aligned}$$

If the damping factor ξ equals 1, the relative phase writes :

$$\Theta_{VCO_{2nd}}(t) = 2\pi A_j \omega_j \left[(-E\omega_n + F)\, e^{-\omega_n t} + E\, e^{-\omega_n t} + \Re(A_3)\cos(\omega_j t) - \Im(A_3)\sin(\omega_j t)\right]$$

If the factor is higher than 1 the relative phase becomes :

$$\Theta_{VCO_{2nd}}(t) = 2\pi A_j \omega_j \left[A_1\, e^{x_1 t} + A_2\, e^{x_2 t} + 2\Re(A_3)\cos(\omega_j t) - 2\Im(A_3)\sin(\omega_j t)\right] \tag{2.42}$$

At the following, only the case of the passive filter without zero is presented. The case where ξ equals to 1 must be avoided because on startup of the PLL, the frequency deviation is proportional to the both amplitude and frequency jitter. This value of the frequency deviation can out the lock range of the PLL. Figure 2.25 presents the frequency deviation for a second order PLL.

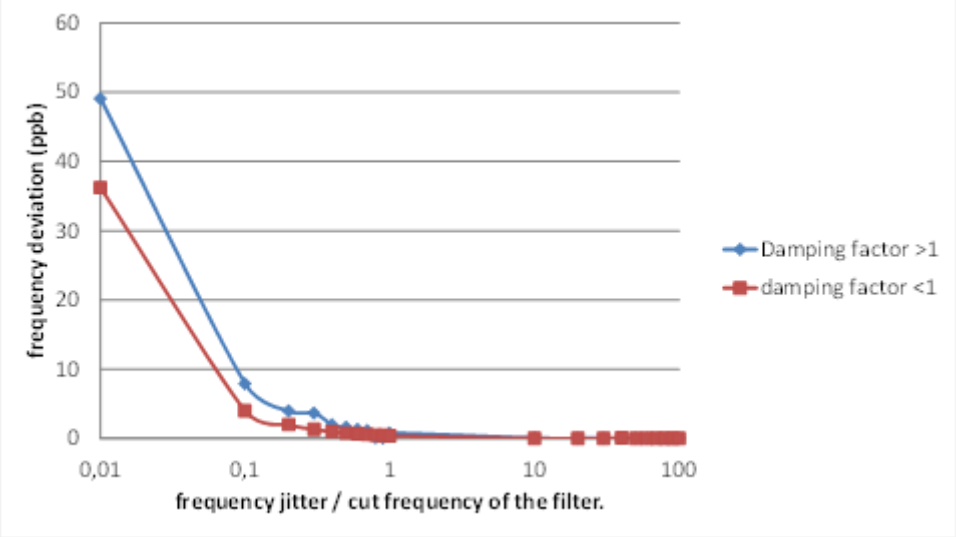

Figure 2.25: Frequency deviation of the second order PLL

The x-axis represents the ratio of the frequency jitter on the cut frequency filter of the PLL. For the both damping factor, two cases are distinguished. The first case concerns the part of the curves where the ratio is less than 1. In the part, the curves depict the influences of frequency of jitter. The frequency deviation is inversely proportional to the frequency of SJ. For the ratio between 1 and 100, the frequency deviation is approximately the same. In addition, for both damping factors, the curves are superimposed from the ratio equals to 10 until to 100. Generally, the curves converge to the zero ppb when the frequency of the jitter increases. The PLL behaves as a filter relative to the SJ. Equation2.42 also shows that the amplitude of the sinusoidal jitter is an important parameter. The frequency deviation is proportional to the amplitude of SJ.

The consequence of the jitter on the radio frequency deviation depends on the cut-off frequency of the filter. The PLL filters the SJ which have frequencies higher than the cut-off frequency.

3. **Third case: third order PLL**

The third order PLL is often used because their features allow increasing the tracking capability of the high dynamics phase fluctuations [74]. This system is characterized by the second order filter $F(P)$ which can be represented by the following equation :

$$F(P) = \frac{(1 + PT_2)(1 + PT_3)}{(PT_1)^2} \tag{2.43}$$

The transfer function of a type 3 PLL writes such as :

$$F(P) = \frac{\omega_c(P+\beta\omega_c)(P+\beta_1\omega_c)}{P^3+\omega_c(P+\beta\omega_c)(P+\beta_1\omega_c)} \tag{2.44}$$

Where :

- $\omega_c = K_1K_2\left(\frac{T_2}{T_1}\right)\left(\frac{T_3}{T_1}\right)$
- $\beta = \frac{1}{\omega_c T_2}$
- $\beta_1 = \frac{1}{\omega_c T_3}$

Unlikely the PLL of first or second order, the stability of this PLL is not unconditional [87]. To achieve the stability of the type 3 orders PLL the condition described beyond must be respected. The gain of the PLL has to be higher than a minimum value estimated as [87]:

$$K_1K_2 > \frac{1}{2T_2}\left(\frac{T_1}{T_2}\right)^2 \tag{2.45}$$

When the stability is achieved for this kind of system, it can be approximated by a second order PLL [87].

In summary, the PLL behaves as a filter relative to the jitter. The frequency deviation is approximately the same for any jitter frequency higher than the cut frequency of the PLL. Considering these frequencies, the amplitude of the jitter becomes the major parameter which influences the performance of the fronthaul. This analysis can justify the results described by the figure 2.12 and figure 2.14. Indeed, in these figures, the operating zone of the system is delimited by the threshold amplitude of SJ and in some cases and not by the frequency of SJ. In order to get a realistic SJ jitter mask and the realistic tool which permit to diagnostic the issue of the jitter on a fronthaul link, the CPRI specifications about jitter must be rethinking.

2.4.3.2 Jitter impact on carrier frequency: experimental tests

In this part an experimental setup is described to measure the frequency deviation of the RRH. The setup is presented beyond.

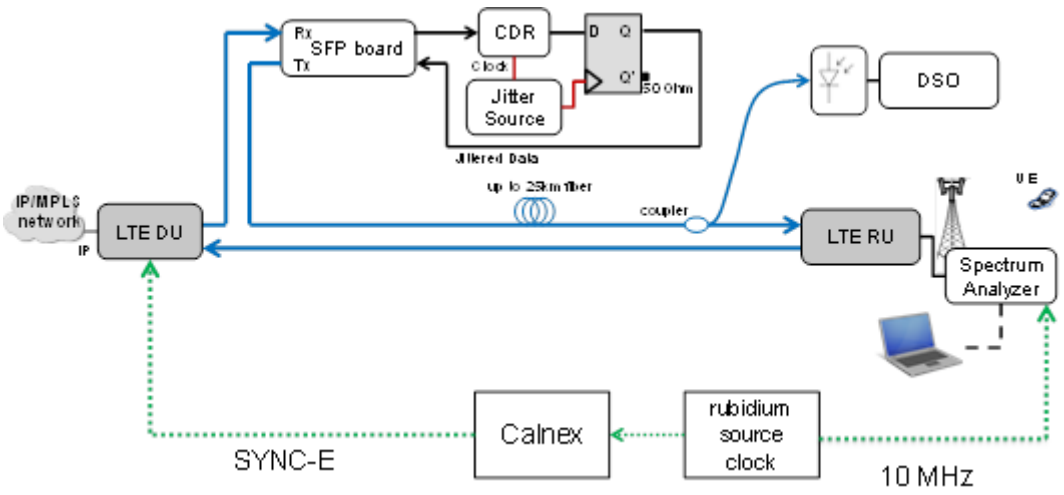

Figure 2.26: Setup to study jitter effects on the carrier frequency deviation

In this experimentation, the Spectrum Analyser measures the spectrum of the radio frequency. It is able to measure the frequency deviation. In Addition, software is installed in the computer to get the information about the frequency deviation. Then, the BBU and the Spectrum Analyzer have to be synchronized with the same stable source clock. In this scheme, the rubidium provides stable clock at 10 MHz. This signal trigs the spectrum analyser. The CALNEX recovers the clock signal and converts it in a Synchronous Ethernet (SYNC-E) signal to trig the BBU (LTE DU). After introduction of jitter the signal (CPRI signal containing the jitter) get the RRH (LTE RU) after has crossed 25 km of optical fiber. In the antenna site, a power coupler is placed to divide the optical power in two parts. One part of received signal is used to measure the jitter, and the other part is sent to the RRH in order to measure the radio frequency deviation.

In the following part, the reference measurements are presented. To obtain these results, the CPRI signal is sent through the dispositive described by the figure 2.26 without jitter is added.

The radio frequency deviation doesn't exceed 1.2 ppb (figure 2.27), but this measurement does not significantly represent the trend of the different recorded samples. In order to have an idea on the repartition of the samples in function of the radio frequency deviation, a normalized histogram is drawn in the next figure (figure 2.28).

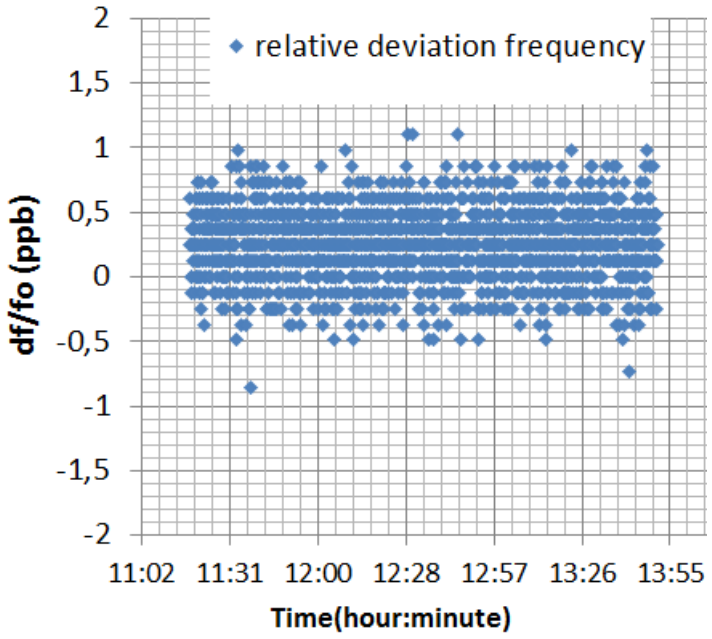

Figure 2.27: Reference radio frequency deviation (without introduced jitter)

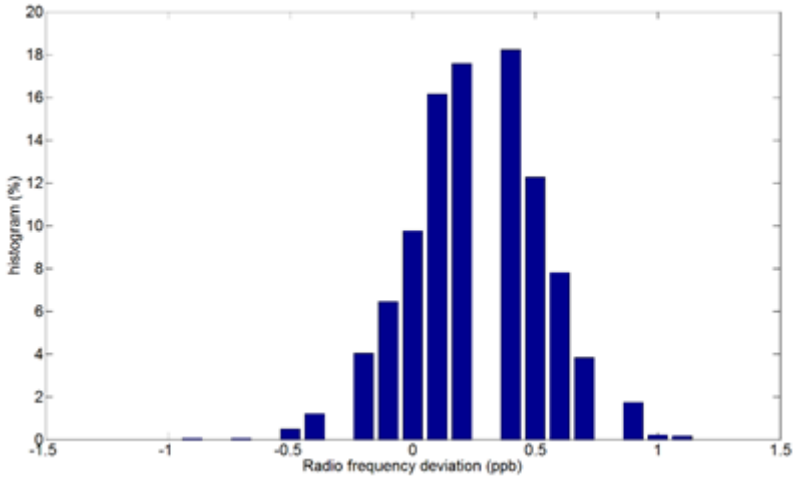

Figure 2.28: Reference radio frequency deviation (without introduced jitter)

This histogram is divided by class and each class has an interval of 0.1 *ppb*. According figure 2.15, the range of the class is described by the interval : $[-1; 1.2]$ *ppb*. More than 95% of the frequency deviations are between -0.2 *ppb* and 0.7 *ppb*. The goal of this figure is to show the distribution of the different measurements in order to propose a representative value of the radio frequency deviation. For this, the mean $\hat{x}_{ref_{dev}}$ £and the standard deviation $\sigma_{ref_{dev}}$ of samples are calculated with the following formulas :

$$\hat{x}_{ref_{dev}} = \frac{1}{N}\sum_{i=1}^{N} x_i \tag{2.46}$$

$$\sigma_{ref_{dev}} = \sqrt{\frac{1}{N}\sum_{i=1}^{N}(x_i - \hat{x}_{ref_{dev}})^2} \tag{2.47}$$

$$Representative \;\; interval = [\hat{x}_{ref_{dev}} - \sigma_{ref_{dev}}; \hat{x}_{ref_{dev}} + \sigma_{ref_{dev}}] \tag{2.48}$$

$$Frequency \;\; deviation = max\left(|\hat{x}_{ref_{dev}} - \sigma_{ref_{dev}}; \hat{x}_{ref_{dev}}, \sigma_{ref_{dev}}|\right) \tag{2.49}$$

Where :

- N : is the total number of samples
- x_i : is the i^{th} sample

After calculation, the mean of reference frequency deviation is 0.25 *ppb* and the standard deviation is 0.27 *ppb*. Considering these two values, the representative interval (equation 2.48) is defined between $[-0.01; 0.53]$. In term of class this interval can be in $[0; 0.5]$. This interval represents approximatively 75% of the samples. After this statistical study, $[-0.01; 0.53]$ can be considered to describe the reference frequency deviation in terms of interval and 0.53 *ppb* can be used to represented these reference measurements as a number.

Now, jitter is introduced in the CPRI signal and the radio frequency deviations are measured. Before the presentation of general results, an example of jitter effects on the frequency deviation is given. Figure 2.16 represents the radio frequency deviation resulting of the fronthaul link containing 0.5 UI of sinusoidal jitter and 0.49 UI of RJ. The comparison between figure 2.29 and the reference measurement (figure 2.28) shows that the standard deviation is rise when the jitter is present in the CPRI signal.

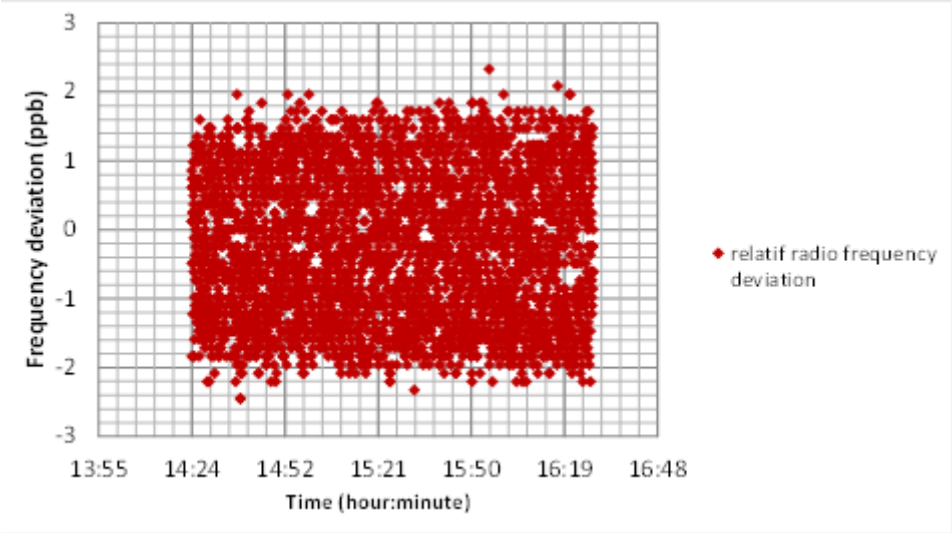

Figure 2.29: Relative radio frequency deviation with a fronthaul link containing 0.5 UI of SJ at 1 MHz and 0.49 UI of RJ

The following figure shows the distribution of different samples. Through this figure the increasing of standard deviation is noted. The results of equation 2.47, equation 2.47, equation 2.48 and equation 2.49 applied on these samples (samples of jitter present in the CPRI signal) are consigned in the table 2.5.

Mean	**Standard deviation**	**Interval**	**Considered value**
-0.24 *ppb*	1.05 *ppb*	$[-1.3; 0.9]$ *ppb*	1.29 *ppb*

Table 2.5: Statistical results of the radio frequency deviation of a fronthaul link containing 0.5 UI of SJ at 1 MHz and 0.49 UI of RJ

The measurements are directly carried out at the output of the RRH. In this way, the tests are performed for several levels of SJ at different frequencies. The results are summarized in figure 2.30. The radio frequency deviation represents the point described by the equation 2.49

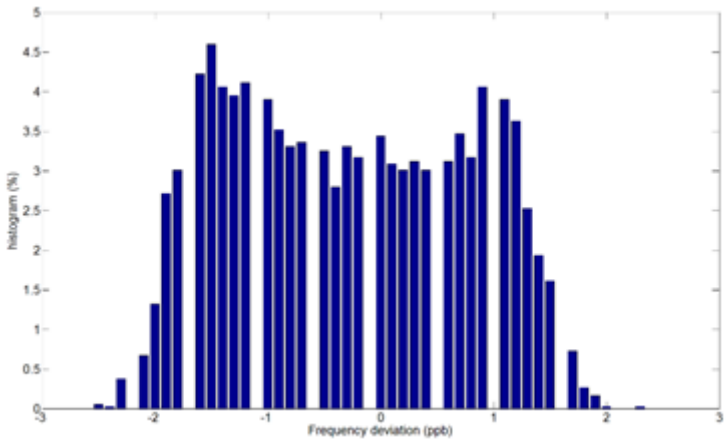

Figure 2.30: Histogram of relative radio frequency deviation with a fronthaul link containing 0.5 UI of SJ at 1 MHz and the 0.49 UI of RJ

SJ is introduced at different frequencies. The radio frequency deviation is measured and the results are summarized at figure 2.31. This figure represents the considered value of the radio frequency deviation. This figure shows that the SJ do not cause a high frequency deviation. The frequency deviations are approximately equal to the reference measurement. These results are due to the cleaner jitter present in the commercial enode B. The cleaner jitter is able to cancel the effects the jitter in the signal and provide a clean signal. For any frequency, when the amplitude jitter is higher than 0.5 UI, there is a failure of the radio link. This result confirms that the amplitude of jitter remains the main factor for the frequencies jitter between 10 Hz and 10 MHz. Therefore, with the actual system dedicated for the fronthaul link, it is not possible to meet the requirement of the CPRI in terms of SJ tolerance for the frequencies between 10 Hz and approximately 1.8 MHz.

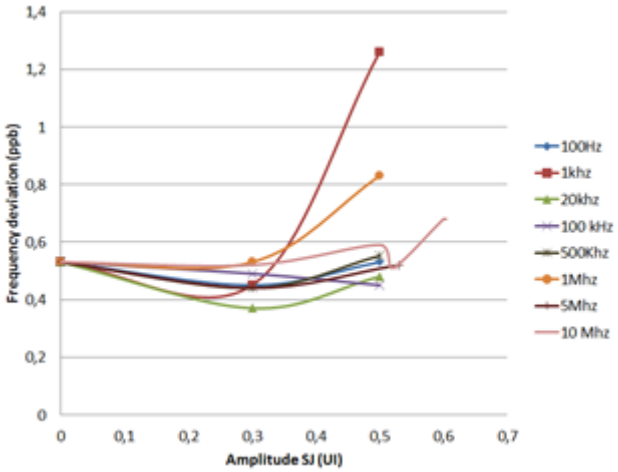

Figure 2.31: Radio frequency deviation relative to the sinusoidal jitter

2.5 Conclusion

The jitter is an electronical phenomenon which causes the variation of the decision instant on the digitalized data transmission. The consequence of the jitter is the introduction of the errors in the transmission. The requirements in term of jitter on the fronthaul link are consigned in the CPRI Specification. These requirements are divided by two. The first specifies the impact of the jitter in the frequency accuracy budget of the CPRI clock signal. Indeed, the contribution of the jitter on the frequency accuracy budget is 2 *ppb* and can be measured in the spectral domain. The second defined the tolerance jitter in the time domain and gives a definition of total jitter different from the conventional representation.

The study of the jitter on the fronthaul link begins by a state of the art about jitter definition. These investigations highlight the different components of the jitter and the method to measure these components. The oscilloscope to measure the jitter uses the conventional jitter decomposition which is different from the CPRI specification. A mapping between these two different representations is proposed in order to compare the measured values to CPRI specification.

From the perspective to have thorough inspection of jitter, a system permitting to introduce different kinds of jitter is proposed and tested. This setup allows assessing the jitter and studying its impact on the fronthaul link. This evaluation of jitter has considered three criteria such as the BER of the CPRI signal, EVM of the LTE signal and the radio frequency deviation of the commercial enode B. Finally, this study shows that the amplitude of SJ is the main criterion which must be considered. The different specifications in terms of jitter proposed by the CPRI do not match with the actual electronic devices. In order to evaluate correctly the fronthaul link it is necesseru to rethinkink the CPRI in terms of Jitter.

Chapitre 3 :

Experimental solutions for a fronthaul link

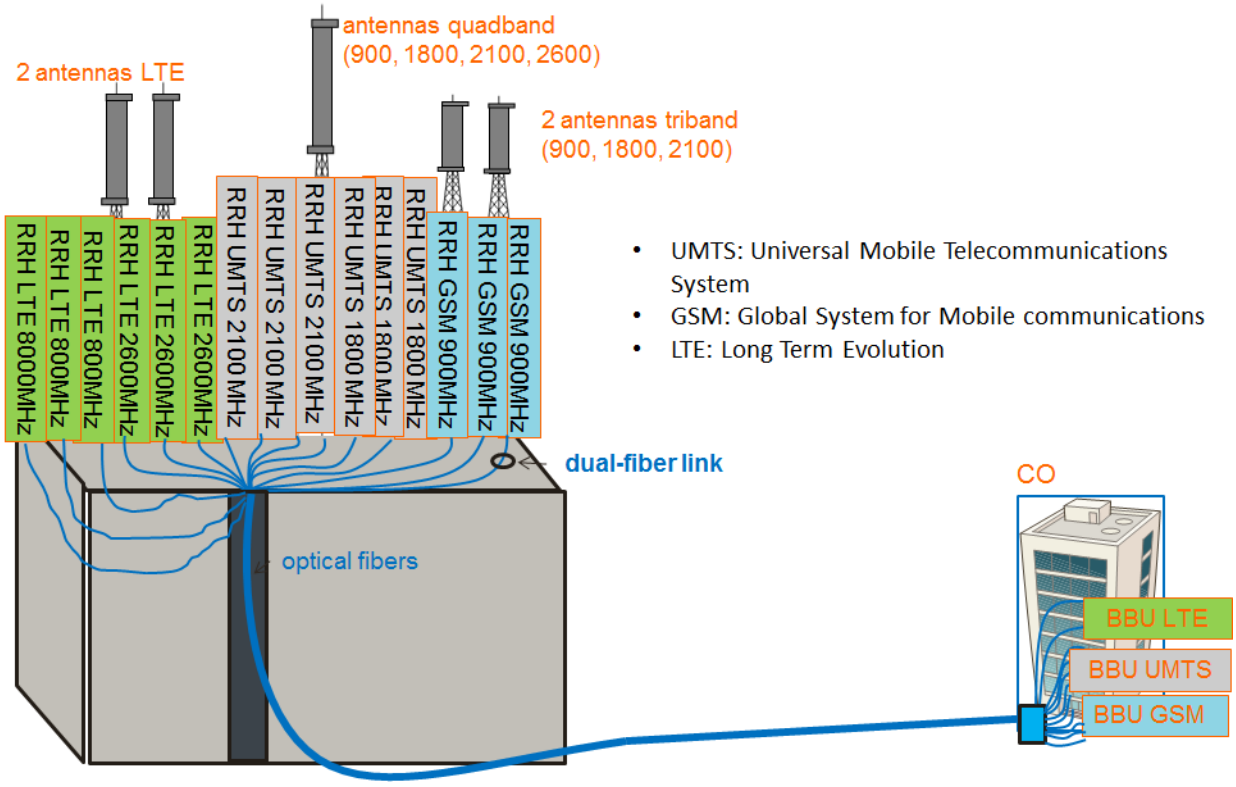

Figure 3.1: Macro cells configuration with 15 RRHs

3.1 Introduction

Since the regulation aspects are considered in the deployment of fronthaul, the fiber provider must to allow the transport of CPRI signal of any mobile Operator. Nowadays, the typical antenna configuration in urban areas can exceed 15 RRHs. The figure 3.1 illustrates the configuration of macro cells sites. The RRHs depend on the different RAT (GSM, UMTS or LTE) and of the different operation frequencies bands. Using the physical point to point topology does not permit to optimize the optical fiber resources. Indeed, with this topology, the bidirectional communication between 15 RRHs and theirs BBUs is guaranteed through 30 optical fibers. The Wavelength Division Multiplexing (WDM) technique is used to reduce the number of optical fibers used between the antenna site and the CO and therefore, the cost of the deployment of fronthaul. In addition to this technique, ORANGE continues to explore different ways to reduce further the cost of deployment of fronthaul while focusing on the passive network as criterion. This objective has permitted us to study two potential solutions low cost for the implementation of fronthaul. The two proposed candidates which have been studied in this chapter are:

- DWDM self-seeded based on a RSOA (O-band)
- WDM Single fiber including a semi passive monitoring scheme

3.2 DWDM self-seeded on a fronthaul link

One of characteristics for fronthaul in Centralized-Radio Access Network (C-RAN) architecture is the capacity to multiplex several fronthaul links on the same fiber by means of Wavelength Division Multiplexing (WDM). Hence, the CWDM is the low cost and a pragmatic option, but inventory management problems for wavelength assignment can burden the network. Moreover, if the number of RRHs on the antenna site exceeds 16, this system will reach its limits in terms of capacity of links. Dense Wavelength Division Multiplexing (DWDM) is then used to face to the limits of CWDM but an increasing of complexity of inventory management issue is observed with this type of WDM technique [88].

DWDM based on the self-seeded Reflective Semiconductor Optical Amplifier (RSOA) has been evoked as potential solution for the fronthaul [89] [90]. This solution is a colorless wavelength and offers the advantage of assigning automatically and passively the wavelength of the laser source thus suppressing the inventory the capacity issues met with the classic WDM system. In this section, DWDM self-seeded solution is implemented for fronthaul link in the O-Band. The particularity of O-Band is the low chromatic dispersion in SMF-28 fiber. This latter can deteriorate the quality of the optical transmission relative to the distance.

3.2.1 Operation of self-seeded system

The self-seeded system is a colorless and low cost laser solution for WDM access [91]. The purpose of the self-seeded source is to assign automatically and passively a desired wavelength. An optical cavity is formed between the reflector in the RSOA and the Faraday Rotator Mirror (FRM) providing a colorless optical source called “self-seeded”. The principle of a self-seeded with a RSOA can be summarized by figure 3.2 in three steps.

At the first step (① in the figure 3.2), the RSOA provides a wide band of an Amplified Spontaneous Emission (ASE). At the second step, this ASE is sliced by an Arrayed Waveguide Grating (AWG) at the desired wavelength (② in the figure 3.2) at the selected wavelength.

A part of the light is reflected by the mirror and return to the RSOA. At the third Step, (③in the figure 3.2) these round trips are carried out several times in the cavity before reaching the steady state. In this manner the signal from the RSOA is passively amplified at the selected wavelength.

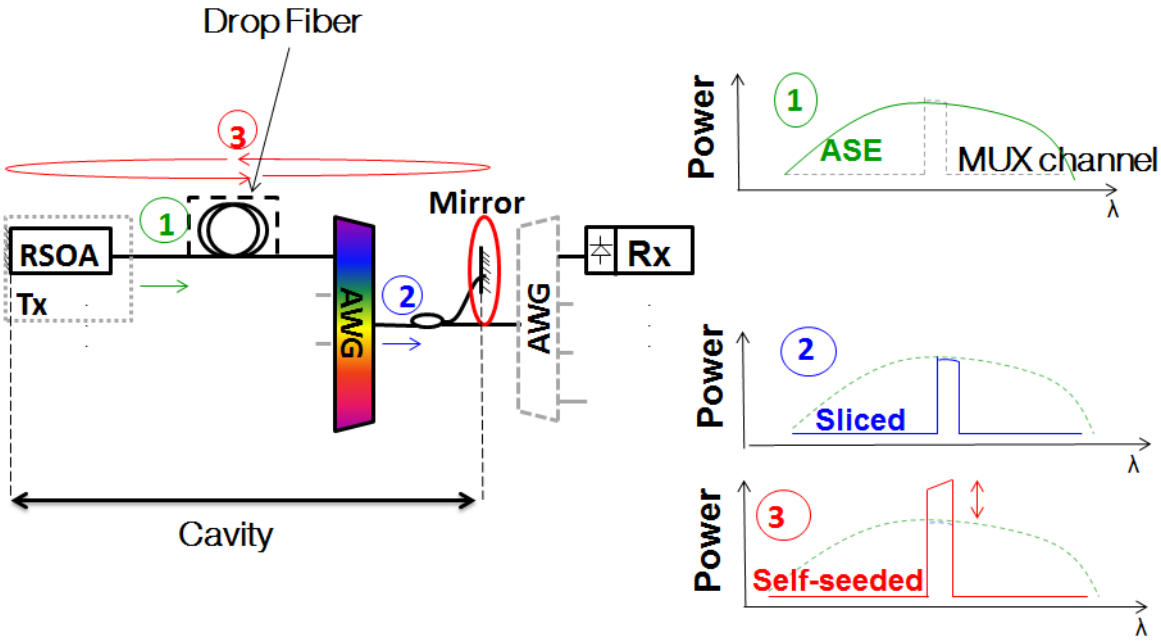

Figure 3.2: Schema of principle of a self-seeded source based on RSOA

Therefore, the emission wavelength is only by the selected AWG port so that every network terminal can be equipped with the same RSOA. Thus, this solution is passive and colorless [91].

The behavior of laser in the cavity has been studied in [91]. Indeed, the presence of cavity modes is observed in the laser cavity and the frequency of apparition modes depends on the length of the cavity as shown the figure 3.3. Indeed, the number of longitudinal modes rises with the length of the cavity. Thus, the self -seeded source is a multimode laser with a low degree of coherence.

3.2.2 Setup of self-seeded based on the RSOA for a fronthaul link

Figure 3.4 describes the setup of the fronthaul link based on the RSOA in the O-Band at 1327.6 nm and the transmitted power is approximatively -9.5 dBm. The RSOA is highly polarization dependent. We use a 45° Faraday Rotator (FR) and a Faraday Rotator Mirror (FRM) to preserve the polarization of the RSOA in the cavity [92]. The common port of a flat top Arrayed Waveguide Grating (AWG) with 3dB losses, 200 GHz of 3 dB bandwidth and 280 GHz of channel spacing is connected to a 50% splitter followed by a reflective 90° FRM. In [93], several combinations with different splitters have been tested. The back to back configuration with a 50% splitter shows the best BER, therefore the same configuration has been used for the fronthaul setup. Thus, an optical cavity is formed between the reflector in the RSOA and the FRM providing a colorless optical

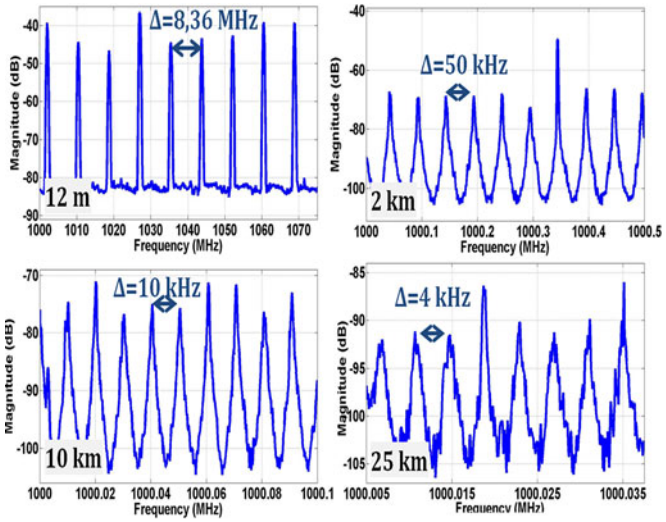

Figure 3.3: Optical Spectral cavities from 12 m to 25 km [91]

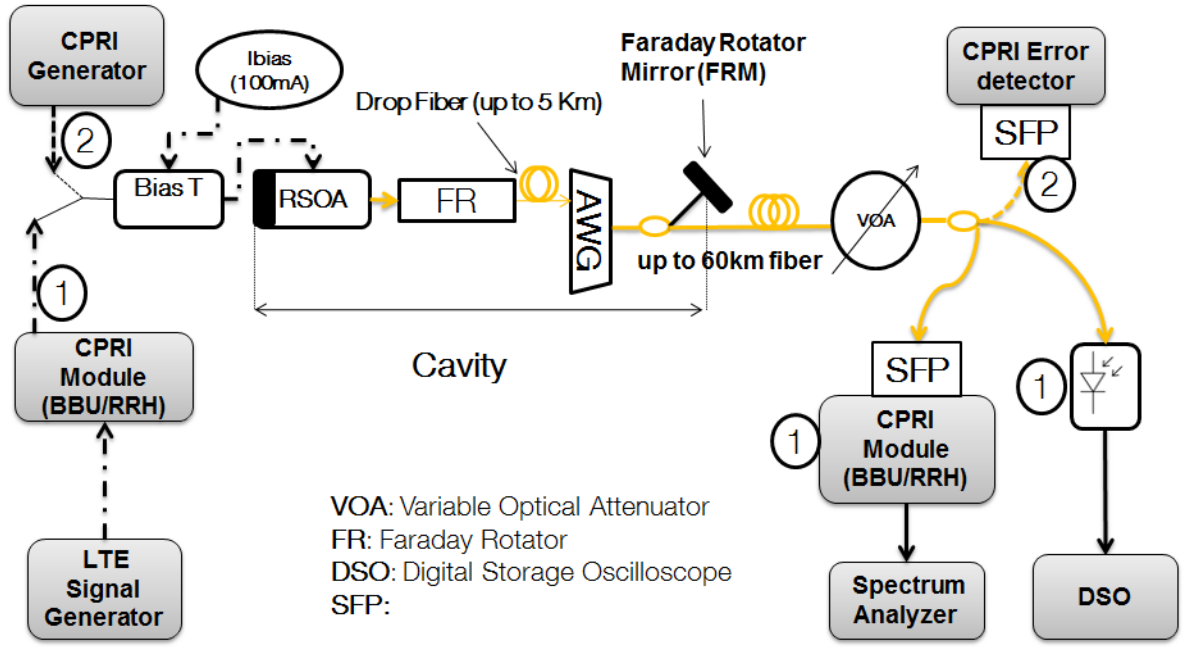

Figure 3.4: Experimental Setup for Self-seeded based on a RSOA for a fonthaul link

source. The tests have been performed on the downlink transmission from BBU to the RRH in order to simultaneously study the quality of the signal and also evaluate the radio frequency deviation at the output of the RRH. However, the BER measurements also hold for the uplink transmission direction. Two different tests have been carried out:

- EVM and jitter measurements respectively on the LTE and CPRI Signals (① in the figure 3.4)
- BER and latency measurement of CPRI frames (② in the figure 3.4).

The RSOA biased with 100 mA current, has been directly modulated by CPRI frames provided by a CPRI module that emulates a BBU and a RRH in case ① or by a CPRI generator in case ②. We have tested CPRI rates at 1.22 Gbit/s and 2.45 Gbit/s for back to back, 30 km and 60 km feeder lengths and short (<10m), 1 km, 2 km and 5 km cavity lengths. Also, remember that the standard of optical fiber SMF-28 is used as transmission and drop fiber.

3.2.3 EVM and BER characterization

The CPRI module converts the LTE baseband signal obtained from a LTE generator to CPRI frames (① in figure 3.4). At the reception, the optical signal is split in two parts. On one side, the CPRI module (RRH) extracts the LTE signal from the received CPRI frames. The Spectrum Analyzer demodulates the LTE signal and measures the EVM. The three modulation types have been tested at for LTE 10MHz and 20MHz corresponding to 1.22 Gbit/s and 2.45 Gbit/s CPRI rates respectively (same filling ratio in the CPRI frames). Single Input Single Output has been used as antenna configuration. At the other output port of the optical splitter, the jitter has been measured on the CPRI signal by means of a calibrated photodiode and a Digital Storage Oscilloscope (DSO). A CPRI generator is used to modulate the RSOA with CPRI frames (② in figure 3.4). At the reception, a CPRI error detector measures the BER and latency on the fronthaul link. During the test, we have increased the attenuation of a Variable Optical Attenuation (VOA) so to identify the receiver sensitivity. The sensitivity is defined as the minimum received power allowing the respect of EVM 3GPP recommendations.

3.2.3.1 EVM

Figure **??** depicts the measured EVM as a function of the received power for back to back (figure 3.5 (a)), 30 km feeder length (Figure 3.4 (b)) and 60 km feeder length (figure 3.5 (c)). $QPSK$, $16-QAM$ and $64-QAM$ modulations have been tested, but only the results with $64-QAM$ are presented in figure 3.5, as this modulation has the

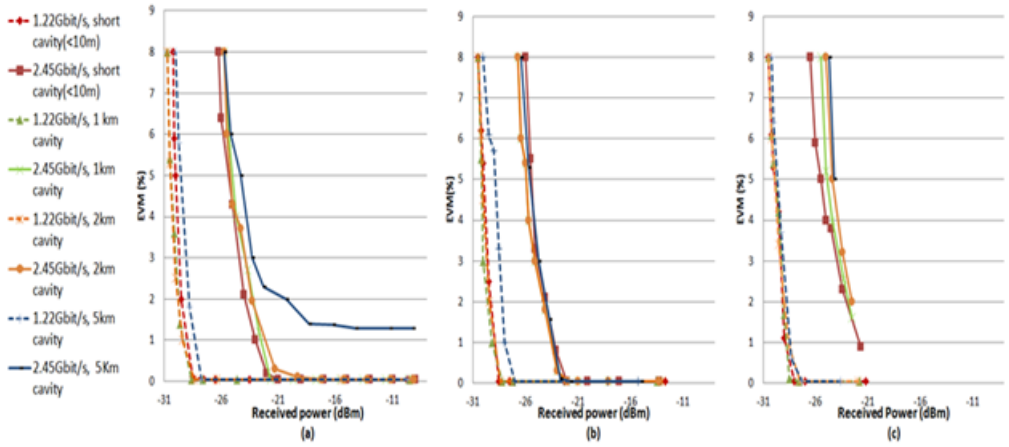

Figure 3.5: EVM measurements for 64-QAM, (a): back to back feeder, (b): 30 km feeder, (c): 60 km feeder

most stringent EVM requirements. The results of the others modulation are presented in the annex. The different curves correspond to short (<10 m), 1 km, 2 km and 5 km cavity length (drop fiber length) for 1.22 Gbit/s (dashed curves) and 2.45 Gbit/s (solid curves) are presented.

A loss of signal is observed when the EVM is higher than 3GPP limit. The performance of LTE signal depends on the received power and the rate. Indeed, the sensitivity is approximately -30 dBm at 1.22 Gbit/s and -25 dBm at 2.45 Gbit/s. In the back to back configuration, the performances for a considered rate and different cavity lengths are approximately the same, except for the 5 km cavity configuration at 2.45 Gbit/s where a small deterioration is registered with a minimum EVM of 1.2%. For 30 km feeder length the results are very similar to the back to back configuration. For 60 km fiber length, the different attenuations (insertion loss of different devices, fiber attenuation) on the transmission link have not allowed to measure a power higher than -21 dBm. For 2.45 Gbit/s data rate at -21 dBm and 60 km feeder, the EVM increases relative to other configurations at the same power. For example, EVM is 5% with 5 km cavity length, whereas it is 0.04% for the same cavity length but shorter feeder lengths (Figure 3.4). Furthermore, we study the impact of CPRI on the modulation of radio LTE signal ($QPSK$, $16-QAM$, $64-QAM$). We consider the case with 30 km feeder, first with short cavity, then with 2 km and finally 5 km of cavity. The results are presented in figure 3.6. A reference measurement has been made by directly connecting the LTE generator to the spectrum analyzer. The value of this reference measurement for the different modulation formats (QPSK, 16-QAM and 64-QAM) is 0.04%. The EVM is approximately the same for different modulations. It is 0.04% for received power of at least -27 dBm at 1.22 Gbit/s and for received power of at least -22 dBm

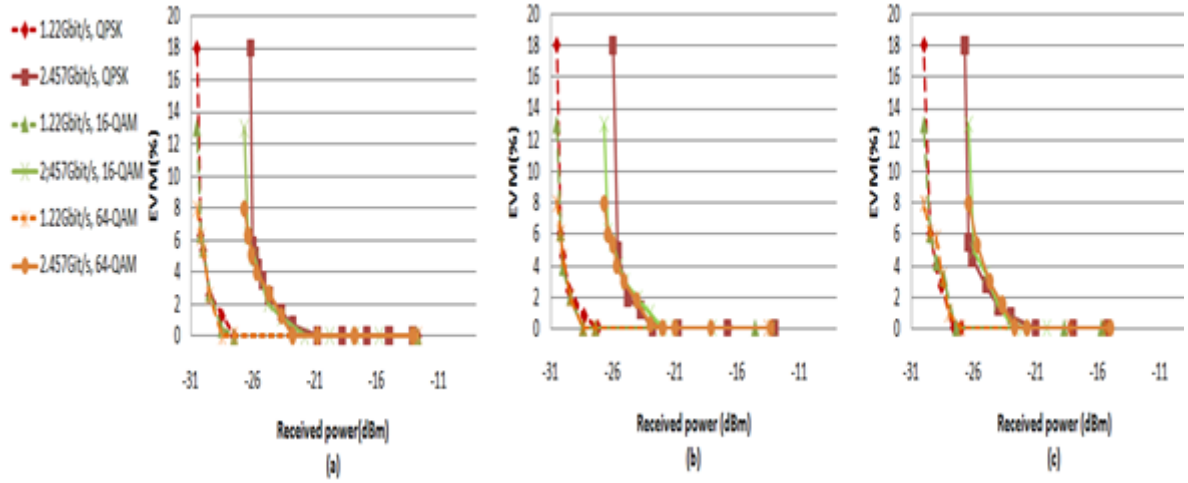

Figure 3.6: EVM measurements at 30 km feeder, (a): with short cavity (<10 m), (b): 2 km cavity, (c): 5 km cavity

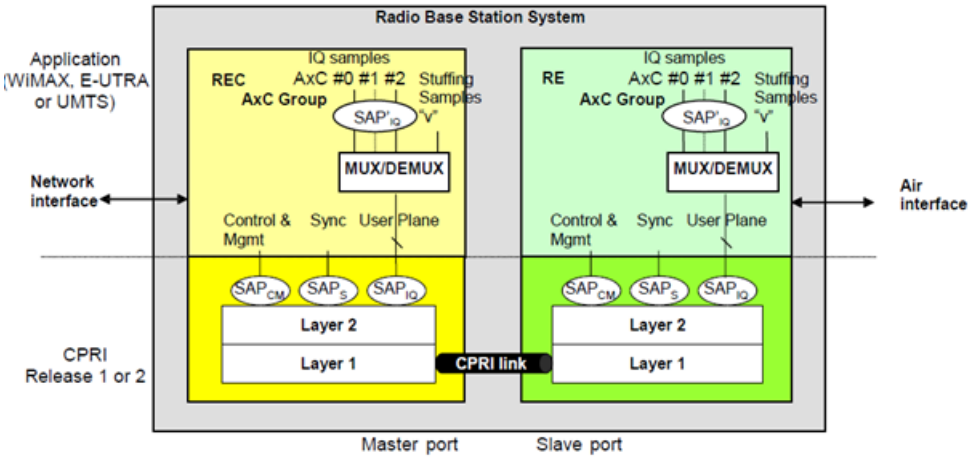

Figure 3.7: LTE data I/Q mapped on the CPRI frame

at 2.45 Gbit/s. For all modulations, the maximum EVM, corresponding to the power sensitivity, is approximately equal to 6%. There is negligible EVM difference between different modulation formats. This little difference between EVM of each modulation format and the lower of the EVM (equals to the reference measurements 0.04%) is due to uses high level of the quantification of LTE I/Q format which has 15 bits of resolution. In order to have a better understanding of these results, a thorough analyze of the setup is made. Indeed, the data I/Q (I: 15 bits, Q: 15 bits) provides by the LTE generator is directly sent toward the spectrum analyzer. This latter is able to demodulate the LTE data I/Q and measures an EVM of 0.04% for the three tested modulation formats. When the CPRI is used to transport the LTE data, the data I/Q samples are mapped to the Antenna Carrier Container (AxC). For LTE, two methods exist to map the data I/Q to the AxC Container. For our analysis the backward compatible method is

considered. In this case, One AxC Container contains exactly one sample of data I/Q. The Figure 3.6 gives an overview of the operating mode of this method [37]. Accordingly, one AxC container corresponding to one data I/Q is placed on the CPRI frame whose length is 15 bits. In this way, there is not any modification on the Data I/Q samples. Therefore, when the Signal to Noise Ratio (SNR) of the optical signal permits to return correctly the CPRI signal, the case of the reference measurement can be reproduced at the spectrum analyzer. For example, for 2.45 Gbit/s, concerning the received power of least -22dBm, the Signal to Noise Ratio (SNR) of the optical signal is enough to recover AxC container (I/Q samples) in order to measure an EVM of 0.04% for any tested modulation format. When the attenuation increases, the SNR decreases. The drop of the SNR affects the AxC container accordingly the data I/Q samples which are independent of the modulation format. Hence, the deterioration of the signal due to the mitigation of the SNR impacts at the same way the different tested modulation formats.

In order to show the influence of the resolution bandwidth of I/Q data, the CPRI modules are directly connected themselves. Then the resolution bandwidth is changed in function of the modulation format provided by the LTE generator. The results are consigned in the following table. In the table 3.1, the EVM decreases when the resolution

	EVM following the modulation formats(%)		
Resolution bandwidth (bits)	**QPSK**	**16-QAM**	**64-QAM**
4	14.12	14.84	21.25
6	3.03	3.33	5.7
8	0.49	0.93	1.41
10	0.12	0.2	0.36
12	0.05	0.05	0.1
15	0.04	0.04	0.04

Table 3.1: EVM relative to the resolution bandwidth and the modulation formats

bandwidth rises. The EVM of the different modulation formats is equal and reach its minimum (0.04%) for 15 bits of resolution bandwidth. This result underpins the previous conclusion which specifies that the low different of EVM between the modulation formats and the low EVM observed for all modulation formats are due to the high resolution bandwidth (15 bits).

3.2.3.2 BER

Figure 3.8 reports the BER measurements for the back to back configuration, 30 km feeder and 60 km of optical fiber transmission with various cavity lengths. At 1.22 Gbit/s, the CPRI BER requirement is respected in back to back and with 30 km feeder length, for received powers of at least -22 dBm. For 60km feeder length, the BER is

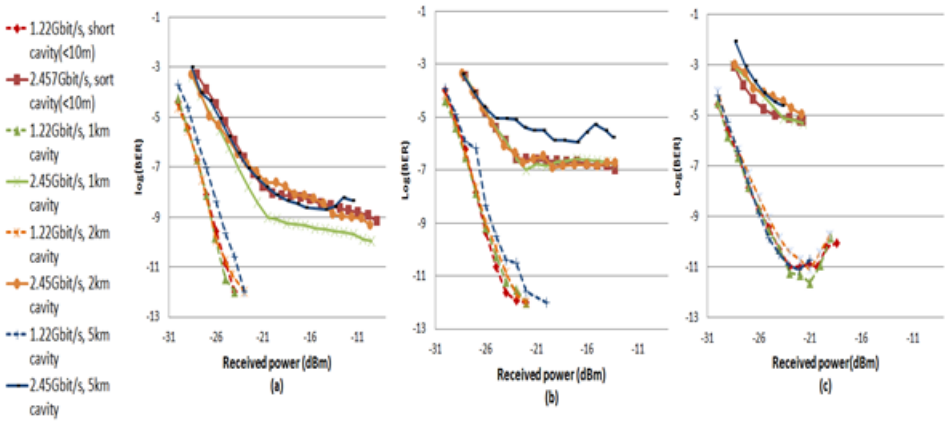

Figure 3.8: BER measurements, (a) back to back, (b) 30 km feeder, (c): 60 km feeder

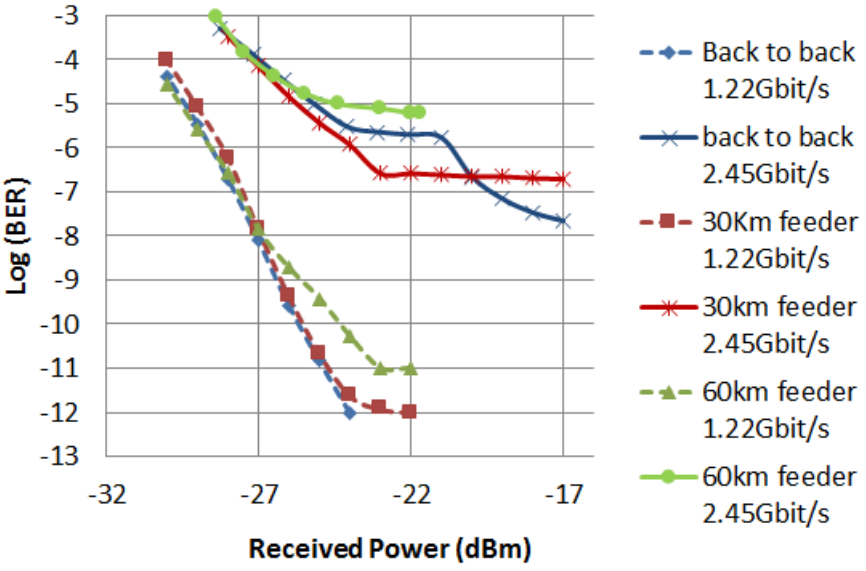

Figure 3.9: Comparison of the BER in function of the fiber length

higher than 10^{-12}. At 2.45 Gbit/s, in all cases, the BER is higher than 10^{-12}. When the different curves of the figure 3.8 are compared, we note a degradation of BER as a function of increasing feeder length. This phenomenon is highlighted in figure 3.9 that depicts the results of short cavity for different feeder length and both data rates.

In figure 3.9, at 1.22 Gbit/s the curves of back to back and 30 km of feeder are superimposed. There are approximately the same performances but for a BER of 10^{-12} a power penalty of 1 dB is measured. About the feeder of 60 km, two parts are distinguished. The first part concerns the curve whereabouts the received power is approximately of at least -27 dBm. In this part, a little penalty is illustrated in terms of BER. For a BER of 10^{-11} a power penalty of approximately -3 dB is measured. At 2.45 Gbit/s, according to the Figure 3.8, after 30 km and for a BER of 10^{-7} a power penalty of about 5 dB is

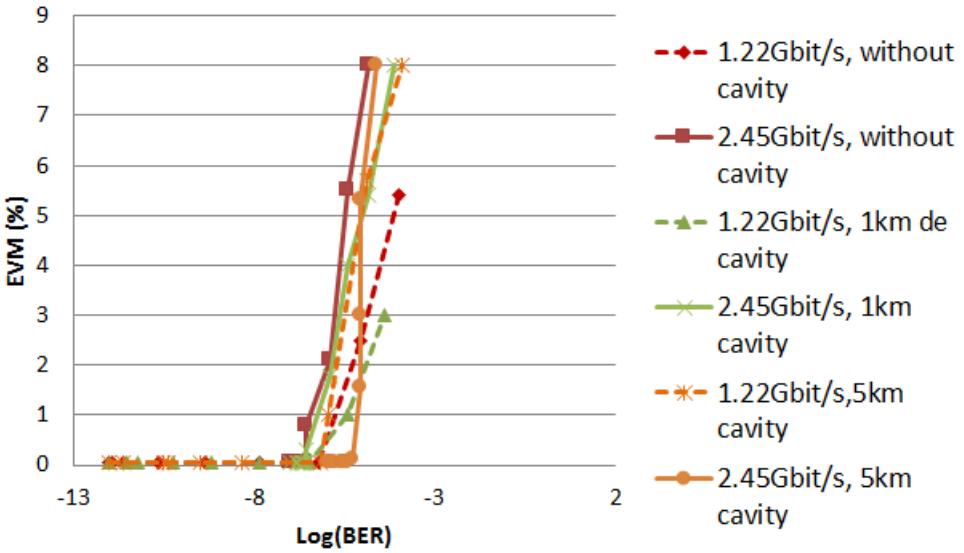

Figure 3.10: EVM measurement vs BER

noticed. At 60 km of optical transmission, for a BER of about 10^{-5} a power penalty of approximately 3dB is noticed.

This power penalty is essentially due to 2 raisons. At first, the cavity modes which appear in the cavity of the self-seeded source [91]. At second, a standard SMF-28 (chromatic dispersion is zero at 1310 nm) fiber is used. Considering the emitted wavelength (1327.76 nm) a small quantity of chromatic dispersion (CD) and Polarization Mode Dispersion (PMD) are introduced by the used fiber. Remember that for a standard SMF-28 the CD is between 0 and 3.5 ps/nm for the wavelength between 1280nm and 1330 nm. The main reason of the observed penalty after the 30 km and 60 km of feeder is that all longitudinal modes present in the cavity [91] suffer the effects of chromatic dispersion and PMD.

The EVM specification is respected for all constellation, even if the BER is higher than CPRI specification. Figure 3.10 shows the correspondence between the EVM and the BER for 30 km of transmission and for different cavity lengths. For both transmission rates, the EVM remains equal to 0.04% until the BER is lower than approximately 10^{-6}. No deterioration on LTE signal quality is observed because the EVM is constant and respects the 3GPP specifications. The end to end signal quality is ensured despite the BER does not comply CPRI specification. One more time, this result shows the strength of the D-RoF technology and ensure the quality of the LTE signal for the low BER performance according the CPRI specifications. This low deterioration of EVM signal is thanks to the high resolution of quantification.

Rate	Short cavity (<10m)			1 km cavity			2 km cavity			5 km cavity		
Rate (Gbit/s)	TJ (UI)	RJ (UI)	DJ (UI)	TJ (UI)	RJ (UI)	DJ (UI)	TJ (UI)	RJ (UI)	DJ (UI)	TJ (UI)	RJ (UI)	DJ (UI)
1.22	1.1	0.35	0.74	1.1	0.38	0.7	1	0.64	0.36	1.1	0.55	0.6
2.45	1.5	0.7	0.8	1.35	0.9	0.4	1.48	1.1	0.4	1.6	1	0.6

Table 3.2: Jitter measurements for fronthaul based on a self-seeded system

3.2.3.3 Jitter and latency characterization

The jitter and latency aspects are very important parameters in the characterization of a fronthaul link. Let remember that the DSO is used to measure the jitter in the time domain and the latency is measured by means of the CPRI errors detectors (figure 3.4). The results about the jitter measurements are consigned in the table 3.2. The TJ, RJ, DJ are measured for different cavity length. According to the table 3.2 , the jitter (TJ, RJ, and DJ) does not depend on the cavity length but it depends on the rate. In all cases, the measured jitter is higher than the maximum tolerated values according to the CPRI specifications. At 2.45 Gbit/s random jitter is very high (approximately 1UI). Indeed, the RJ is mainly due to thermal noise [94]. The power of thermal noise P depends of temperature and bandwidth (equation 3.1).

$$P = K_B T B \tag{3.1}$$

Where:

- P: The power of thermal noise
- K_B: The constant Boltzmann
- B: The bandwidth.

When we compare RJ between the two rates, at the same temperature, RJ at 2.45 Gbit/s is approximately two times than at 1.22 Gbit/s. When the bandwidth increases, the thermal noise increases at the same proportion and causes the rise of the RJ. In order to reduce random jitter, we can study the temperature influence on the self-seeded source based on a RSOA or the influence of the CPRI compression which permits to reduce the bandwidth of signal. Despite the high jitter level, the quality of LTE signal is not impacted.

The table 3.3 lists the latency measurements. The introduction of cavity length increases latency. To obtain the total latency on the transmission, we add the delay of the cavity and the delay of the feeder. Indeed, for 5 km of cavity, 24 μs on the latency has been added compared to the back to back configuration. This latency corresponds

to the signal propagation in the optical fiber. To estimate the round trip delay, we can multiply by two the values of table when we consider that the transmission on the uplink and the downlink use the same self-seeded setup. According to [32], the round trip delay is 400 μs for LTE-A and 700μs for LTE. In terms of round trip delay, the self-seeded DWDM can be used until 60 km with 5 km of cavity (644 μs of round trip delay) for LTE and until 30 km with 5 km of cavity (349 μs of round trip delay) for LTE-A. But remember that the values of the round trip delay proposed by [32] are not a standard. The works of the standardization of these values are ongoing.

Rate	Short cavity (<10m)			1 km cavity			2 km cavity			5 km cavity		
Rate (Gbit/s)	0 km	30 km	60 km	0 km	30 km	60 km	0 km	30 km	60 km	0 km	30 km	60 km
1.22	0 μs	149.6 μs	297.2 μs	4.8 μs	154.6 μs	302 μs	9.8 μs	159.5 μs	306.8 μs	24.5 μs	174.3 μs	321.7 μs
2.45	0.02 μs	149.7 μs	297.2 μs	5 μs	154.7 μs	302.2 μs	9.3 μs	159.6 μs	307 μs	24 μs	174.4 μs	321.8 μs

Table 3.3: Latency measurements for fronthaul based on a self-seeded system

3.2.4 Radio frequency deviation

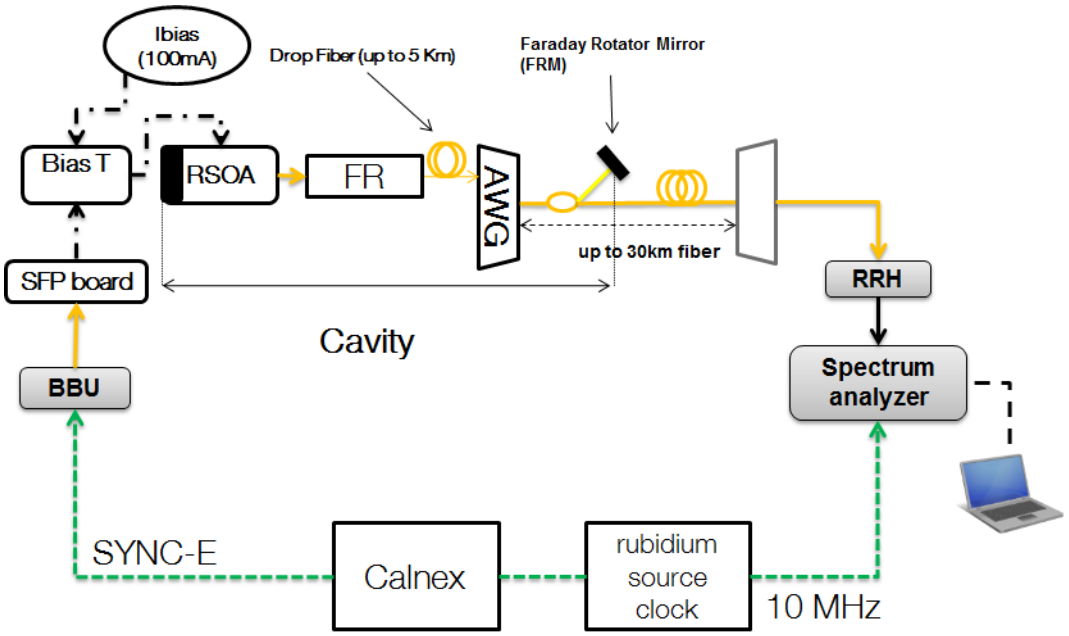

Figure 3.11: Setup of frequency deviation measurements

The Radio frequency accuracy is the precision of the RU radio frequency transmitter to synchronize on a nominal frequency. Interdependence between CPRI clock, jitter and radio frequency accuracy budget exist [95] [96] and this latter can be influence the performance of the LTE signal. The maximum allowed radio frequency deviation at the air interface of LTE eNode B is ±50 ppb [83]. In this experience, we measure the frequency deviation on a commercial eNode B platform as shown in figure 3.11. The CPRI signal provided by the BBU (2.45 Gbit/s) is converted from optical to electrical thanks to a SFP board. This signal is transmitted on the fiber by the self-seeded device. The spectrum analyzer measures the frequency deviation and the EVM. It is important to synchronize the BBU and the spectrum analyzer with the same source (rubidium source with 10^{-9} precision at 10 MHz) in order to have stable measurements. The Calnex allows delivering SYNC-E to synchronize the BBU. The RRH transmits at 816 MHz. The frequency deviation is directly measured at the output of RRH. In this manner, we are sure that the measured frequency deviation is essentially due to the self-seeded system. At first, a reference measurement without the self-seeded device (the BBU is directly connected to the RRH) has been done. The figure 2.27 shows the results of the reference measurement: 0.5 ppb of frequency deviation is measured. The measurements respect the 3GPP standard (50ppb).

At the following, the radio frequency deviation is measured with the self-seeded setup.

	Reference measurements		**Short cavity**		**Other Cavity length**	
Length of transmission (km)	**Back to back**	**30**	**Back to back**	**30**	**Back to back**	**30**
Frequency deviation (ppb) / rate of measured samples (%)	0.7/ 99		0.9/ 99	0.9/ 60 35/ 25 ≥50/ 15	No radio signal (system is down)	

Table 3.4: Frequency deviations results

The Figure 3.11 and the Figure 3.12 present the results for the short cavity, which is implemented with back to back feeder and with 30 km of feeder. Figure 3.11 describes back to back configuration. The measurements of frequency deviations are generally between 0 and 0.9 ppb. The EVM is constant at 0.24%. When 30 km of feeder is added (figure 3.12), most of measured points are between 0 and 0.9 ppb (approximately 60% of measured samples), but several of them are higher than 50 ppb. In the case where the frequency deviation is above 50 ppb, the radio link is failed and the EVM is higher than the 3GPP recommendations. For when the frequency deviation is below 50 ppb, the EVM equal to 0.24%. The combination of jitter and the propagation of the longitudinal modes (present in the cavity of self-seeded) in the standard fiber (SMF-28) do not permit the RRH to properly synchronize to the frequency of the CPRI signal. When cavity length is added, the system does not operate. In this case the number of longitudinal mode increases and affects the Relative Intensity Noise (RIN) which is an important parameter in the performance of the self-seeded transmission. The level of the RIN depends of the competition of the longitudinal mode [91]. The RIN and the cavity losses affect the performance of the transmission and do not allow the RRH to operate. Finally, for the tested commercial eNobe B, only the configuration of short cavity without fiber transmission properly operates. The different results are summarized in the table 3.4.

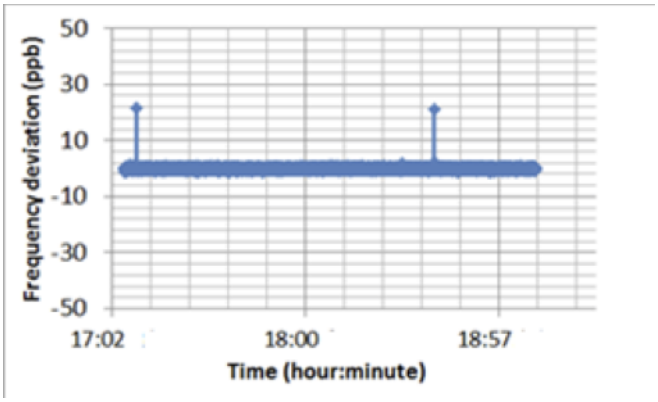

Figure 3.12: Frequency deviation for short cavity and back to back feeder

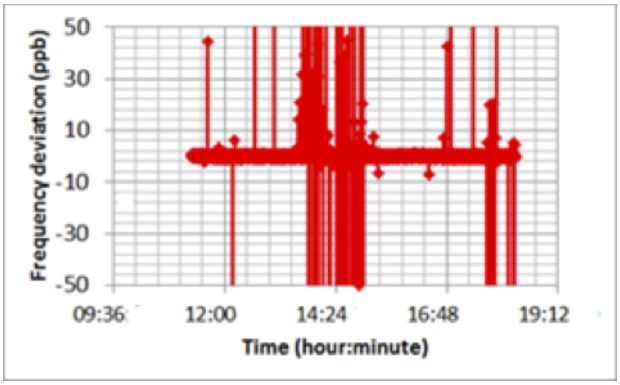

Figure 3.13: Frequency deviation for short cavity and 30 km feeder

3.3 CWDM single fiber solution for fronthaul

To achieve fronthaul, different physical configurations exist. Among them, the point to point topology can be used be used but its deployment uses a lot of optical resources. Indeed, this physical topology links each RRH to its BBU by two fibers. The pair of fibers is used to downlink and uplink transmission between BBU and RRH. Since the optical fiber is a scarce resource, a Wavelength Division Multiplexing (WDM) technic is used in order to reduce the number of fiber. Concerning the Coarse WDM (CWDM), it is possible to multiplex up to 18 optical links. In addition, the CWDM proposes 2 configurations. First of all, the dual fiber CWDM can be used to reduce the number of fiber. Indeed, between the demarcation points only 2 fibers are necessary to connect 18 RRHs to their BBU instead of 36 fibers for the point to point physical topology. Typical macro cell configurations in urban areas can reach up to 15 RRHs corresponding to 3 sectors for each radio access technology that must be connected to the BBUs in the CO. Dual fiber CWDM is a low cost option that allows the reduction of the CAPEX and OPEX relative to the point to point physical topology by connecting 15 RRHs to their BBU through 2 transmission fibers (figure **??**).

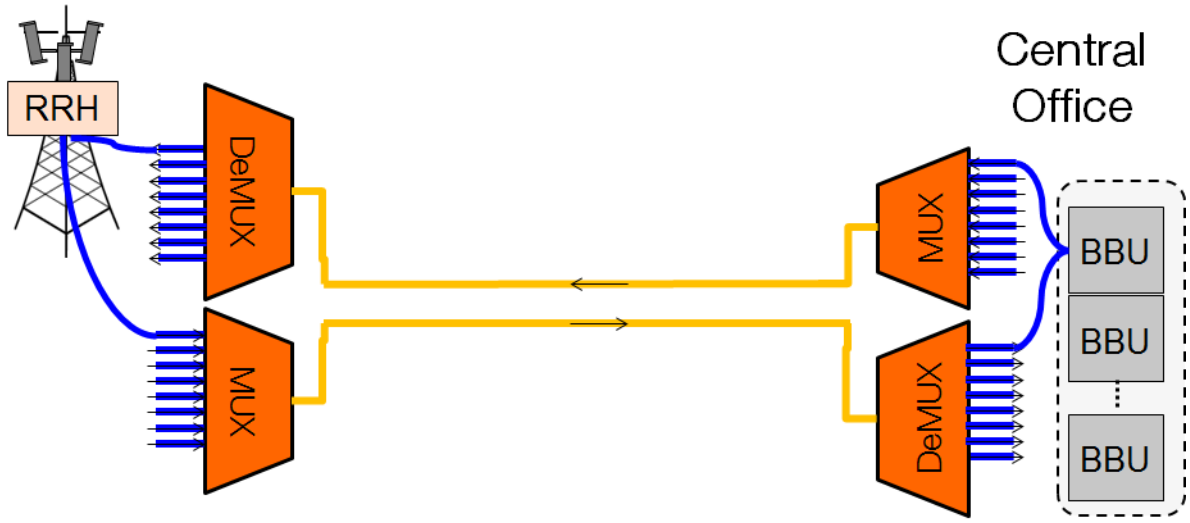

Figure 3.14: Dual optical fiber transmission of fronthaul link

3.4 CWDM single fiber solution for fronthaul

To achieve fronthaul, different physical configurations exist. Among them, the point to point topology can be used but its deployment implements a lot of optical resources. Indeed, this physical topology links each RRH to its BBU by two fibers. The pair of fibers is used to downlink and uplink transmission between BBU and RRH. Since the optical fiber is a scarce resource, a Wavelength Division Multiplexing (WDM) technic is used in order to reduce the number of fibers. Concerning the Coarse WDM (CWDM), it is possible to multiplex up to 18 optical links. In addition, the CWDM proposes 2 configurations. First of all, the dual fiber CWDM can be used to reduce the number of fibers. Indeed, between the demarcation points only 2 fibers are necessary to connect 18 RRHs to their BBU instead of 36 fibers for the point to point physical topology. Typical macro cell configurations in urban areas can reach up to 15 RRHs corresponding to 3 sectors for each radio access technology that must be connected to the BBUs in the CO. Dual fiber CWDM is a low cost option that allows the reduction of the CAPEX and OPEX relative to the point to point physical topology by connecting 15 RRHs to their BBU through 2 transmission fibers (figure **??**).

In spite of the simplicity of this solution, its reliability and its robustness for outdoor environment, dual fiber CWDM has also some drawbacks. At the cell site and at CO level, the requirement of two fibers can burden the exploitation. A single fiber bidirectional solution would be privileged in comparison to dual fiber CWDM to connect up to 18 RRHs. Moreover, a single fiber link would provide a symmetric link that is preferable for synchronization issues in LTE-A. For this raison, this study is going to focus on the bidirectional single fiber to achieve fronthaul link. In order to build a

fronthaul solution, several aspects must be considered like legal and regulation aspects, operation, administration, monitoring system and cost efficiency of CPRI transport. In terms of legal and regulation aspects, it is important to know the part on the fronthaul link which will be managed by the fiber provider. In order to situate the different responsibility between the mobile operator and the fiber provider, the Demarcation Points (DPs) must be defined. In our case, we consider like a fiber provider. Deploying fronthaul solution based on single fiber systems requires the implementation of an optical link monitoring for fault detection. In dual fiber CWDM, the monitoring scheme consists in injecting an optical power at a dedicated wavelength (e.g. about 1600 nm) from active equipment at CO. This monitoring signal is looped with passive equipment situated at antenna site. Following the received power measured in the active equipment, we can diagnose the fiber link between the MUXs and DeMUX. This monitoring system is not able to precisely detect the cause or to situate exactly the fault on the fiber. It just able to diagnostic if the fiber has a fault which causes the failure of the fronthaul.

Unlike dual fiber CWDM, it is difficult to implement monitoring system on single fiber CWDM. For the time being, there is no monitoring solution for fronthaul CWDM single fiber links. Furthermore, the fixed and mobile network convergence aspects presented by COMBO project, the CWDM single fiber is proposed as solution to integrate fronthaul in the reference architecture but the issue about the monitoring scheme is addressed. Our objective is to demonstrate the possibility to have a complete CWDM single fiber solution for fronthaul. This solution implements CPRI data traffic and a monitoring scheme based on reduction of Rayleigh Backscattering (RB). Like the monitoring system of dual fiber CWDM, the proposed monitoring scheme permits to diagnostics if the fiber transmission is damaged and not to detect the source of the damage or to localize where the fiber is cut. In this section, at first, the monitoring aspects are going to present, and then the issue about the single fiber for fronthaul is going to discuss.

3.4.1 Monitoring Scheme for single fiber for fronthaul

The reflection of the light in a mono fiber can be caused by [97]:

- Rayleigh scattering: due to non-homogeneous structural changes at the molecular level. The light propagates in all directions
- Reflections scattered light: due to localized changes in the optical refractive index glass of the glass. The light also propagates in all directions
- Reflection diameter: due to the geometrical glass differences

- Fresnel peaks: appear where there is a sudden change in the material density. For example, from glass to air transitions at near perpendicular cleaved fiber ends.

Indeed, the non-homogeneous of particles always exist in the fiber, the presence of Rayleigh scattering is so permanent and cannot be avoided [98] [99]. Rayleigh scattering is one of main causes of the attenuation in the fiber. The attenuation due to the Rayleigh scattering is inversely proportional to the wavelength ($\sim\lambda^{-4}$ where λ is the wavelength).

When a cut of fiber occurs, the reflected power light depends on refractive index difference (between the core of single fiber mode and the air), the angle of incidence and the polarization incident ray. The worst case which can appear is when the cut of fiber is straight. In this case, the reflective power is approximately estimated at 4% of the incident radiation at the silica-air interface (less 14 dB under the incident power) [100]. This kind of reflection corresponds to Fresnel peaks. In the practice, when a cut of fiber occurs, it is rare that the cut is straight. Generally, the cut makes an angle at the silica-air interface thereby the reflected power is less than 4% and becomes negligible relative to the power of Rayleigh scattering light. The objective of this experimental study is to propose a monitoring scheme based on the Rayleigh Backscattering.

Two monitoring setups are presented. The first is the setup which is described in the figure 3.15. It permits to measure the reflected power of an injected signal and the intrinsic Rayleigh Backscattering level. The second setup (figure 3.16) improves the performance of the first by reducing the power of Rayleigh Backscattering at the reception thanks to a Polarization Beam Combiner (PBC) and a Faraday Rotator Mirror (FRM).

Monitoring a CWDM single fiber link is possible thanks to a probe wavelength with bidirectional CWDM transmission between BBU and RRH (figure 3.15, figure 3.16)

The figure 3.15 describes the method allowing a single fiber monitoring system. The principle of the system is to introduce a probe signal in the fiber. This probe situated at Central office (CO) is modulated by a low frequency signal (50 MHz) in order to limit Brillouin backscattering because about +7 dBm optical power is launched in the fiber in our experiments. At CO, an optical circulator is used to separate the signal probe which is injected in the MUX/DeMUX from the reflected signal. The probe signal is reflected by a mirror situated at Demarcation Point (DP). Whatever the probe optical power injected in the optical fiber, a Rayleigh Backscattering (RB) light is detected and has a power level at least 30 dB below the optical power injected in the optical link [98]. When a fiber cut occurs on the fronthaul link, the power monitor measures essentially the RB power. In order to understand our monitoring scheme, we give the following example.

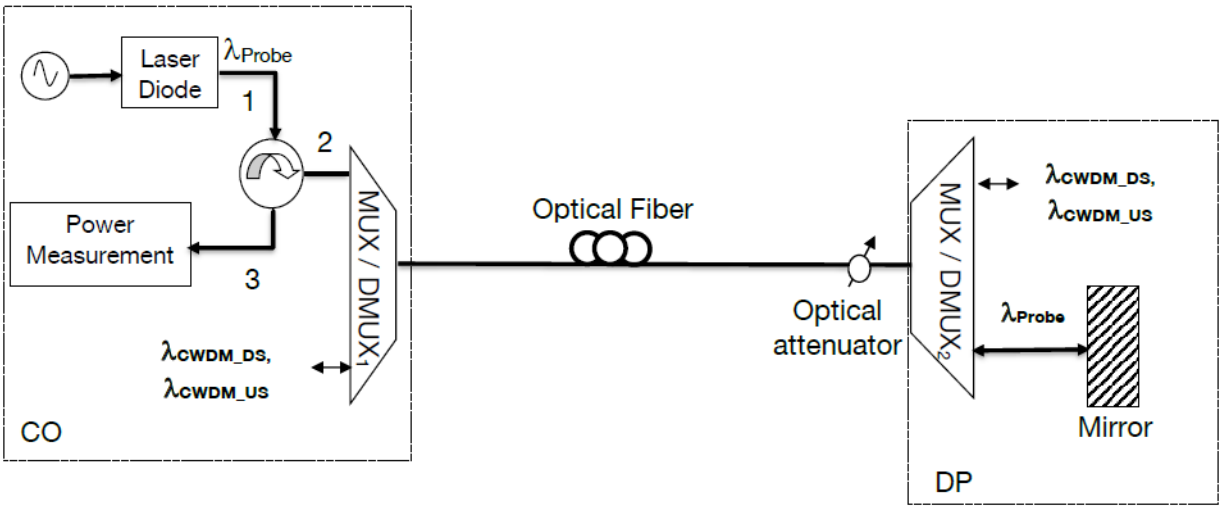

Figure 3.15: Single optical fiber link monitoring based on reflective mirror and an optical circulator

We assume that the CWDM single fiber whose the attenuation of round trip link is 30dB. In addition, we assume that the RB power is 30 dB below the injected power of probe. In other words, 15 dB of optical attenuation are sufficient to have a reflected power equal to the RB power. in this case, the reflected power measured by the power meter and the power of RB should be equal. Therefore, it will be difficult to dissociate RB light from the attenuated probe once reflected. This type of monitoring scheme is thus limited to approximately a 30 dB round trip optical budget (laser diode emission / power monitor in the CO). We consider the optical link has a fault when the measured power is equal to the RB power. A margin of 1 or 2 dB above the RB power can be considered in practice as threshold of detection. The performance of this monitoring system depends on the gap between the power of the injected signal probe and the level of RB light. In other word, more this gap is important, more it is possible to detect some failures on a CWDM single fiber system whose the optical budget is high. In order to increase this gap, a method to reduce RB light measured by the power meter is proposed. This method consists to replace the optical circulator and the mirror by a PBC and a FRM, respectively. The Figure 3.16 depicts the setup of this method.

This monitoring scheme reduces RB impact by decomposition of its State of Polarization (SoP). Notice that RB light SoP is the same as the incoming light SoP [98]. Moreover, the Degree of Polarization (DoP) of Rayleigh backscattered light is equal to 33 %, and its state of polarization is the same than the incoming signal [98]. Thus only 33% of RB light is polarized and will be treated by the PBC. The FRM is used to reflect the probe and rotate its SoP by $\pi/2$. This change of polarization permits to maximize

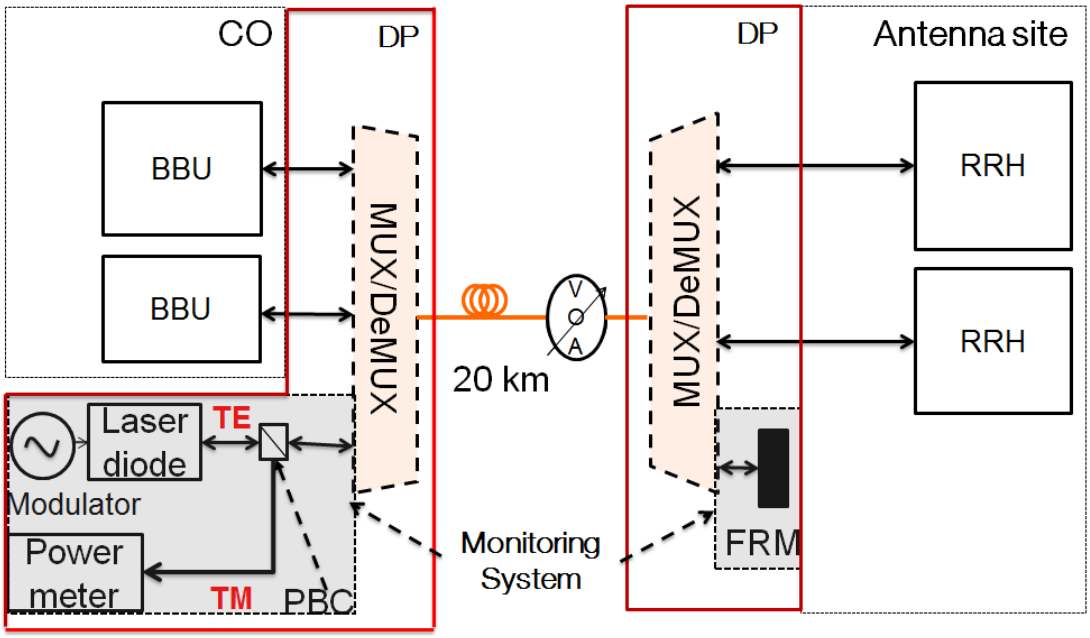

Figure 3.16: Single optical fiber link monitoring based on FRM and an PBC

the power on the TM port of the PBC and to protect the laser probe of the reflected signal. Indeed, in the setup shown in Fig. 2.30, solely light in TM mode is measured, i.e. probe with a rotated state of polarization and TM mode of RB light. When the fiber cut occurs, only the TM mode of the polarized RB light (33% of the total RB light) is measured. In this way the measure power at the CO due to the RB light is reduced. Thereby the reduction of RB effect allows increasing of the round trip optical budget to detect the fiber faults. Additionally, a polarization scrambler is introduced. It permits a rapid variation of SoP of the injected signal of probe in the fiber in order to study the influence of different SoP.

3.4.1.1 Experimental Results

At the following, setup 1 and setup 2 describe respectively the setup depicted by the figure 3.15 and figure 3.16. The laser diode used for monitoring probes has 10.2 dBm of output power at a wavelength of 1610 nm. For the two setups, this results in 6.9 dBm of injected power in the optical fiber, considering insertion losses (optical circulator, PBC, MUX/DeMUX, polarization scrambler). The insertion losses of the different components involved in setup 1 and setup 2 are detailed in the table 3.5 and the table 3.6.

Generally, all optical measured powers converge to RB Level when the attenuation value increases as illustrated by figure 3.17. Indeed, round trip Optical Budget (OB) is estimated to 21.5 dB (resp. 22.5 dB) with 0 dB of variable attenuation for setup 1 (resp. setup 2). The estimation of the round trip OB permits to estimate the received power.

Designation	Insertion Loss (dB)
Optical circulator, port 1 → port 2	2.2
Optical circulator, port 2 → port 3	1.7
Optical circulator isolation, port 1 → port 3	56
CWDM MUX/DMUX1	1.1
CWDM MUX/DMUX2	1.5
Optical fiber of 20km	4
Optical attenuator	1.5
Mirror	1.4

Table 3.5: Insertion Losses of components involved in setup 1

Designation	Insertion Loss (dB)
PBC, port 1 → port 2	0.6
PBC, port 2 → port 3	1.1
Faraday Mirror Rotator	1.4
CWDM MUX/DMUX1	1.1
CWDM MUX/DMUX2	1.5
Optical fiber of 20km	4
Optical attenuator	1.5

Table 3.6: Insertion Losses of components involved in setup 2

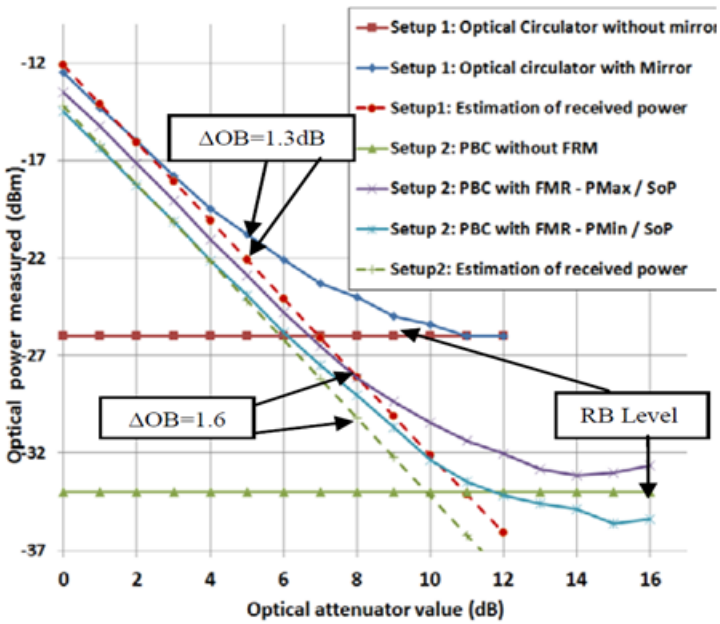

Figure 3.17: Received Optical Power measurement in function of the optical attenuator value on 20 km of optical fiber

We define the round trip OB error (ΔOB) as the difference between measured power and estimated received power. For example, ΔOB is equal to 1.3 dB (resp. 1.6 dB) for 5 dB (resp. 8 dB) of attenuation in setup 1 (resp. setup 2). ΔOB increases (figure 3.17) as the value of attenuation rises and the measured power at the power meter becomes to be constant because RB light comes to be predominant.

In order to study the influence of SoP variation, a polarization scrambler is introduced in setup 2. The difference between PMax/SoP and PMin/SoP which increases following attenuation value highlights this influence. PMax/SoP (resp. PMin/SoP) is the measured power which corresponds to the SoP introducing the maximum (resp. the minimum) power in the fiber. The difference between PMax/SoP and PMin/SoP is due to the difference of the injected power of signal.

3.4.2 CWDM single fiber link for fronthaul

A fronthaul single fiber CWDM bidirectional link is achievable thanks to single fiber Small Form factor Pluggable (SFP) [101] which operates at CWDM wavelengths. The figure 3.18 shows a CWDM single fiber SFP and the figure 3.19 describes the experimental setup.

Figure 3.18: CWDM single fiber SFP

These tests are performed on a 20 km optical fiber. Several types of SFP transceivers are used and modulated by CPRI signal. The first transceiver is Single Wavelength Single Fiber (SWSF) SFP which uses only one CWDM wavelength for transmission and reception thanks to a 3 dB optical splitter. An isolator is placed after the laser diode and a CWDM filter positioned before the photodiode. It operates up to 2.45 Gbit/s at 1531nm and it emits at -7 dBm. Signal reflection impact can be reduced by using Angle Physical Contact (APC), but it is not practically feasible. This SFP makes an angle of 8° with a fiber to reduce the impact of the reflected signal. If the conventional SMF 28 is considered, this angle of 8° is larger than the critical angle θ_c defined by the following formula:

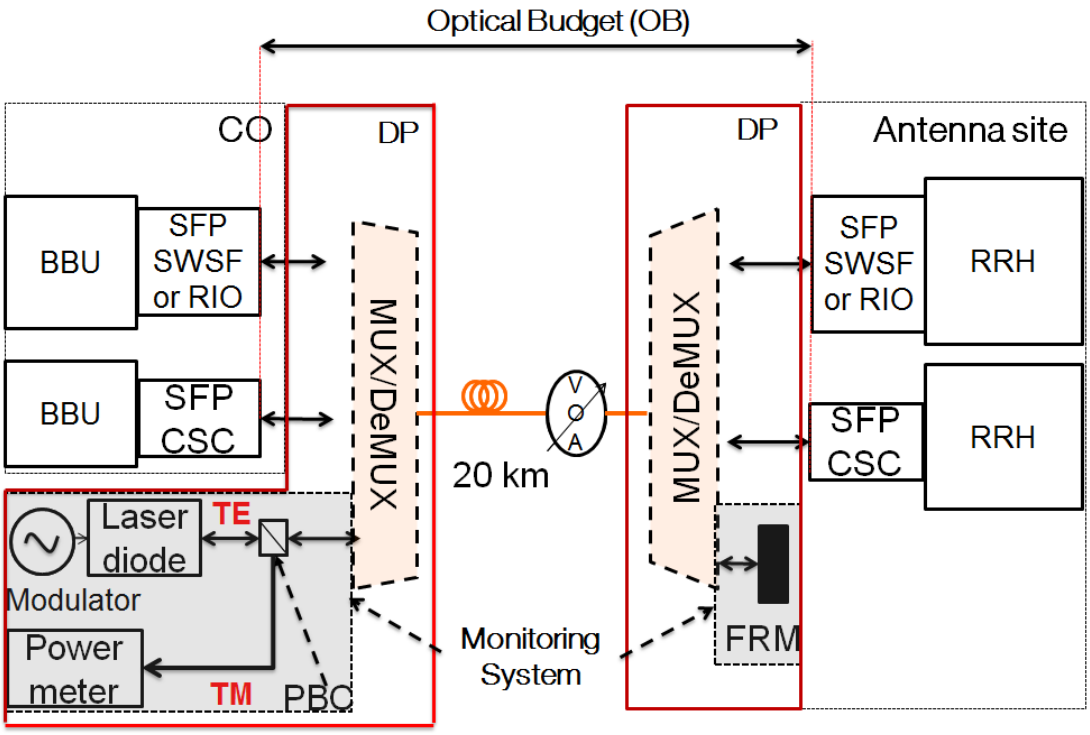

Figure 3.19: A complete CWDM single fiber solution for fronthaul

$$\theta_c = \arcsin(\frac{n_{cladding}}{n_{core}}) \tag{3.2}$$

Where:

- $n_{cladding}$: Cladding refractive indice
- n_{core}: Core refractive indice

This kind of connector is not used in the networks of fiber provider. It has the same description as simple SWSF SFP in terms of emitted power, data rate and wavelength. The figure 3.20 shows the schema of APC SWSF.

Then we consider a SWSF Reflection Immune Operation (RIO) SFP, which recognizes reflected signals in order to cancel electronically the reflection impact [102].

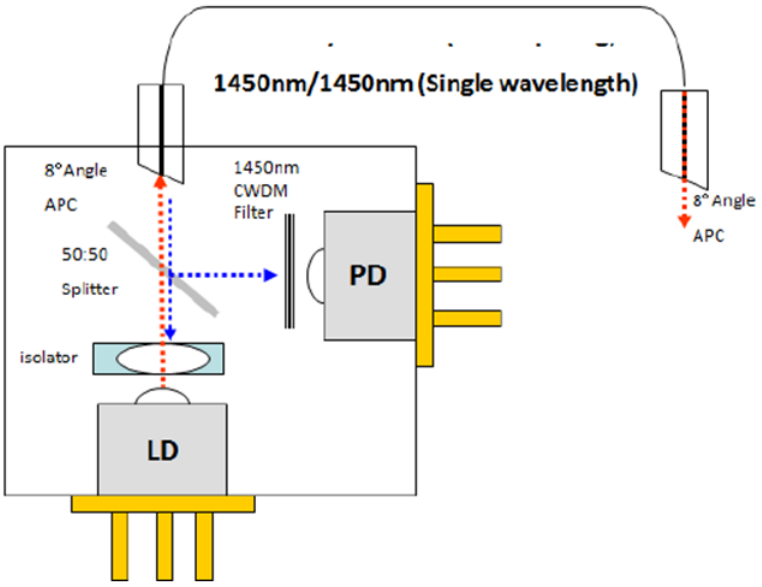

Figure 3.20: APC SWSF at 1450 nm. (LD: Laser Diode, PD: Photodiode)

It operates up to 1.22 Gbit/s at 1511 nm and emits at -3 dBm. Figure 3.21 shows the schema of RIO SFP.

At last, Cooled Single Channel (CSC) SFP divides each 20 nm CWDM channel in two sub-channels [103]. It can reach 4.9 Gbit/s CPRI data rate. The couple of CSC SFP operating up to 2.45 Gbit/s emits -1 dBm and has the couple of wavelength at 1547nm and 1556nm. The power of couple of CSC SFP operating up to 4.9 Gbit/s is 0 dBm and has 1567 nm and 1576 nm as operating couple of wavelength. The CSC SFP roadmap indicates that 10 Gbit/s can be reached. The Figure 3.21 gives a descriptive of the CSC SFP principle.

To build a fronthaul solution, some requirements like Bit Error Rate (BER), must be considered. Let remember that the CPRI specification fixes the maximum BER at 10^{-12} for all data rates [37]. Figure 3.23 presents measured BER for different SFPs (SWSF, SWSF APC, RIO and CSC). The Optical Budget (OB) is defined between the Tx and Rx of the transceivers face to face, and the Rx sensitivity is characterized for a BER equal to 10^{-12}.

According to figure 3.23, the performances at 1.22 Gbit/s (dashed curves) and at 2.45 Gbit/s are approximately the same. Concerning SWSF SFP type, simple SWSF SFP has poor performances due to the reflected signal. It has -17 dBm of receiver sensitivity and 10 dB of OB. Using APC allows improving the optical budget by 5 dB at 1.22 Gbit/s and 2.45 Gbit/s. Indeed, the angle at the end of connector reduces reflected power. In practice, for 1.22 Gbit/s SWSF RIO SFP improves the performance of about

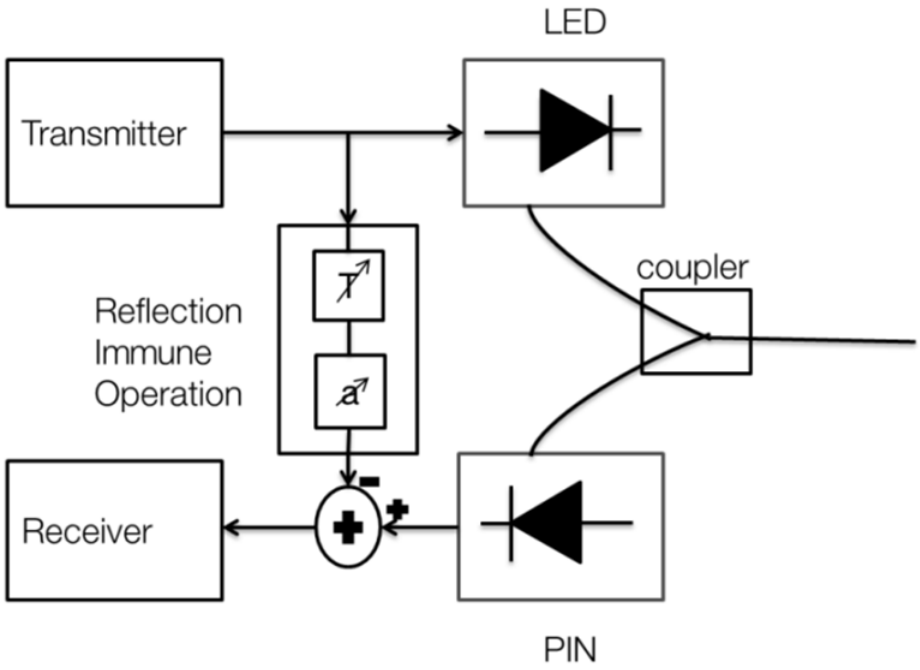

Figure 3.21: RIO SFP. (LED: Light Emitting Diode, PIN: Positive Intrinsic Negative diode)

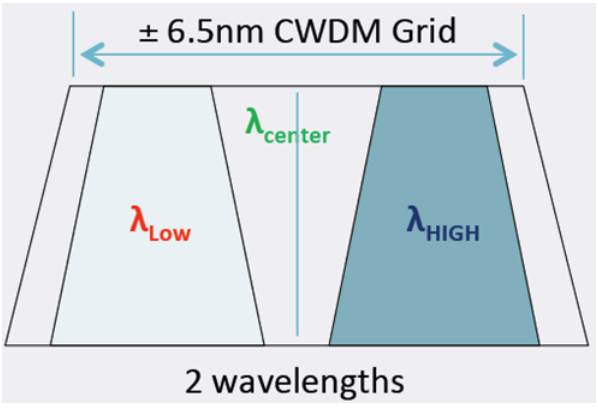

Figure 3.22: CSC SFP

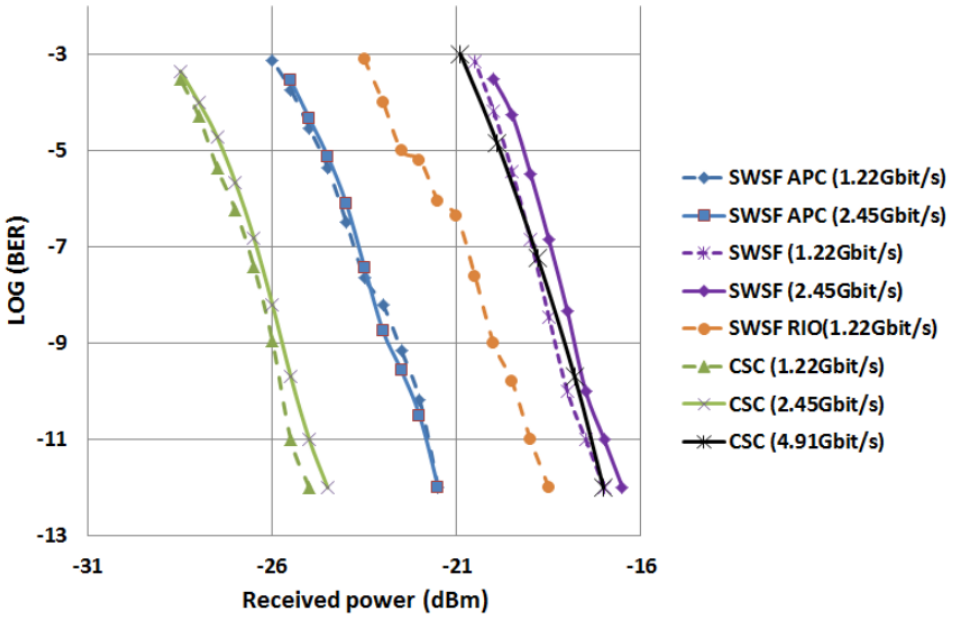

Figure 3.23: BER on fronthaul CWDM single fiber in function of received power

1.5 dB relative to the receiver sensitivity of simple SWSF SFP. It has 15.5 dB of OB and -18.5 dBm of receiver sensitivity. For this data rate, CSC SFP is the best transceiver with 24 dB of OB. At 2.45 Gbit/s CPRI rate, CSC SFP has best performances with approximately -25 dBm receiver sensitivity and 24 dB of OB. Only CSC SFP can reach 4.9 Gbit/s CPRI rate. It has 17 dB of OB and -17 dBm of receiver sensitivity at this CPRI rate.

3.4.3 Diagnostic results

Sometime on the optical link, the bends can appear. These bend can strongly attenuate the signal. For the wavelengths of about 1600 nm and regard the radius of the curvature, the attenuation can exceed 100dB/m [104]. Therefore, the bends can cause an important attenuation such that the measured reflected power is equal to the power of RB. But when the optical budget of the SFP is higher than the half of the round trip OB which characterizes our monitoring scheme, the communication between the BBU and the RRH is possible. For better understanding, the following example is given.

Aforesaid, our monitoring system has a round trip optical budget equal to 40.9 dB. On a fronthaul link, the attenuation between the BBU and the RRH is 8.7dB. Let assume that this is a bend which introduces an additional attenuation of 14 dB on the optical link. The total attenuation on the fronthaul link is 22.7 dB. Indeed, this attenuation in the fronthaul link permits to have a BER of 10^{-12}. However, on the monitoring link, the

Case1	Case 2	Case 3	Alarm
✓	×	×	flawless link
✓	✓	×	default link (strong attenuation)
×	✓	×	cut link or strong attenuation
✓	×	✓	minor default link

Table 3.7: Different alarms of the monitoring scheme

total round trip attenuation is 50.5dB. The measured power at the power meter has the same power level that the Rayleigh Backscattering. Thus, when the power of Rayleigh Backscattering is measured does not automatically mean that the cut fiber occurs. To diagnostic the optical fiber failure, three cases are distinguished:

- Case 1: Received power by the SFP is higher than the sensitivity of the SFP. *Received power by the SFP* $\geq$ *sensitivity*
- The measured power by the power meter equals to Rayleigh Backscattering level. The measured power by the power meter equals to Rayleigh Backscattering level
- The measured power by the power meter is less than -28.5 dBm which corresponds to the measured power where le RB comes to be predominant in the optical fiber link, and higher than RB level. in other terms:
  RB level $\leq$ *Measured power by power meter* $\leq -28.5dBm$.

The table 3.7 gives the alarm for the diagnostic results following the different cases.

3.5 Conclusion

In this Chapter 3 kinds of solution for the implementation of fronthaul are studying. The first presented solution is the DWDM self-seeded based on a RSOA O band and the second solution is the WDM single fiber implementing a semi passive monitoring scheme based on the reduction of RB light.

Concerning the first solution, the fronthaul requirements in terms of BER, jitter, round trip delay and radio frequency accuracy budget have been evaluated. A fronhaul link is implemented including the radio signal generation (LTE) and the CPRI module. The radio performances are measured in terms of EVM. The implemented self-seeded technology guarantees the respect of the LTE quality signal in terms of EVM (3GPP indications). In addition, BER of 10-12 is reached with a rate of 1.22 Gbit/s for back to back and 30 km feeder transmission configuration. Considering the rate of 2.45 Gbit/s, the BER is not complied with the CPRI specification. Moreover, the jitter specifications

are not respected for both rates 1.22 Gbit/s and 2.45 Gbit/s. The quantity of RJ depends on bandwidth. It is proportional with the data rate. The RJ is approximately multiplied by two (2) when the bitrate is changed from 1.25Gbis/s to 2.45 Gbit/s. However, even the CPRI specifications in terms of BER and jitter are not respected; the EVM of LTE signal meets the 3GPP recommendations. The latency of the fronthaul link allows evaluating an important parameter which is the roundtrip delay. In our study, the total latency is the addition of cavity latency and the feeder latency. These latencies correspond to the time of signal propagation in the optical fiber. The round trip delay can be obtained from the latency measurements. Considering round trip delay we can use LTE and LTE-A with the self-seeded transmission system until 30km of feeder and with 5 km of cavity length. The radio frequency accuracy budget is generally compliant when the self-seeded system with short cavity ($<$10m) is implemented. Some peaks higher than 50ppb are observed when feeder transmission is added. These peaks are generally due to the combination of jitter and the propagation of longitudinal modes in the transmission fiber. When long cavity length is introduced, the EVM requirement is not respected. A loss of signal (LoS) is observed. These results are due to the high quantity of jitter and the number of longitudinal modes which increases and is not supported by the RRH.

Concerning the second solution, several transceivers such SWSF SFP, SWSF RIO SFP, SWSF APC SFP and CSC SFP are studied to achieve bidirectional WDM single fiber system in the fronthaul link. The best transceiver which provides approximately the same performance that a dual fiber SFP is the CSC SFP but all of them meet the CPRI BER and jitter requirements. The monitoring scheme is possible thanks to the association of PBC and FRM. This association allows monitoring a single optical fiber with roundtrip optical budget up to 40 dB by reduction of RB influence.

General conclusion and perspectives

1. Summary

This thesis is generally focused on the new architecture C-RAN and specifically on the fronthaul segment appeared in the novel architecture concept. The objective of these studies is to provide the operator ORANGE a first approach on the issue of the fronthaul for the possible deployment of C-RAN.

The state of the art presented in the chapter 1 described the evolution of mobile networks. Indeed, this description presents the traditional architecture of 2G, 3G, and 4G. Concerning the 4G, some requirements of LTE as EVM or HARQ time are highlighted. The EVM of the signal allows an assessment of the quality of radio signal and the HARQ time is involved in the calculation of maximum length of optical fiber on a fronthaul link. In addition, to understand the context and the challenges of C-RAN, the wired technologies used in backhaul network are presented. After this brief description of traditional RAN and technologies of backhaul, the C-RAN and the fronthaul segment are introduced. The third step consists to move the BBU from antenna site to the CO where the BBU are stacked. The following step consists to pool the resources of several BBUs so one BBU could manage several antenna sites. Up to now, no prototype is presented concerning the fourth step of C-RAN but the works are ongoing through the virtualization of BBUs. The fronthaul appears when the BBU is moved towards the CO. The fronthaul uses the D-RoF technology to transport the data on optical fiber. Some specifications such as OBSAI, CPRI or ORI define the fronthaul interface. In our work, we focus only on the CPRI specifications because it is more used than the others. From where, the constraints and the requirements are defined for the fronthaul interface. These latter are:

- The data rate
- The latency and timing parameters
- The jitter
- - The synchronization parameter.

The jitter, the latency and the EVM constitute the main measurements in this thesis. The different operation principles of different evaluated solutions are presented in the chapter 1 and have been divided into three parts which are:

- The passive solution
- The passive solution

- The semi active solution
- The active solution

Since the regulation aspects have to be considered, only the semi active and the active solution could be deployed in the operator network.

Among the different requirements defined by the CPRI specification, we pay attention to the jitter parameters. One the important challenge on fronthaul link is to know the impact of the jitter. Indeed, the issue of jitter is addressed in the chapter 2. The different components of jitter are presented. During this study, different setups are proposed and evaluated in order to introduce or measure the jitter impacts on a fronthaul link and on the radio frequency of the RRH. The first proposed setup permits to introduce jitter on the fronthaul link. This dispositive has permitted to test the jitter tolerance of different devices under test. In addition, another dispositive to measure the contribution of jitter on stable frequency has been implemented. The study of the influence of SJ on the fronthaul link shows that the effect of jitter does not depend on frequency of SJ but on the intensity of the jitter. A theoretical study is done on the effects of jitter on the radio frequency deviation of the RRH. During this investigation, basic electronics circuits (PLL) is considered. The results show that the PLL circuit behaves as a filter relative to the jitter and explain the low effect of high jitter frequency on the frequency deviation of RRH observed during the test. Finally, the impact of jitter on the radio frequency is tested on a commercial enode B. The result of this test confirms that the frequency of SJ has few influence on the radio frequency of the RRH. This is due to the behavior of the PLL and the cleaner jitter present in the RRH.

The chapter 3 highlights two low cost solutions for the implementation of fronthaul segment. The DWDM self-seeded based on a RSAO is assessed. The advantage is its colorless property. As the previous tested systems, the EVM of radio signal, BER, jitter parameter, latency and radio frequency deviation are measured. Two data rates are evaluated. The 1.22 Gbit/s is the first tested data rate. The CPRI BER requirement is met and the link is not affected by the chromatic dispersion. The jitter requirement is not respected but the end to end transmission is ensured because a low EVM is measured. At 2.45Gbit/s, no requirement in terms of jitter and BER are met by this system a low quantity of chromatic dispersion affects the optical link. However, like the transmission at 1.22 Gbit/s the transmission end to end is guaranteed on our platform. Concerning the latency, it corresponds to the time propagation of the signal in the cavity and the fiber transmission. The LTE-A and LTE are supported in terms of latency by the system implementing up to 5 km of cavity and 30 km of fiber transmission. This system has

been tested on a commercial eNode B. Only the back to back configuration with a short cavity has permitted the implementation of fronthaul and the communication between the RRH and the BBU. The result of this test shows that the fonthaul link is sensible to the longitudinal modes which appear in the laser cavity and which affect the performance of fronthaul link.

The second evaluated setup allows the realization of a complete solution of CWDM single fiber for fronthaul links. This complete solution consists of a data transmission part and a monitoring system. Regarding the CPRI signal transmission, several transceivers have been evaluated and the best of them which has performances approaching that of the dual fiber transceivers is the CSC SFP. Concerning to the monitoring scheme, it is based on the reduction of RB light thanks to a PBC and a FRM. The implementation of the proposed solution is possible in the realistic network scenarios. Indeed, all used elements to achieve this solution exist at lower cost in the commercial version. The fronthaul link is dimensioning to operate with the SFPs and the proposed monitoring scheme can easily be realized with the commercial CWDM systems.

2. Perspectives

One of major challenges of C-RAN is to rethink fronthaul through function split equipment of RAN. But at first, the CPRI over Ethernet constitutes a preliminary step towards the redefinition of fronthaul. Indeed, the realization of CPRI/ORI over Ethernet should permit the study of packetized fronthaul frames. It also should allow the dynamic allocation of resources and the use of the existing backhaul network. Also, once the CPRI/ORI over Ethernet should be realized, the jitter issue will be addressed. Indeed, in this case, the jitter is defined as the fluctuation of the time taken by data frames to be transmitted from RRH to BBU. Indeed, when different packets take different paths in the Ethernet network to reach their destination, the transmission time of the packet could vary causing the jitter apparition. The impact of this jitter on synchronization parameters or on the performance radio signal could be studied in the future.

Appendix

Appendix 1

The backhaul et fronthaul Network

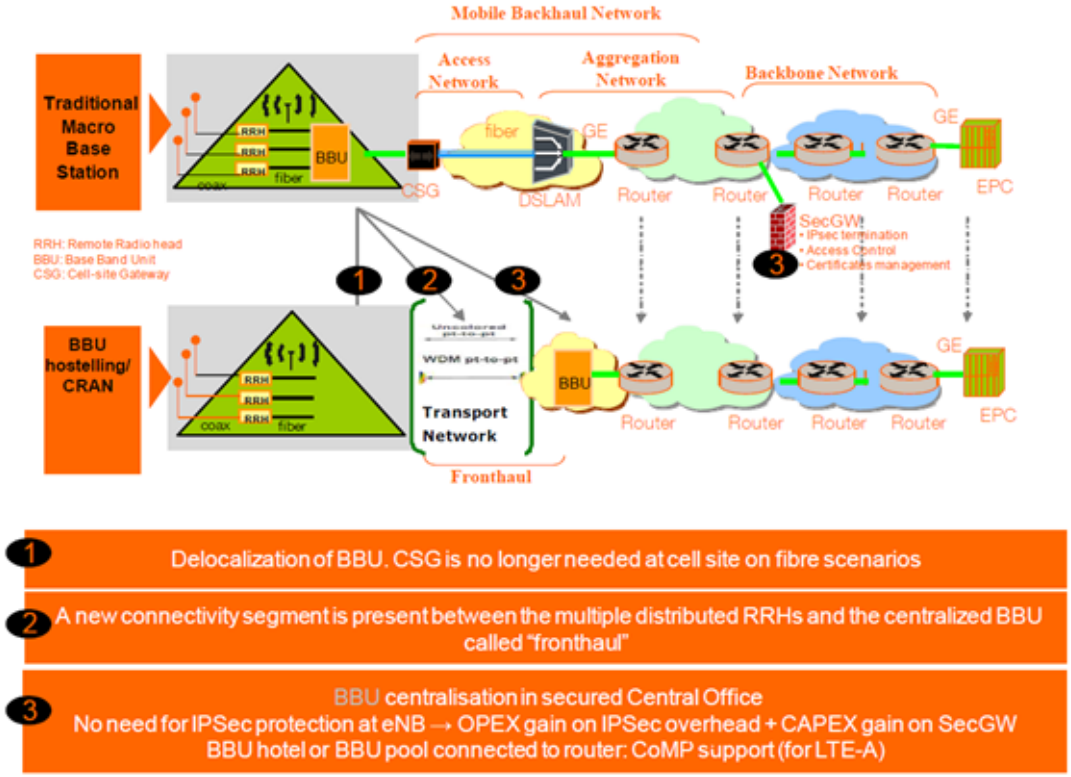

Figure: Backhaul and Fronthaul architecture

Appendix 2

Time parameter calculation

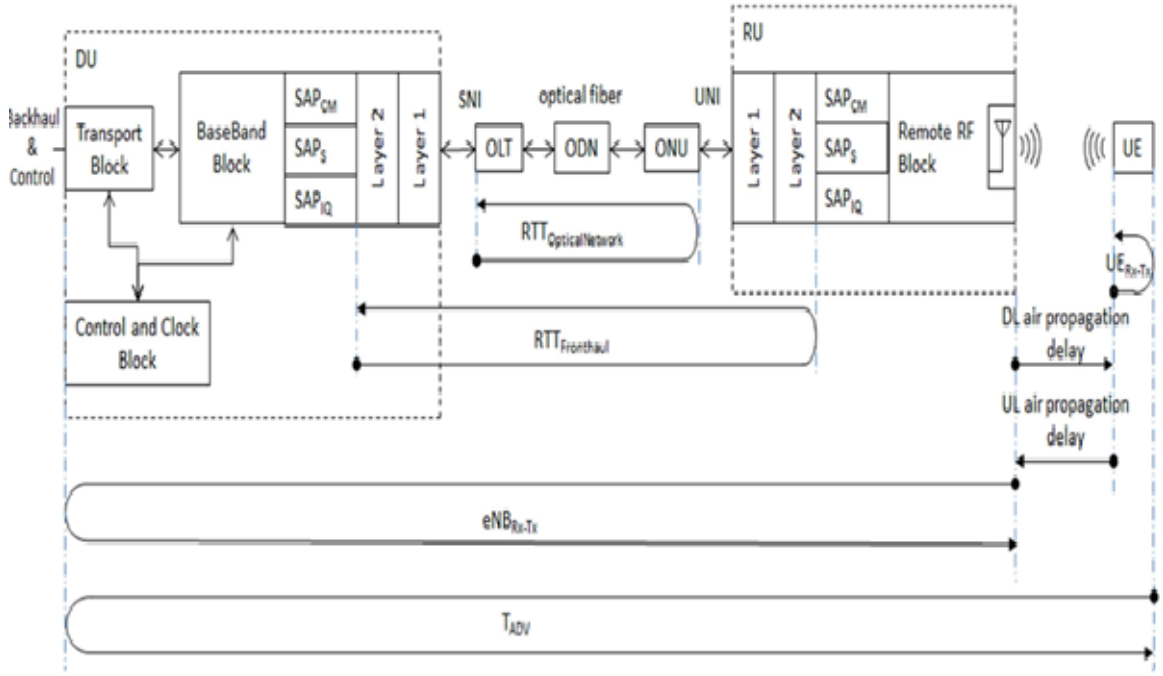

Figure: Time parameters that should be considered in the calculation of around trip delay on fronthaul link

UERX-TX (UE: User Equipment) :time difference which is defned as the difference of the UE received timing of downlink radio frame #i , defined by thefirst detected path in time and the UE transmit timeof uplink radio frame #i. The reference point for the UERx-Tx time difference measurement shall be the UE antenna connector.

eNBRX-TX : time difference which is defined as thedifference of the eNB received timing of uplink radio frame #i, defined by the first detected path in time and the eNB transmit time of downlink radio frame #i. The reference points for the eNBRx-Tx time difference measurement shall be the Rx and Tx antenna connector.

RTTfronthaul: Round Trip Time which has the reference point the layer 2 of BBU The timing Advance (TADV) should be defined as the time difference based on the sum eNBRx-Tx, UERx-Tx, and DownLink (DL) and UpLink (UL) propagation delay.

Appendix 3

CPRI Basic Frame

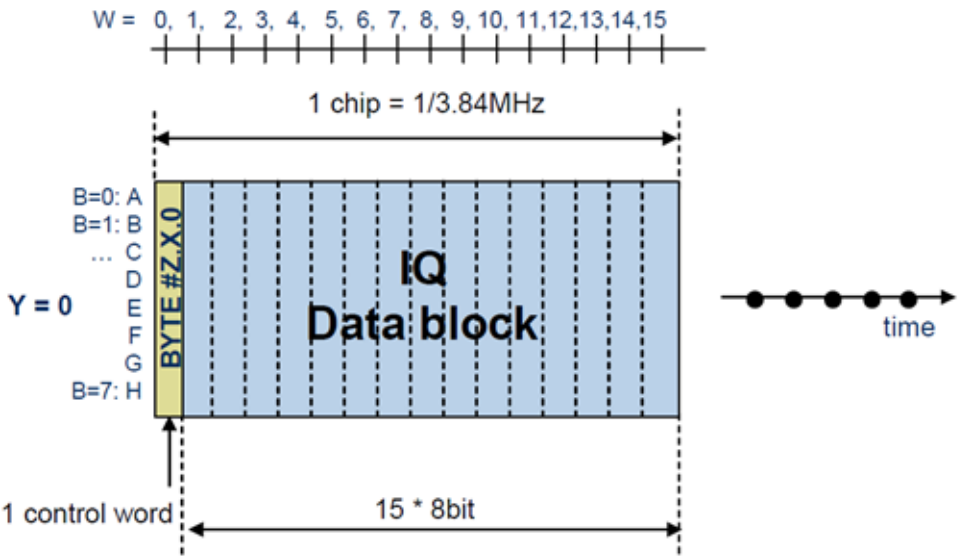

Figure: CPRI basic frame structure for 614.4 Mbit/s

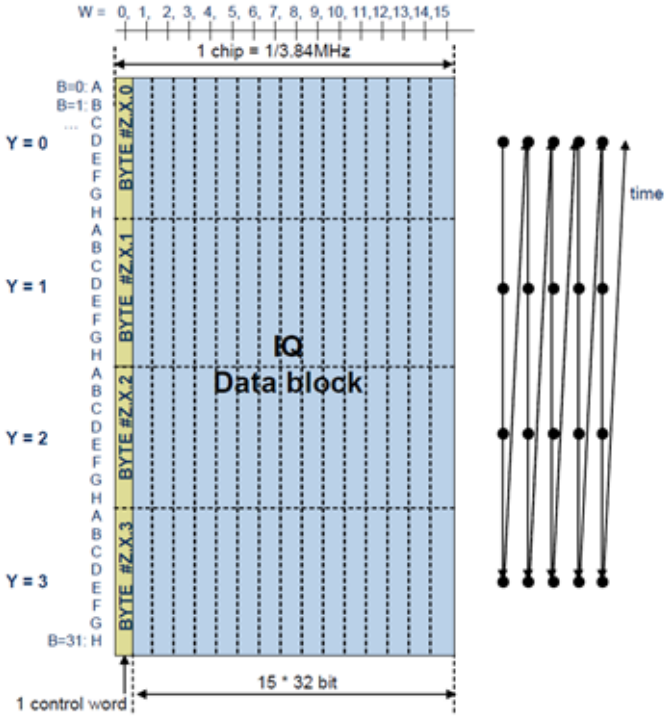

Figure: CPRI basic frame structure for 2.457 Gbit/s

Appendix 4

EVM

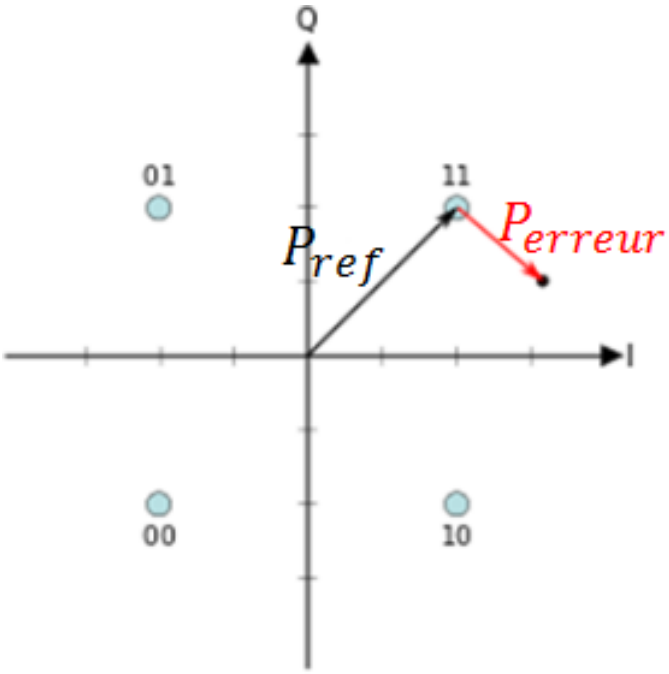

Figure: EVM

The error vector magnitude or EVM is a measure used to quantify the performance of a digital radio transmitter or receiver. A signal sent by an ideal transmitter or received by a receiver would have all constellation points precisely at the ideal locations, however various imperfections in the implementation cause the actual constellation points to deviate from the ideal locations. Informally, EVM is a measure of how far the points are from the ideal locations [105]. EVM can be described in dB or % as shown by the following equations.

$$EVM(dB) = 10\log_{10}(\frac{P_{error}}{P_{reference}})$$

$$EVM(\%) = \sqrt{\frac{P_{error}}{P_{reference}}} \times \ 100\%$$

Appendix 5

EVM measurements with self-seeded laser based on RSOA at 30 km and with 2 km of cavity length

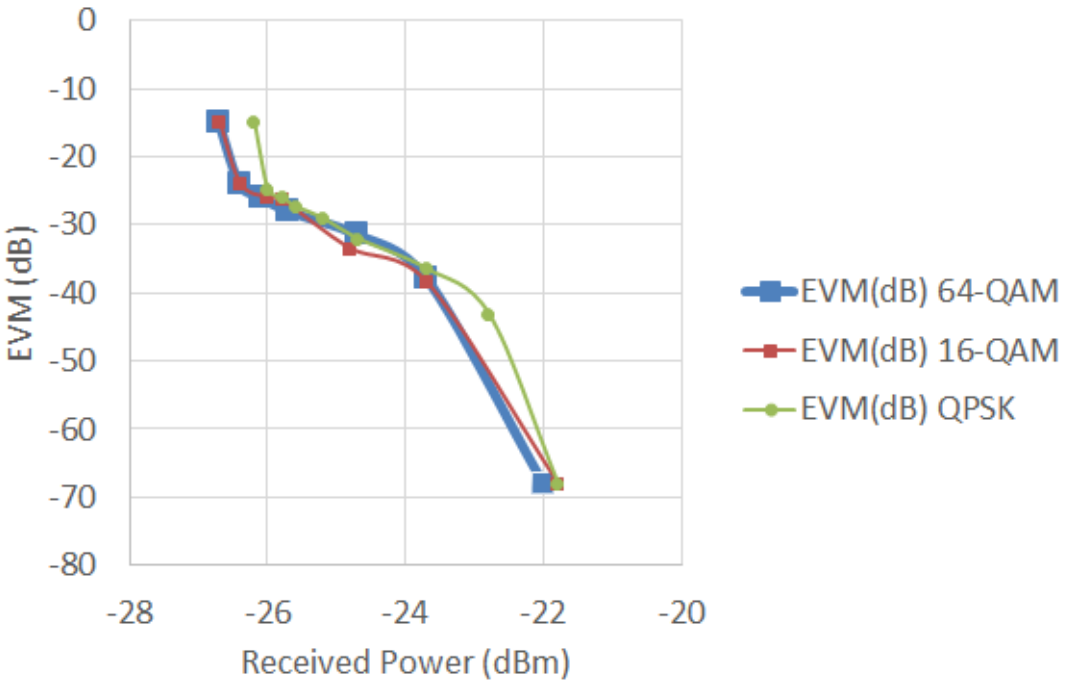

Figure: EVM measurements with self-seeded laser based on RSOA at 30 km and with 2 km of cavity length

This figure shows that the performances of different tested constellations are similar. This result is valid for any tested cavity length and any fronthaul link length tested during our experimental study.

Appendix 6

X-Haul

The X-Haul term describes the capacity of the network to be transparent to the different used specifications on fronthaul interface (CPRI, OBSAI, ORI). These different specification will be encapsulated in Ethernet.

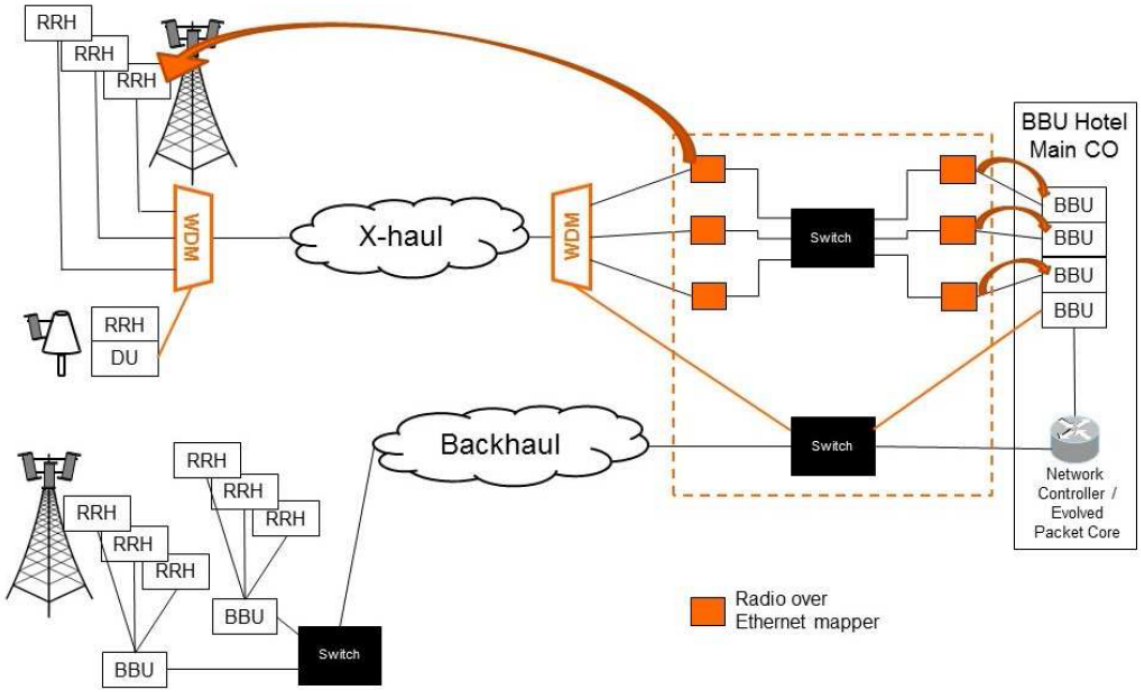

Figure: Ethernet based network including back- and front-haul [59]

Publications

International journal

ANNA PIZZINAT; PHILIPPE CHANCLOU; FABIENNE SALIOU; **THIERNO DIALLO**, « Things You Should Know About Fronthaul », Journal of Lightwave Technology, Vol. 33 Issue 5, pp 1077 - 1083, DOI: 10.1109/JLT.2014.2382872, 2015

THIERNO DIALLO; ANNA PIZZINAT; FABIENNE SALIOU; PHILIPPE CHANCLOU; GAËL SIMON; CHRISTELLE AUPETIT-BERTHELEMOT, « Self-Seeded DWDM Solution for Fronthaul Links in Centralized-Radio Access Network», Journal of Lightwave Technology, Vol. 34 Issue 21, pp 4965 - 4971, DOI: 10.1109/JLT.2016.2588520, 2016.

International conferences

CHANCLOU P. PIZZINAT A; LE CLECH F; REEDEKER T; LAGADEC Y and SALIOU F, LE GUYADER B; GUILLO L; DENIEL Q; GOSSELIN S; LE S. D; **DIALLO T**; BRENOT R; LELARGE F; MARAZZI L; PAROLARI P; MARTINELLI M; O'DULL S; GEBREWOLD S. A; HILLERKUSS D; LEUTHOLD J; GAVIOLI G; and GALLI P., "Optical fiber solution for mobile fronthaul to achieve cloud radio access network"; Future Network Mobile Summit, 2013, pp. 1-11

DIALLO, T.A. ; PIZZINAT, A. ; CHANCLOU, P. ; SALIOU, F. ; DELETRE, F. ; AUPETIT-BERTHELEMOT, C., " Jitter impact on mobile fronthaul links", Optical Fiber Communications Conference and Exhibition (OFC), DOI: 10.1364/OFC.2014.W2A.41, pp. 1-3, 2014

T.A. DIALLO, A. PIZZINAT, P. CHANCLOU, F. SALIOU, F. DELETRE, C. AUPETIT-BERTHELEMOT, « Study of jitter impact on radio frequency accuracy budget in C-RAN architecture" , European C-RAN Conference, Paris, May 2014.

T. A. DIALLO; B. LE GUYADER; A. PIZZINAT; S. GOSSELIN; P. CHANCLOU; F. SALIOU; A. ABDELFATTATH; C. AUPETIT-BERTHELEMOT, "A complete fronthaul CWDM single fiber solution including improved monitoring scheme", European Conference on Networks and Communications (EuCNC), 2015, Pages: 325 - 329, DOI: 10.1109/EuCNC.2015.7194092.

Z. TAYQ, B. LE GUYADER, P. CHANCLOU, S. GOSSELIN, **T. DIALLO**, D.P.VENMANI, S. PACHNICKE, M. EISELT, A. AUTENRIETH, J. ELBERS and C. AUPETIT-BERTHELEMOT, 25th European Conference on Networks and

Communications (EuCNC 2016), Athens, Greece, 27-30 June 2016.

Z. TAYQ, P. CHANCLOU, **T. DIALLO**, K. GRZYBOWSKI, F. SALIOU, S. GOSSELIN, O. FOUCAULT, C. AUPETIT-BERTHELEMOT, et al. "Performance demonstration of fiber and wireless fronthaul combination with remote powering" Optical Fiber Communications Conference and Exhibition (OFC),W3C.4, 2016.

National conferences

Z. TAYQ, P. CHANCLOU, F. SALIOU, **T. DIALLO**, C. AUPETIT-BERTHELEMOT, « IMPACT DE LA MONTEE EN DEBIT SUR LE CWDM BIDIRECTIONNEL DANS UNE ARCHITECTURE C-RAN », 35ème Journées Nationales d'Optique Guidées JNOG2015, Rennes, 6-9 juillet 2015.

Bibliography

[1] F. J. Effenberger, "Mobile backhaul and fronthaul systems," in *2016 21st OptoElectronics and Communications Conference (OECC) held jointly with 2016 International Conference on Photonics in Switching (PS)*, July 2016, pp. 1–3.

[2] M. Hadzialic, B. Dosenovic, M. Dzaferagic, and J. Musovic, "Cloud-ran: Innovative radio access network architecture," in *ELMAR, 2013 55th International Symposium*, Sept 2013, pp. 115–120.

[3] A. Pizzinat, "Cloud ran architecture evolution and migration stream," Orange, (Confidential document), 2012.

[4] J. E. Mitchell, "Integrated wireless backhaul over optical access networks," *Journal of Lightwave Technology*, vol. 32, no. 20, pp. 3373–3382, Oct 2014.

[5] Q. Yang, N. Deng, X. Zhou, and C.-K. Chan, "A mobile fronthaul system architecture for dynamic provisioning and protection," in *2016 21st OptoElectronics and Communications Conference (OECC) held jointly with 2016 International Conference on Photonics in Switching (PS)*, July 2016, pp. 1–3.

[6] K. Lee, J. H. Park, and H. Jung, "Comparison of digitized and analog radio-over-fiber systems over wdm-pon networks," in *2013 International Conference on ICT Convergence (ICTC)*. IEEE, 2013, pp. 705–706.

[7] E. Bogenfeld, F. Geihardt, J. Torrijos, L. Cucala, M. Attoyo, J. D. Biasio, G. Akpoli, T. Diallo, X. Grall, V. Sestito, A. Hamidian, A. Magee, P. Tumbull, R. M. S. Host, A. Krendzel, A.Pattavina, M. D. Andrade, K. Grobe, and J. V. Galan. (2014) Roadmaps for independant fixed and mobile network evolution. COMBO project, Grant Agreement number: 317762. [Online]. Available: http://ict-combo.eu/data/uploads/pdf-combo-v2/combo_d2.2_wp2_20june2014_tid_v2.0_sec.pdf

[8] X. L. Philippe Godlewski, Sami Tabbane, *Réseaux GSM*, H. S. Publication, Ed., 1999.

[9] *Universal Mobile Telecommunications System (UMTS) Technical Specifications and Technical Reports for UTRAN-based 3GPP system (3GPP TS21.101 version 3.15.0 Release 1999)*, 3GPP Std., 2005. [Online]. Available: http://www.etsi.org/deliver/etsi_ts/121100_121199/121101/03.15.00_60/ts_121101v031500p.pdf

[10] Z. Choukair and S. Tabbane, *Ingénierie des services télécoms UMTS et WiFi*, H. Science/Lavosier, Ed., 2005.

[11] H. Holma, A. Toskala *et al.*, *Wcdma for umts*. Wiley Online Library, 2000, vol. 2.

[12] H. Holma and A. Toskala, *WCDMA for umts: hspa evolution and lte.* John Wiley & Sons, 2010.

[13] H. Holma, A. Toskala, K. Ranta-Aho, and J. Pirskanen, "High-speed packet access evolution in 3gpp release 7 [topics in radio communications]," *IEEE Communications Magazine*, vol. 45, no. 12, pp. 29–35, 2007.

[14] ETSI, *3rd Generation Partnership Project; Technical Specification Group Services and System Aspects; Technical Specifications and Technical Reports for an Evolved Packet System based 3GPP System (Release 8)*, 3GPP Std., 2009. [Online]. Available: http://www.arib.or.jp/IMT-2000/V740Dec09/5_Appendix/Rel8/21/21201-810.pdf

[15] ——, *LTE; Evolved Universal Terrestrial Radio Access (E-UTRA) and Evolved Universal Terrestrial Radio Access Network (E-UTRAN); Overall description; Stage 2 (3GPP TS 36.300 version 10.2.0 Release 10)*, 3GPP Std., 2011. [Online]. Available: http://www.etsi.org/deliver/etsi_ts/136300_136399/136300/10.02.00_60/ts_136300v100200p.pdf

[16] M. Rumney *et al.*, *LTE and the evolution to 4G wireless: Design and measurement challenges.* John Wiley & Sons, 2013.

[17] A. Ghosh, R. Ratasuk, B. Mondal, N. Mangalvedhe, and T. Thomas, "Lte-advanced: next-generation wireless broadband technology [invited paper]," *IEEE Wireless Communications*, vol. 17, no. 3, pp. 10–22, June 2010.

[18] E. Dahlman, S. Parkvall, and J. Skold, *4G: LTE/LTE-advanced for mobile broadband.* Academic press, 2013.

[19] X. Zhang and W. Wang, "Carrier aggregation for lte-advanced mobile communication systems," *IEEE Communications Magazine*, p. 89, 2010.

[20] M. Sawahashi, Y. Kishiyama, A. Morimoto, D. Nishikawa, and M. Tanno, "Coordinated multipoint transmission/reception techniques for lte-advanced [coordinated and distributed mimo]," *IEEE Wireless Communications*, vol. 17, no. 3, pp. 26–34, June 2010.

[21] Y. Wang and K. I. Pedersen, "Performance analysis of enhanced inter-cell interference coordination in lte-advanced heterogeneous networks," in *Vehicular Technology Conference (VTC Spring), 2012 IEEE 75th*, May 2012, pp. 1–5.

[22] E. Hossain and M. Hasan, "5g cellular: key enabling technologies and research challenges," *IEEE Instrumentation Measurement Magazine*, vol. 18, no. 3, pp. 11–21, June 2015.

[23] W. J. Goralski, *ADSL et XDSL Nouvelles technologies d'accès à Internet.* Osman Eyrolles Multimedia, 2000.

[24] Wikipedia, "Ftth," https://fr.wikipedia.org/wiki/FTTx, 2015.

[25] R. Ramaswami, K. Sivarajan, and G. Sasaki, *Optical networks: a practical perspective.* Morgan Kaufmann, 2009.

[26] F. N. Raharimanitra, "Contribution à l'étude des architectures basées sur le multiplexage en temps et en longueur d'onde dans le réseau d'accès, permettant la migration vers la nouvelle génération de pon (ng-pon) à 10 gbits/s," Ph.D. dissertation, Télécom Bretagne, Université de Bretagne-Sud, 2012.

[27] F. Saliou, "Etude des solutions d'accès optique exploitant une extension de portée," Ph.D. dissertation, Télécom ParisTech, 2010.

[28] S. Hardy, "Iut- approves xgs-pon, and amends ng-pon2 specifications," http://www.lightwaveonline.com/articles/2016/03/itu-t-approves-xgs-pon-new-ng-pon2-specifications.html, Mar. 2016.

[29] Y. Luo, X. Zhou, F. Effenberger, X. Yan, G. Peng, Y. Qian, and Y. Ma, "Time- and wavelength-division multiplexed passive optical network (twdm-pon) for next-generation pon stage 2 (ng-pon2)," *Journal of Lightwave Technology*, vol. 31, no. 4, pp. 587–593, Feb 2013.

[30] D. Nesset, "Ng-pon2 technology and standards," *Journal of Lightwave Technology*, vol. 33, no. 5, pp. 1136–1143, March 2015.

[31] K. Grobe, A. Mitcsenkov, S. Krauss, E. Weis, J. Belschner, D. Breuer, A. Hamidian, B. Skubic, Z. Ghebretensaé, S. Gosselin, Z. Tayq, M. Tornatore, N. Carapellese, M. de Andrade, J. Vicente, and J. T. Gijón. (2015, Jun.) Analysis of transport network architectures for structural convergence. COMBO Prohect, Grant Agreement number: 317762. [Online]. Available: http://www.ict-combo.eu/data/uploads/deliverables/combo_d3.3_pu.pdf

[32] P. Chanclou, A. Pizzinat, F. L. Clech, T. L. Reedeker, Y. Lagadec, F. Saliou, B. L. Guyader, L. Guillo, Q. Deniel, S. Gosselin, S. D. Le, T. Diallo, R. Brenot, F. Lelarge, L. Marazzi, P. Parolari, M. Martinelli, S. O'Dull, S. A. Gebrewold, D. Hillerkuss, J. Leuthold, G. Gavioli, and P. Galli, "Optical fiber solution for

mobile fronthaul to achieve cloud radio access network," in *Future Network and Mobile Summit (FutureNetworkSummit), 2013*, July 2013, pp. 1–11.

[33] A. Pizzinat, F. L. Clech, F. Jounay, G. Akpoli-johson, and P. Chanclou, "Bbu hostelling opportunity for lte transport over fibre," Orange (confidential document), Tech. Rep., 2011.

[34] C. Paganus, "Consommation électrique des reseaux mobiles d'orange france. analyse et scenario d'évolution," Orange(confidential document), Tech. Rep., 2011.

[35] A. Pizzinat, "Perspectives on mobile fronthaul," Broadband World Forum 2013, 2013, amterdam.

[36] A. Pizzinat, P. Chanclou, F. L. Clech, F. Saliou, T.-L. Reedeker, T. Diallo, Y. Lagadec, A. Stidwell, Z. Shi, G. Calvignac, S. Gosselin, B. Landousies, F. Herviouand, and Y. Loussouarn, "C-ran architecture and fronthaul challenges," LTE World Summit, 2013, amsterdam.

[37] E. AB, H. Technologies, N. Corporation, A. Lucent, and N. Siemens, *CPRI Specification v7.0*, Std., Oct. 2015. [Online]. Available: http://www.cpri.info/downloads/CPRI_v_7_0_2015-10-09.pdf

[38] OBSAI, *Open Base Station Architecture Initiative (Reference Point 3 Spectification)*, Std., Mar. 2010. [Online]. Available: www.obsai.com

[39] ETSI, *Open Radio equipment Interface (ORI); ORI interface Specification; Part 1: Low Layers (Release 4)*, ETSI Std., Oct. 2014. [Online]. Available: http://www.etsi.org/deliver/etsi_gs/ORI/001_099/00201/04.01.01_60/gs_ori00201v040101p.pdf

[40] China-Mobile, *C-RAN The Road Towards Green RAN*, Dec. 2013. [Online]. Available: http://labs.chinamobile.com/cran/wp-content/uploads/CRAN_white_paper_v2_5_EN.pdf

[41] K. Sundaresan, M. Y. Arslan, S. Singh, S. Rangarajan, and S. V. Krishnamurthy, "Fluidnet: a flexible cloud-based radio access network for small cells," *IEEE/ACM Transactions on Networking*, vol. 24, no. 2, pp. 915–928, 2016.

[42] "Ieee standard for information technology–telecommunications and information exchange between systems–local and metropolitan area networks–specific requirements part 3: Carrier sense multiple access with collision detection (csma/cd) access method and physical layer specifications," *IEEE Std 802.3-2008 (Revision of IEEE Std 802.3-2005)*, pp. 1–2977, Dec 2008.

[43] ETSI, "Open radio interface (ori)," http://www.etsi.org/technologies-clusters/technologies/ori, 2010. [Online]. Available: http://www.etsi.org/technologies-clusters/technologies/ori

[44] ——, *Open Radio equipment Interface (ORI); Requirements for Open Radio equipment Interface (ORI) (Release 4)*, ETSI Std., Oct. 2014. [Online]. Available: http://www.etsi.org/deliver/etsi_gs/ORI/001_099/001/04.01.01_60/gs_ORI001v040101p.pdf

[45] X. Zhang and X. Zhou, *LTE-advanced air interface technology*. CRC Press, 2012.

[46] H. J. Son and S. Shin, "Fronthaul size: Calculation of maximum distance between rrh and bbu," 2014. [Online]. Available: http://www.netmanias.com/en/post/blog/6276/c-ran-fronthaul-lte/fronthaul-size-calculation-of-maximum-distance-between-rrh-and-bbu

[47] S. Shin and S. M. Shin, "Why should jitter be minimized in cpri fronthaul? - frequency accuracy," Jul. 2014. [Online]. Available: http://www.netmanias.com/en/?m=view&id=blog&no=6460

[48] A. Pizzinat, P. Chanclou, F. Saliou, and T. Diallo, "Things you should know about fronthaul," *J. Lightwave Technol.*, vol. 33, no. 5, pp. 1077–1083, Mar 2015. [Online]. Available: http://jlt.osa.org/abstract.cfm?URI=jlt-33-5-1077

[49] Y. Ma, X. Huo, J. Li *et al.*, "Optical solutions for fronthaul application," in *Optical Communications and Networks (ICOCN), 2015 14th International Conference on*. IEEE, 2015, pp. 1–3.

[50] F. Labs, "Dense wavelength division multiplexing (dwdm) iut grid: C-band 100 ghz spacing," 2014. [Online]. Available: http://www.fiberdyne.com/products/itu-grid.html

[51] ITU-T, *ITU-T G.694.1 Spectral grils for WDM applications: DWDM frequency grid*, ITU-T Std., 2012, geneva. [Online]. Available: http://www.itu.int/rec/T-REC-G.694.1-200206-S/en

[52] Transmode, "Mobile fronthaul transmode's unique passive, semi-passive and active options enable mobile operators to migrate small and micro cells to a cloud-ran architecture," Application Note, 2015. [Online]. Available: https://www.infinera.com/wp-content/uploads/2015/10/AN_Mobile-Fronthaul_G-1.pdf

[53] ITU-T, *Recommendation ITU-T G.709/Y.1331: Interfaces for the optical transport network*, ITU-T Std., 2016. [Online]. Available: https://www.itu.int/rec/T-REC-G.709-201606-I/fr

[54] ——, *Recommendation ITU-T G798 Characteristics of optical transport network hierarchy equipment functional blocks*, ITU-T Std., 2012. [Online]. Available: https://www.itu.int/rec/T-REC-G.798-201212-I/fr

[55] D. Temple and L. Pedersen, "Superior cpri over otn front-haul solutions," ALTERA, White Paper, 2016, wP-01263-1.0. [Online]. Available: https://www.altera.com/content/dam/altera-www/global/en_US/pdfs/literature/wp/wp-01263-superior-cpri-over-otn-front-haul-solutions.pdf

[56] ITU-T, *Recommendation ITU-T G Supplement 56 OTN transport of CPRI signals*, ITU-T Std., 2016. [Online]. Available: https://www.itu.int/rec/T-REC-G.Sup56-201602-I/en

[57] M. Jamgochia and S. Trowbridge, "Understanding otn, optical transport network (g.709)," Alcatel Lucent, Tech. Rep., 2010. [Online]. Available: http://www.cvt-dallas.org/March2010.pdf

[58] T. P. Walker, "Optical transport network (otn) tutorial," AMCC, techreport, 2005. [Online]. Available: https://www.itu.int/ITU-T/studygroups/com15/otn/OTNtutorial.pdf

[59] N. J. Gomes, P. Chanclou, P. Turnbull, A. Magee, and V. Jungnickel, "Fronthaul evolution: From cpri to ethernet," *Optical Fiber Technology*, vol. 26, pp. 50–58, 2015.

[60] B. Varga, "Cpri over ethernet, towards cpri parameters," Ericsson, Presentation, 2015, iEEE P202.1CM, Dallas. [Online]. Available: http://www.ieee802.org/1/files/public/docs2015/cm-varga-towards-cpri-parameters-1115-v01.pdf

[61] T. Wan and P. Ashwood, "A performance study of cpri over ethernet," *IEEE 1904.3 Task Force*, 2015.

[62] L. Valcarenghi, K. Kondepu, and P. Castoldi, "Analytical and experimental evaluation of cpri over ethernet dynamic rate reconfiguration," in *2016 IEEE International Conference on Communications (ICC)*, May 2016, pp. 1–6.

[63] T. Wan and P. Ashwood-Smith, "A performance study of cpri over ethernet with ieee 802.1qbu and 802.1qbv enhancements," in *2015 IEEE Global Communications Conference (GLOBECOM)*, Dec 2015, pp. 1–6.

[64] S. Pachnicke, J. Zhu, M. Lawin, A. Wonfor, M. Eiselt, R. V. Penty, R. Cush, R. Turner, P. Firth, M. J. Wale, I. H. White, and J. P. Elbers, "First demonstration of a full c-band tunable wdm-pon system with novel high-temperature ds-dbr lasers," in *OFC 2014*, March 2014, pp. 1–3.

[65] S. Pachnicke, S. Mayne, B. Quemeneur, D. Sayles, H. Schwuchow, J. Zhu, A. Wonfor, P. Marx, M. Lawin, M. Fellhofer, R. Turner, P. Neuber, M. Dietrich, M. J. Wale, R. V. Penty, I. H. White, and J. P. Elbers, "Field demonstration of a tunable wdm-pon system with novel sfp+ modules and centralized wavelength control," in *2015 Optical Fiber Communications Conference and Exhibition (OFC)*, March 2015, pp. 1–3.

[66] C. F. Lam, *Passive optical networks: principles and practice*. Academic Press, 2011.

[67] Z. Tayq, P. Chanclou, T. Diallo, K. Grzybowski, F. Saliou, S. Gosselin, O. Foucault, C. Aupetit, L. Bellot, T. Boukour, J. C. Plumecoq, and J. Sayed, "Performance demonstration of fiber and wireless fronthaul combination with remote powering," in *2016 Optical Fiber Communications Conference and Exhibition (OFC)*, March 2016, pp. 1–3.

[68] C. l. I, Y. Yuan, J. Huang, S. Ma, C. Cui, and R. Duan, "Rethink fronthaul for soft ran," *IEEE Communications Magazine*, vol. 53, no. 9, pp. 82–88, September 2015.

[69] China-Mobile-Research-Institute, Alcatel-Lucent, N. Networks, Z. Corporation, B. Corporation, and I. C. R. Center, "White paper next generation fronthaul interface," China Mobile, resreport, Jun. 2015, white Paper. [Online]. Available: http://labs.chinamobile.com/cran/wp-content/uploads/White%20Paper%20of%20Next%20Generation%20Fronthaul%20Interface.PDF

[70] China-Mobile, "China mobile's view on next generation fronthaul interface," China Mobile, Tech. Rep., 2015. [Online]. Available: http://www.ieee1904.org/email/pdfLV66u9TRJ8.pdf

[71] J. Hancock *et al.*, "Jitter–understanding it, measuring it, eliminating it. part 1: Jitter fundamentals," *High Frequency Electronics*, vol. 4, no. 4, pp. 44–50, 2004.

[72] N. Ou, T. Farahmand, A. Kuo, S. Tabatabaei, and A. Ivanov, "Jitter models for the design and test of gbps-speed serial interconnects," *IEEE Design & Test of Computers*, vol. 21, no. 4, pp. 302–313, 2004.

[73] ——, "Jitter models for the design and test of gbps-speed serial interconnects," *IEEE Design & Test of Computers*, vol. 21, no. 4, pp. 302–313, 2004.

[74] S. Bregni, *Synchronization of digital telecommunications networks*. Wiley New York, 2002, vol. 27.

[75] IEEE, *IEEE Standard 802.3 , Carrier Sense Multiple Access with Collision Detection (CSMA/CD) access methode and Physical Layer specifications*, IEEE Std., 2008, clause 47.

[76] OBSAI, *Reference Point 3 Specification*, OBSAI Std., 2010, version 4.2. [Online]. Available: http://www.obsai.com/specs/RP3_Specification_V4.2.pdf

[77] Maxim-Intergrated, "Converting between rms and peak-to-peak jitter at a specified ber," Maxim integrated, Application Note, Apr. 2008, application Note: HFAN-4.0.2. [Online]. Available: http://pdfserv.maximintegrated.com/en/an/AN462.pdf

[78] ITU, *ITU-T Recommendation O.171: Timing jitter and wander measuring equipment for digital systems which are based on the plesiochronous digital hierarchy (PDH)*, ITU Std., Apr. 1997. [Online]. Available: https://www.itu.int/rec/T-REC-O.171-199704-I/en

[79] ——, *ITU-T Recommendation O.172: Timing jitter and wander measuring equipment for digital systems which are based on the synchronous digital hierarchy (SDH)*, ITU Std., Apr. 2005. [Online]. Available: https://www.itu.int/rec/T-REC-O.172-200504-I/en

[80] R. Stephens, "Jitter analysis: The dual-dirac model, rj/dj, and q-scale," *Agilent Technologies Whitepaper, Literature Number*, 2004.

[81] Agilent-Technologies, "Precision jitter analysis using the agilent 86100c dca-j," Agilent Technologies, Application Note 5989-1146EN, Mar. 2007. [Online]. Available: http://cp.literature.agilent.com/litweb/pdf/5989-1146EN.pdf

[82] C. Lanzani, G. Bergamo, M. Hoegdal, R. ApS, and H. Denmark, "Analysis of clock distribution and delay measurements for multi-hop remote radio applications," in *6th Karlsruhe Workshop on Software Radios (I.. KI of Technology Communications Engineering Lab, ed.),(Karlsruhe, Germany)*, 2010, pp. 146–152.

[83] ETSI, *3GPP TS 36.104 LTE; Evolved Universal Terrestrial Radio Access (E-UTRA); Base Station (BS) radio transmission and reception*, 3GPP Std., Apr. 2013, version 11.4.0 Release 11. [Online]. Available: http://www.etsi.org/deliver/etsi_ts/136100_136199/136104/11.04.00_60/ts_136104v110400p.pdf

[84] N. J. Gomes, P. P. Monteiro, and A. Gameiro, *Next generation wireless communications using radio over fiber*. John Wiley & Sons, 2012.

[85] Texas-Instruments. (2013) Telecom tower: Remote radio unit (rru). Texas Instruments. [Online]. Available: http://www.ti.com/solution/telecom_tower_remote_radio_unit_rru

[86] A. Nirmalathas, P. A. Gamage, C. Lim, D. Novak, and R. Waterhouse, "Digitized radio-over-fiber technologies for converged optical wireless access network," *Journal of Lightwave Technology*, vol. 28, no. 16, pp. 2366–2375, 2010.

[87] H. Meyr and G. Ascheid, *Phase-, frequency-locked loops and amplitude control*. Wiley, 1990.

[88] T. Diallo, A. Pizzinat, F. Saliou, P. Chanclou, G. Simon, and C. Aupetit-Berthelemot, "Self-seeded dwdm solution for fronthaul links in centralized-radio access network," *Journal of Lightwave Technology*, vol. 34, no. 21, pp. 4965–4971, Nov 2016.

[89] P. Parolari, L. Marazzi, M. Brunero, M. Martinelli, A. Maho, S. Barbet, F. Lelarge, R. Brenot, G. Gavioli, G. Simon *et al.*, "Operation of a rsoa wdm pon self-seeded transmitter over more than 50 km of ssmf up to 10 gb/s," in *Optical Fiber Communication Conference*. Optical Society of America, 2014, pp. W3G–4.

[90] Q. Deniel, F. Saliou, P. Chanclou, and D. Erasme, "Self-seeded rsoa based wdm-pon transmission capacities," in *Optical Fiber Communication Conference*. Optical Society of America, 2013, pp. OW4D–3.

[91] A. Maho, G. Simon, S. Barbet, F. Lelarge, F. Saliou, P. Chanclou, P. Parolari, L. Marazzi, M. Brunero, M. Martinelli, S. A. Grebewold, J. Leuthold, and R. Brenot, "Demystification of the self-seeded wdm access," *Journal of Lightwave Technology*, vol. 34, no. 2, pp. 776–782, Jan 2016.

[92] M. Martinelli, L. Marazzi, P. Parolari, M. Brunero, and G. Gavioli, "Polarization in retracing circuits for wdm-pon," *IEEE Photonics Technology Letters*, vol. 24, no. 14, pp. 1191–1193, July 2012.

[93] G. Simon, F. Saliou, P. Chanclou, Q. Deniel, D. Erasme, and R. Brenot, "70km external cavity dwdm sources based on o-band self seeded rsoas for transmissions at 2.5gbit/s," in *OFC 2014*, March 2014, pp. 1–3.

[94] A. Technology, "Jitter fundamentals: Agilent 81250 parbert jitter injection and analysis capabilities," Agilent Technology, Application Note 5988-9756EN, Jul. 2003. [Online]. Available: https://fenix.tecnico.ulisboa.pt/downloadFile/3779572188795/AG03.pdf

[95] T. Diallo, A. Pizzinat, P. Chanclou, F. Saliou, F. Deletre, and C. Aupetit-Berthelemot, "Jitter impact on mobile fronthaul links," in *Optical Fiber Communication Conference*. Optical Society of America, 2014, p. W2A.41. [Online]. Available: http://www.osapublishing.org/abstract.cfm?URI=OFC-2014-W2A.41

[96] T. A. Diallo, A. Pizzinat, P. Chanclou, F. Saliou, F. Deletre, and C. Aupetit-Berthelemot, "Jitter impact on radio frequency accuracy budget in c-ran architecture." in *C-RAN Europe Conférence*, 2014.

[97] R. Ellis, "Explanation of reflection features on optical fiber as sommetimes observed in otdr measurement traces," Tech. Rep., 2015. [Online]. Available: http://www.corning.com/media/worldwide/coc/documents/Fiber/RC-%20White%20Papers/WP-General/WP1281_11-2015.pdf

[98] M. O. V. Deventer, "Polarization properties of rayleigh backscattering in single-mode fibers," *Journal of Lightwave Technology*, vol. 11, no. 12, pp. 1895–1899, Dec 1993.

[99] W. Yan-Hong, N. Guo-Qiang, G. Pan, and G. Kun, "Theoretical analysis on coherent noise by rayleigh backscattering in bidirectional transmission system with single mode fiber," in *2009 International Forum on Information Technology and Applications*, vol. 1, May 2009, pp. 209–212.

[100] F. Couny, F. Benabid, and P. S. Light, "Reduction of fresnel back-reflection at splice interface between hollow core pcf and single-mode fiber," *IEEE Photonics Technology Letters*, vol. 19, no. 13, pp. 1020–1022, July 2007.

[101] T. Hashimoto, A. Kinda, R. Kasaliara, I. Ogawa, Y. Shuto, M. Yanagisawa, A. Obki, S. Mino, M. Ishii, Y. Suzuki, R. Nagase, and T. Kilagawa, "A bidirectional single fiber 1.25 gb/s optical transceiver module with sfp package using plc," in *53rd Electronic Components and Technology Conference, 2003. Proceedings.*, May 2003, pp. 279–283.

[102] N. Parkin, M. Bartur, D. Nesset, and D. Jenkins, "Gigabit sfp transceiver with integrated optical time domain reflectometer for ethernet access services," in *39th European Conference and Exhibition on Optical Communication (ECOC 2013)*, Sept 2013, pp. 1–3.

[103] J. Shin, S. Hong, J. Y. Lim, S. Cho, H. Y. Rhy, and G. Y. Yi, "Cwdm networks with dual sub-channel interface for mobile fronthaul and backhaul deployment," in *16th International Conference on Advanced Communication Technology*, Feb 2014, pp. 1099–1102.

[104] L. Faustini and G. Martini, "Bend loss in single-mode fibers," *Journal of Lightwave Technology*, vol. 15, no. 4, pp. 671–679, Apr 1997.

[105] Wikipedia. (2015) Error vector magnitude. Wikipedia. Web page. [Online]. Available: https://en.wikipedia.org/wiki/Error_vector_magnitude

Abstracts

La Fibre en support du Mobile Cloud

Résumé : résumé français.

Abstract

De nos jours, la montée en débit observée dans les réseaux mobiles est une problématique. A long terme, la densification des réseaux radios mobiles s'avèrera inefficace. En plus de cela cette densification entrainera une baisse de rentabilité des réseaux d'accès mobiles et augmentera la complexité au niveau de la gestion des fréquences mobile qui accroîtra inéluctablement le risque de la présence des interférences. Pour pallier ce manque de rentabilité et pour faciliter le déploiement de certaines techniques d'optimisation et d'amélioration de l'interface air comme le « Coordinated MultiPoint (CoMP) », les acteurs des télécommunications proposent une nouvelle architecture innovante désignée par les termes « Mobile Cloud » ou « Centralized or Cloud Radio Access Network (C-RAN) » Le C-RAN consiste à déporter l'entité de traitement des données numérisées appelée « Base Band Unit (BBU) » du site d'antenne vers un local plus sécurisé nommé « Central Office (CO) ». L'entité de traitement radio dénommée « Remote Radio Head (RRH)» est toujours localisée sur le site d'antenne. Cette délocalisation crée un nouveau segment réseau appelé « fronthaul ». Le fronthaul est un segment réseau très gourmand en bande passante par conséquent la fibre est désignée comme le support idéal pour assurer la communication bidirectionnelle entre la RRH et la BBU. Dans notre thèse, nous avons étudié les solutions de déploiement du fronthaul. Etant donné que l'interface fronthaul utilise de grands débits pour la transmission de données numérisées, elle est soumise à un phénomène physique nommé gigue qui a tendance à dégrader les performances de transmission. Les effets et l'impact de la gigue sur l'interface fronthaul et sur l'interface air ont été aussi étudiés.

Mots clés : C-RAN, Fronthaul, CPRI, WDM, Gigue.

Mobile Cloud supported by the optical fiber

Abstract: résumé anglais.

Abstract

In Europe, the competition between the mobile operators is so strong that the profitability of the mobile network has decreased. The cost to implement, to operate and to upgrade the mobile network is increasing while the revenues generated by the latter are not sufficient. Therefore, the operators should find the way to reduce the CAPEX and the OPEX. To keep competitive, the operators have begun to think about a novel RAN architecture. This new architecture is called Centralized or Cloud Radio Access Network. The traditional antenna site consists of the Radio Remote Head (RRH) which performs the radio processing, and the Base Band Unit (BBU) which carries out the digital processing. The principle of C-RAN consists to move the BBU from antenna site towards the local secured belonging to an operator called Central Office (CO). The move of BBU from antenna site to CO leads to the appearance of a new network segment called fronthaul. During this thesis, the different solutions to the deployment of fronthaul are studied. Since the fronthaul is a digitized interface with great data rate, it is affected by a physical phenomenon called jitter. The jitter affects the performance of the system and can lead the break of the communication between the RRH and the BBU.Therefore, the effects and the impacts of jitter on the fronthaul interface are addressed in this thesis.

Keywords: C-RAN, Fronthaul, CPRI, WDM, Jitter.

LABO XLIM - UMR CNRS n° 7252
11 Boulevard Marie et Pierre Curie - BP 30179 - 86962 Futuroscope Chasseneuil CEDEX